UCRL 9835

UNIVERSITY OF CALIFORNIA

Ernest O. Lawrence

Radiation Laboratory

PION-HYPERON RESONANCES

BERKELEY, CALIFORNIA

UCRL-9835
UC-34 Physics
TID-4500 (16th Ed.)

UNIVERSITY OF CALIFORNIA
Lawrence Radiation Laboratory
Berkeley, California

Contract No. W-7405-eng-48

PION-HYPERON RESONANCES

Stanley G. Wojcicki

(Thesis)

August 24, 1961

Printed in USA. Price $2.25. Available from the
Office of Technical Services
U. S. Department of Commerce
Washington 25, D.C.

PION-HYPERON RESONANCES

Table of Contents

Abstract vii

I. Introduction 1

II. Experimental Procedure

A. Description of the beam 2

B. Operating Conditions 4

III. Data Analysis

A. Scanning 5

B. Sketching and Measuring 5

C. Digital-Computer Analysis 7

IV. Treatment of Experimental Data

A. The $\Sigma^+\pi^-$, $\Sigma^-\pi^+$, and $\Sigma^0\pi^0$ Reactions 10

1. Angular Distributions for $K^-+p \rightarrow \Sigma^{\pm}+\pi^{\mp}$ . . 10

2. Separation and Angular Distribution for Single-V Events 17

3. Polarization of Charged Σ and Single-V Events 23

B. The $\Sigma 2\pi$ Reactions 30

1. The $\Sigma^{+-0}\pi\pi$ and $\Sigma^-\pi^+\pi^0$ Final States 30

2. The $\Sigma^0\pi^+\pi^-$ Final State 31

3. Representation of the Data 32

C. The $\Sigma 3\pi$ Events 32

1. The $\Sigma^{\pm}\pi^{\mp}\pi^+\pi^-$ Reactions 36

2. The $\Sigma^{\pm}\pi^{\mp}\pi^0\pi^0$ Reactions 36

3. The $\Sigma^0\pi^+\pi^-\pi^0$ Reaction 36

V. Discussion of Results

A. Discussion of the Reactions $K^-+p \rightarrow \Sigma+\pi$ . . . 39

B. The T=1 Resonance (Y_1^*) 42

1. Global Symmetry Description of Y_1^* . . . 42

2. $\bar{K}N$ Bound-State-Model Description of Y_1^* . 45

3. The $\Sigma 2\pi$ Experimental Results 47

Table of Contents (continued)

C. The T=0 Resonance (Y_0^*) 51
1. The $\Sigma^{\pm}\pi^{\mp}\pi^{+}\pi^{-}$ Events 52
2. The $\Sigma^{0}\pi^{0}\pi^{+}\pi^{-}$ Events: Determination of the Isotopic Spin of the Resonance 57
3. The $\Sigma^{\pm}\pi^{\mp}\pi^{0}\pi^{0}$ Reactions 63
4. Discussion of $\Sigma^{\pm}\pi^{+}\pi^{0}$ Events in Light of T=0 Resonance 63
5. Mass Discrepancy 68
D. Influence of Other Possible Σ-π Resonances . 68
1. The T=2 Global-Symmetry Resonance . 69
2. The 1520-Mev T=0 Resonance 71
Acknowledgements 73
Appendices
A. Path-Length Determination 75
B. Study of Measurement Errors 79
C. Determination of the Beam Momentum . . . 89
D. Estimate of Rates for Different Reactions in Single-V Events 92
E. Study of Ambiguities in Σ2π Reactions . . . 94
References 102

PION-HYPERON RESONANCES

Stanley G. Wojcicki

(Thesis)

Lawrence Radiation Laboratory
University of California
Berkeley, California

August 24, 1961

ABSTRACT

This report describes the study of 1.15-Bev/c K^--meson interactions in the Berkeley 15-in. hydrogen bubble chamber. The discussion is limited mainly to some 600 events in which the final state consists of a Σ hyperon and one or more pions.

The mechanics of analysis with the PANG, KICK, and EXAMIN programs are described in the first part of the report. A detailed discussion is given of the treatment of ambiguities between the various hypotheses, a problem that becomes quite severe at this energy.

The discussion of results emphasizes the effect of strong final-state interactions in the Σ-π system. The relationship of the data to the recently discovered Y_1^* resonance in the $\Lambda\pi^+\pi^-$ reaction is discussed, and it is shown that the Σ/Λ branching ratio of Y_1^* is less than 16%. Evidence is presented for the existence of a T=0 resonance in the Σ-π system with a mass of about 1400 Mev. It is shown that $K^- + p \rightarrow \Sigma + \pi$ reactions at this energy seem to proceed almost entirely from the T=0 initial state, which might be because the reactions are still dominated by the T=0 resonance in the K^-p system at ~1 Bev/c.

I. INTRODUCTION

In the fall of 1958 a high-energy K^- beam was set up[1] at the Berkeley Bevatron to search for the Ξ^0 hyperon, a neutral counterpart of Ξ^- in the strangeness scheme of Gell-Mann and Nishijima.[2] The hydrogen bubble chamber was used as a detector, because it alone would permit an unambiguous identification of the production and decay of the Ξ^0. In addition to one example of the Ξ^0 particle,[3] several thousand K^-p interactions were observed in the Berkeley 15-in. hydrogen bubble chamber. These are of considerable interest in the study of properties of strange particles, as the only previous investigation of K^--nucleon interactions above 400 Mev/c had been limited to a counter measurement of K^- total cross sections on hydrogen and deuterium at 0.9 Bev/c.[4] Since a discussion of the reaction $K^- + p \rightarrow \Lambda + \pi^+ + \pi^-$ has been published already in reasonable detail,[5] this study will be limited mainly to those reactions in which the final state consists of a Σ hyperon and one or more pions. Other Λ reactions will be discussed insofar as they are experimentally connected with the Σ reactions. Part of these data have been published previously in an abbreviated version.[6] The nonhyperon-producing interactions will be reported separately.[7]

Sections II and III deal with the description of the experimental setup and running conditions, and the mechanics of the analysis of data. A more detailed description of some of the aspects of analysis is given in the first three appendices.

Section IV deals with the experimental results, with emphasis on those features of analysis that were specific to a given class of interactions, namely the resolution of ambiguities and the elimination of experimental biases. The last section concerns itself with the interpretation of the data in terms of the existing theories and the relationship of the data to other strange-particle phenomena.

II. EXPERIMENTAL PROCEDURE

A. Description of the Beam

The K^- beam used in this experiment was designed by Eberhard, Good, and Ticho and is described in detail elsewhere.[1] Accordingly, only a summary will be given here. The schematic diagram of the beam setup is shown in Fig. 1.

The K^- mesons were separated from a much more copious pion and muon flux by means of two Cork-Wentzel-Lambertson velocity spectrometers,[8] each forming a separate stage of separation. The crossing E and H fields were set for transmission of K mesons, which in turn resulted in the deflection of the lighter pions and muons out of the median plane. At the end of the first stage of separation, a 0.2-in.-wide slit backed up by a uranium collimator was used to stop the deflected pions. The slit, in turn, served as the source of the K mesons for the second part of the system. The bending magnet just before the bubble chamber was used to sweep away the off-momentum particles that might have gotten through the system up to that point. Finally, another slit--this one 0.34-in-wide--followed by a lead collimator was placed just before the entrance to the chamber to stop the pions and muons deflected by the second spectrometer.

The final accepted momentum interval was defined by using the first quadrupole to focus the beam in the horizontal plane at the second quadrupole. Because of the initial momentum dispersion due to the Bevatron field, different momenta are focused at different points along a line normal to the beam direction. Thus a collimator located in the second quadrupole was used to define the momentum bite. The nominal momentum was 1.15 Bev/c and the momentum interval accepted $\pm$ 1-1/4%.

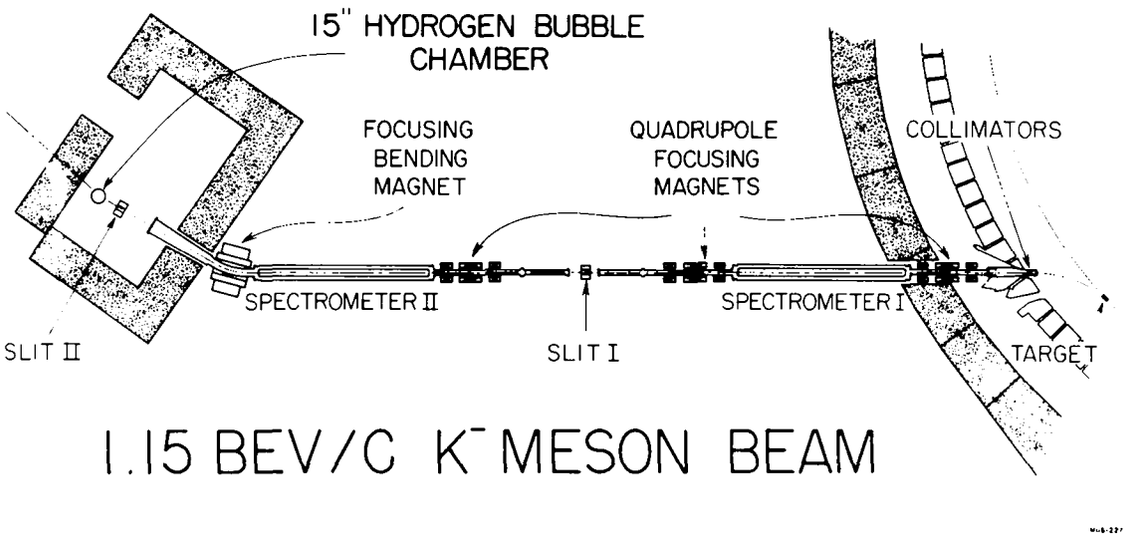

Fig. 1. Schematic diagram of 1.17-Bev/c K^--beam.

B. Operating Conditions

During the actual running time of about 6 weeks some 70,000 pictures were taken in the Berkeley 15-in. hydrogen bubble chamber exposed to the K^- beam. The total K^- flux through the chamber was about 100,000. The average picture contained about 10 tracks, less than half of which satisfied beam criteria on direction, position, and curvature. The majority of the beam tracks were muons, there being typically one or two kaons and less than one pion in each picture. The nonbeam tracks were also principally muons, but with a larger admixture of pions than in the proper beam. Because the total K path length was determined solely by counting K decays (described in detail in Appendix A) and the reactions we will discuss are characteristic of K mesons, the knowledge of the exact amount of pion and muon contamination is not essential for the purposes of our discussion.

III. DATA ANALYSIS

A. Scanning

All film used was scanned twice:--once immediately after exposure mainly to search for double V^0 events (i.e. possible Ξ^0 productions) and to check on the chamber and beam conditions. However, all other interactions as well as the decays were also searched for and recorded. Before the second scan, the film was edited, and approximately 25% of it was rejected because of poor sensitivity of the chamber, failure of a camera, or some other conditions that rendered it below the desired standard. All of the accepted film was then rescanned. The results of the two scans were subsequently used to prepare a master list of all the events found for the next stage in analysis, which is called "sketching". Both of the scans were strictly topological and no effort was made to assign a physical interpretation to a given event.

B. Sketching and Measuring

The purposes of the sketching stage are basically (a) to check the scanner's identification of the event; (b) to scan once again that particular frame for any possible correlated tracks, e.g. V's, recoil protons, or electron pairs; and (c) to prepare a sketch of the event for the subsequent measurement. A fiducial boundary was imposed at this time, its boundaries determined by the condition that all of the area under consideration be sufficiently well illuminated and that all the tracks of the accepted interactions have at least 4 cm of measurable length, regardless of the direction in which they were emitted. The fiducial volume was defined in terms of a projected area in one of the four views.

At this energy the same topological configuration can be due to many types of interaction. For example, a two-prong interaction

with an associated V can be any of the following:

$$\begin{aligned} K^- + p &\rightarrow \bar{K}^0 + p + \pi^- \\ &\rightarrow \bar{K}^0 + \pi^- + \pi^+ + n \\ &\rightarrow \Lambda + \pi^- + \pi^+ \\ &\rightarrow \Sigma^0 + \pi^- + \pi^+ . \end{aligned}$$

Furthermore, each of these reactions can be produced along with additional neutral pions. Very often, ionization, subsequent interaction or decay of one of the secondary tracks, or the fact that the positive track stops and does not decay can be used to eliminate some of these hypotheses by inspection. However, this is not always true, and thus for the sake of simplicity and limiting the number of event types, the classification of events at this stage was determined strictly by the topology of the main interaction vertex. Every distinct topological configuration corresponded to a different event type. If a secondary track interacted or decayed in the chamber (connected event), then this vertex was also listed for measurement so that all available information could be utilized.

In making the sketch, the sketcher assigned an event-type number to every event and decided which two of the four possible views should be used to measure each track. The criteria here were good stereo angle and quality of the film. Stereo angle is the angle made by the track with the line joining the two cameras used. The maximum resolution is obtained when the two intersect at right angles. Furthermore, if any track stopped in the chamber, that information was also recorded on the sketch card.

The next stage in the data-processing system is the actual measurement of the event by means of the automatic measuring projector (Franckenstein) developed at the Lawrence Radiation Laboratory. For each track, several coordinate points are measured on the film in the two views chosen and then punched on IBM cards along with the

master information for the whole event (roll and frame number, fiducials on the top glass, event-type number, etc.). If any track stops, this is also indicated on the IBM cards by means of an appropriate code word. Connected events, if any, associated with the main vertex are also measured at this time.

C. Digital-Computer Analysis

The three stages in the digital computer analysis are the PANG, KICK, and EXAMIN programs. These are interrelated by means of output binary tapes, which serve as input for the following program.

The IBM cards with the track coordinates are used as the input for the track-reconstruction 704 program PANG.[9] This program uses the two projected views of each track to reconstruct it in space and calculates the momenta from curvature and range, and azimuth and dip angles, as well as the uncertainties in these quantities. Some account is taken of the nonlinear effects in the optics of the bubble chamber Nonlinear effects means not only higher-order lens corrections, but also correction for small imperfections in the alignment of the optical system. This is done by calculating a set of optical parameters by a least-squares fit to the grid of fiducials on the top glass. The PANG program calculates statistical errors which include the contribution due to the multiple Coulomb scattering as well as that due to the measurement uncertainties. The latter, however, are obtained merely by propagating a certain intrinsic measuring uncertainty on each point, and take no account of turbulence or imperfections in the optics of the system, as these depend very much on specific running conditions. It was necessary, therefore, to modify parts of PANG to take account of these two effects so as to obtain errors corresponding to the actual experimental conditions. A full discussion of this study is given in Appendix B. To summarize the results of this study here, we can say that the final errors in general are of the right magnitude. However,

there are small systematic shifts in the measured quantities which are at most equal to one third of the typical quoted errors and which will cause the observed χ^2 distributions to be spread out by a factor of ~ 1.2 over the expected distributions.

The PANG binary tape serves as input for the kinematical constraints program KICK.[10] At a vertex where the momenta and angles of all tracks are measured, KICK does a four constraint least-squares fit in the 3n dimensional space (n being the number of tracks), the four constraints being the three equations of conservation of linear momentum and conservation of energy. The 3n variables are taken to be the azimuth, tangent of the dip angle, and the curvature of each track. This choice is dictated because it is in these quantities that the measurement errors come closest to being normally distributed. Sometimes when some of the input variables are missing, (e.g. the momentum of the neutral track), the number of constraints is necessarily reduced. The reason for this constraint reduction is that for each variable that is missing a constraint equation is required (and thereby eliminated) to solve for the missing variable in terms of the known variables. The final fit is obtained when the χ^2 is minimized with the simultaneous satisfaction of the constraining equations.

The input quantities for each vertex fit are ordinarily PANG-calculated quantities with the following exceptions. Often an event type by its nature is a two vertex event, e.g. a two-prong plus a V^0, in which case the V decay is fitted first, and the fitted information on the neutral replaces the original PANG information in fitting the primary interaction vertex. Sometimes a secondary interacts or decays in the chamber (connected event); the second vertex is then fitted first and the resulting data on the secondary is used for the primary vertex. If one of the secondaries stops, momentum from range measurement is used instead of curvature. Finally as the beam momentum is known much more accurately from $K\mu_2$ study (see Appendix C) than from the curvature measurement of the track in PANG, the two values are weighted by the inverse of the square of their errors and then averaged.

This procedure is known as beam averaging and amounts essentially to the substitution of the nominal beam momentum for the measured value, since the former is known to a much better accuracy.

As mentioned previously, most of the event types are ambiguous, i. e. they allow for more than one interpretation. Each one of the hypotheses is then tried in turn and the fitted quantities are then output for each. Frequently the kinematics of two hypotheses are similar enough so that they both give a satisfactory fit. The treatment that was followed for these ambiguities of necessity depends on the specific interaction and will be more appropriately discussed in the following section. We define the satisfactory fit to a given hypothesis as one that yields a χ^2 for that hypothesis which is smaller than the χ^2 corresponding to 1% probability of occurrence.

The KICK binary output tape in turn serves as input for the final step in the data-analysis process, i.e. program EXAMIN.[11] Here are computed quantities like polarizations, escape probabilities, center-of-mass (c. m.) quantities, etc., for each individual event. The calculations performed by EXAMIN by its very nature are much more specific to each event type than those of PANG and KICK and so are better discussed in the following section.

IV. TREATMENT OF EXPERIMENTAL DATA

In this section we shall discuss the experimental results with emphasis on the treatment of data. The following section will stress the theoretical interpretation of the results discussed below. The total cross sections for all hyperon producing channels are given in Table I. The errors quoted show both the purely statistical contributions as well as more realistic estimates; specific experimental uncertainties and ambiguities contributing to these errors will be discussed below. We now discuss in turn the $\Sigma\pi$, $\Sigma 2\pi$, and $\Sigma 3\pi$ reactions.

A. The $\Sigma^+\pi^-$, $\Sigma^-\pi^+$, and $\Sigma^0\pi^0$ Reactions

The experimental problems involved with the study of the first two reactions (charged Σ) are relatively minor when compared with those accompanying the study of the $\Sigma^0\pi^0$ system. Accordingly we discuss the charged-hyperon final states first.

1. Angular Distributions for $K^-+p \rightarrow \Sigma^\pm+\pi^\mp$.

Even though topologically $\Sigma^\pm\pi^\mp$ final states are indistinguishable in most cases from the final states containing additional one or two neutral pions, the kinematics are sufficiently different so that unambiguous isolation of two-body events is relatively straightforward. Specifically, out of some 171 events fitting $\Sigma^+\pi^-$ and $\Sigma^-\pi^+$, only 19 gave also a satisfactory fit to $\Sigma 2\pi$ interpretation. Of these 19, 10 had a higher χ^2 for the three-body interpretation than for the two-body interpretation (see Table II for data on χ^2 distributions of these 19 events). Because the latter is a much more overconstrained hypothesis (no particles are missing), it seems reasonable to assume that the ambiguous events are examples of the two-body reaction.

Table I. Cross sections for the hyperon producing interactions at 1.15 Bev/c.

Reactions	No. events observed	Cross section (mb)
$K^- + p \rightarrow \Sigma^- + \pi^+$	87	1.4 ± 0.2
$\rightarrow \Sigma^+ + \pi^-$	84	1.3 ± 0.2
$\rightarrow \Sigma^0 + \pi^0$	~50	1.2 ± 0.3 (± 0.45)[a]
$\rightarrow \Lambda + \pi^0$	~90	2.1 ± 0.2 (± 0.35)[a]
$\rightarrow \Sigma^+ + \pi^- + \pi^0$	57	1.0 ± 0.2 (± 0.3)[a]
$\rightarrow \Sigma^- + \pi^+ + \pi^0$	54	0.8 ± 0.2 (± 0.3)[a]
$\rightarrow \Sigma^0 + \pi^- + \pi^+$	27	1.0 ± 0.2[b] $\left(^{+0.4}_{-0.2}\right)$[a]
$\rightarrow \Lambda + \pi^+ + \pi^-$	141	3.1 ± 0.4[b]
$\rightarrow \Lambda + a\pi^0$, $\rightarrow \Sigma^0 + a\pi^0$ $\}$ $a \geq 2$	~65	1.5 ± 0.2 (± 0.35)[a]
$\rightarrow \Sigma^+ + \pi^- + \pi^0 + \pi^0$	13	0.18 ± 0.06 (± 0.12)[a]
$\rightarrow \Sigma^- + \pi^+ + \pi^0 + \pi^0$	9	0.12 ± 0.05 (± 0.08)[a]
$\rightarrow \Sigma^+ + \pi^- + \pi^+ + \pi^-$	19	0.19 ± 0.06
$\rightarrow \Sigma^- + \pi^+ + \pi^- + \pi^+$	13	0.12 ± 0.05
$\rightarrow \Lambda + \pi^+ + \pi^- + a\pi^0$, $\rightarrow \Sigma^0 + \pi^+ + \pi^- + a\pi^0$ $\}$ $a \geq 1$	39	1.1 ± 0.2[b]

[a] The first error quoted is purely statistical. The error in parentheses allows for biases and ambiguities in the analysis.

[b] The data for V2P reactions come from reference 5.

Table II. The χ^2 distributions for the 19 events giving satisfactory fit to both the $\Sigma\pi$ and the $\Sigma 2\pi$ hypotheses.

Interpretation	No. of constraints	Observed median	Expected median	Observed average	Expected average
$\Sigma^{\pm} \pi^{\mp}$	4	3.2	3.4	3.6	4.0
$\Sigma^{\pm} \pi^{\mp} \pi^0$	1	2.1	0.4	2.8	1.0

The procedure followed in fitting all charged Σ events consists first in using the data on the Σ track and its charged decay prong to obtain the fit to the decay vertex. Subsequently (by using the range-energy relationship for the Σ and the value of the magnetic field) the fitted variables of the Σ track are transformed to its production point. Fits are then attempted to the two- and three-body hypotheses. In most cases, the Σ track is so short that its momentum from curvature is unreliable; in this case no decay fit is possible. However, by using the measured quantities at the decay vertex along with the constraining equations of energy and momentum conservation, we can solve for the momentum of the Σ. This often results in a two-fold ambiguity, corresponding to forward or backward c.m. decay (fourfold for Σ^+ because of additional protonic decay mode). In these cases several production fits are made, one to each Σ momentum. For two-body events, the final fitted quantities are determined mainly by the angles of the tracks and π and K momenta, which are known ordinarily to a much higher precision that the Σ momentum obtained in the previously described manner. Thus, even for a widely different input Σ momentum, the final fitted quantities are very similar. For the sake of uniform procedure, the fit with the lowest χ^2 of the two or four fits was always used.

In obtaining the angular distributions of these two-body processes, we must be careful of the following experimental biases:

a. For small decay angles of the Σ, the likelihood that the event will be missed is very high. This is especially serious for the forward-produced Σ^+ hyperon decaying via the protonic mode, because then the angle in the laboratory (lab) system is always less than 9.5 deg. Furthermore, one sees then no sudden change of ionization, as in low-energy $\Sigma \rightarrow \pi$ decay. The event thus is very likely to be misclassified as two-prong with a small-angle proton scatter, or (if Σ^+ is short) two-prong with turbulence close to the vertex.

b. Short Σ hyperons tend to be missed by scanners more often than the longer ones. This is a bias against backward-produced

Σ hyperons. As an example, the probability that a backward-produced Σ^+ will decay in the first millimeter is ~30%. Thus this can be a serious bias if not corrected for.

c. At this energy, the escape probability becomes significant, as a forward produced Σ^- has a mean path length of ~6 cm, a relatively large distance in a 15-in. chamber.

For a bias-free distribution, the following requirements were imposed on all events:

a. The projected decay angle between the Σ and its charged decay product must be more than 10 deg in at least one of the four views. This requirement was sufficient insofar as all events were inspected for kinks in all four views during sketching.

b. The Σ must be at least 4 mm long.

c. The Σ must be produced and decay inside a specified fiducial volume. This more stringent fiducial volume was somewhat different from the one used in sketching insofar as it was defined in terms of volume rather than projected area. However, it was contained entirely in the previous definition of the fiducial volume. An appropriate correction was made for this change in computing the path length (see Appendix A).

All the events were then processed through an EXAMIN program which checked to see that all these conditions were satisfied (if they were not, the event was rejected) and computed the probability that this given physical configuration would meet all these requirements. The final probability of detecting an event with a given physical configuration is given by:

$$P\,(\text{detection}) = [\,P(3) - P(1)\,]\,P(2),$$

where $P(3)$ is the probability of decay within the fiducial volume, $P(1)$ is the probability of decay in the first 4 mm, and $P(2)$ is the probability that the largest projected decay angle be greater than 10 deg. Probabilities $P(3)$ and $P(2)$ were calculated by numerical integration over

(a) the azimuthal angle of the Σ around the beam track, and (b) the longitudinal position of the interaction point along the beam track. In addition, for P(2) integration was performed over (c) polar and azimuthal decay angles of the Σ. Isotropic decay was assumed, because even large up-down asymmetry would not affect the result.
The quantities kept constant were the angle that the Σ made with the beam track, the Σ momentum, and the lateral position of the beam track. This took account of the actual distribution of the beam particles along a lateral direction.

Each event satisfying all three of the criteria that were imposed to assure a bias-free distribution was then weighted by 1/P (detection). The statistical error associated then with each histogram interval is the square root of the sum of the squares of the weights.

This method of treating biases is satisfactory as long as there are no physical states that have very low probability of detection, since then any one of these low-detection-efficiency (highly weighted) events can significantly alter the shape of the histogram. This is true of forward-produced Σ^+ hyperons decaying by the protonic mode, because these will give a projected decay angle ordinarily smaller than 10 deg. For this reason, only pionic decay angles were used for the forward part of the histogram for Σ^+ production, and all the numbers in this region were multiplied by 2 to take account of this fact (as the rates of two decay modes of Σ^+ are experimentally known to be equal). As a check we can compare the weighted frequencies of the two decay modes for backward Σ^+ hyperons. The numbers are 39.0 ± 8.8 for proton decay and 30.2 ± 7.2 for the π decay mode, in reasonable agreement with the expected 1:1 ratio. After the removal of the forward produced Σ^+ hyperons which decay into protons, the weights run from about 1.25 to 2.5, and our method of correcting biases is quite satisfactory.

The angular distribution histograms for the $\Sigma^+\pi^-$ and $\Sigma^-\pi^+$ reactions are shown in Fig. 2. The ordinate is the sum of the weights for each interval. The errors are statisical only, but they should be quite realistic as there do not appear to be any unaccounted-for experimental uncertainties. Because of the method used to correct for

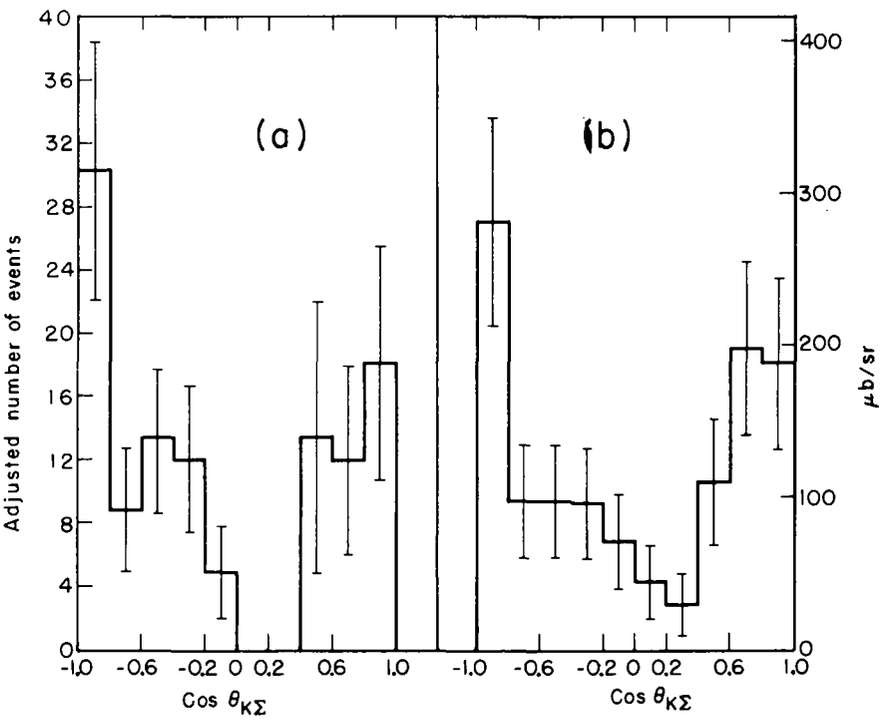

Fig. 2. Angular distribution of $\Sigma^{\pm}$ in the K^-p c.m. system for the reactions (a) $K^- + p \rightarrow \Sigma^+ + \pi^-$ and (b) $K^- + p \rightarrow \Sigma^- + \pi^+$.

scanning biases, the weighted number of events depends on the Σ lifetime used in calculating the corrections. However, only the extreme backward interval is very sensitive to the lifetime of the hyperon. Even in this worst case, the present uncertainty on the lifetimes of Σ^+ and Σ^- contribute an additional error of less than 10%, which is small compared with the statistical error.

2. Separation and Angular Distribution for Single-V Events

We discuss next the $\Sigma^0\pi^0$ events. Topologically they consist of a disappearance of a beam track (zero-prong) associated with a V. The reactions that can give this configuration are quite numerous, and a complete separation is impossible. The possibilities that must be considered are:

$$
\begin{aligned}
K^- + p &\rightarrow \Lambda + \pi^0 \\
&\rightarrow \Sigma^0 + \pi^0 \\
&\rightarrow \left.\begin{array}{l} \Lambda + a\pi^0 \\ \Sigma^0 \quad a\pi^0 \end{array}\right\} a \geq 2 \\
&\rightarrow \bar{K}^0 + n \\
&\rightarrow \bar{K}^0 + n + \pi^0 .
\end{aligned}
$$

For the last two reactions the V is due to a $\bar{K}^0$ decay rather than a Λ. This coupled with some restrictions on the production vertex--i.e. for every angle of $\bar{K}^0$ emission there is a maximum momentum kinematically possible--and the fact that ionization of the tracks is sometimes helpful in distinguishing between the decay proton of the Λ and decay π^+ of the $\bar{K}^0$ allows us to separate these events out relatively easily. The subsequent discussion will be restricted accordingly to Λ and Σ^0 events.

The fitting of the Λ (as opposed to $\bar{K}^0$) part of the single-V event type is as follows: first, a fit is made to the decay hypothesis. Then, if a satisfactory χ^2 is obtained for the Λ decay interpretation, $K^- + p \rightarrow \Lambda + \pi^0$ production is attempted using the fitted quantities. This is the only interpretation constrained enough that a fit can be made.

The difficulty associated with determining the rates for different reactions--a process possible only on a statistical basis because

one cannot assign a definite interpretation to each event--is illustrated in Table III. For a given beam momentum each reaction has a certain range of c.m. kinetic energies available to it. The extreme values of each spectrum are listed in Table III. In addition there is a smearing of about ±3 Mev because of a beam momentum spread of ~±20 Mev/c. We know that the $\Lambda\pi^0$ spectrum is a line and the $\Sigma^0\pi^0$ spectrum must be flat between its two limits (because $\Sigma^0 \rightarrow \Lambda + \gamma$ is the decay of spin-1/2 particle). To see this, we recall that spin-1/2 particles must decay isotropically in their own rest frame if parity is conserved, as in $\Sigma^0 \rightarrow \Lambda + \gamma$ decay. Furthermore, T_Λ in the K^-p c.m. system is linearly related to $\cos\theta_{\Lambda\Sigma}$ in the Σ^0 rest frame; so the T_Λ spectrum must be flat. However, we do not know anything about the expected shape of spectra of other reactions. One possibility is the assumption that phase-space distribution is followed. We know, however, that phase space plays almost no role in determining the $\Lambda\pi^+\pi^-$ spectrum[5] and the $\Sigma^\pm\pi^\mp\pi^+\pi^-$ spectrum (see discussion of $\Sigma^\mp + \pi^\pm + \pi^+ + \pi^-$ events in Section V C). Furthermore, the relative rates of different reactions are unknown, so even if the hyperon-energy spectra were known for each reaction, the composite energy spectrum would still be uncertain. Finally, the typical errors on the c.m. kinetic energy of the Λ after fitting its decay, due to both the measurement errors and the uncertainty in the exact velocity of the K^-p c.m. system because of the finite beam-momentum spread are anywhere from 3 to 15 Mev. Thus we can see that aside from any theoretical uncertainties in the spectra, they all merge together due to experimental errors.

In analyzing the single V events, we must correct for both escape of the Λ from the chamber before decay and also the immediate decay of the Λ. If the Λ decayed immediately, it would be misclassified as two-prong. We used here a similar procedure to that for charged Σ hyperons, computing for each event the probability that it would decay inside the fiducial volume minus the probability that it would decay in the first 4 mm. The former was calculated in the same manner as P(3) for the charged Σ reactions. Each event was then

Table III. Kinematical limits on Λ kinetic energy in $K^- p$ c.m. system for different single-V reactions.[a, b]

Final State	$T_{\Lambda\ min}$(Mev)	$T_{\Lambda\ max}$(Mev)
$\Lambda\pi^0$	145.3	145.3
$\Sigma^0\pi^0$	78.2	144.9
$\Lambda\pi^0\pi^0$	0	130.6
$\Sigma^0\pi^0\pi^0$	0	128.8
$\Lambda\pi^0\pi^0\pi^0$	0	106.2
$\Sigma^0\pi^0\pi^0\pi^0$	0	101.7

[a] The values quoted are for the nominal beam momentum of 1150 Mev/c ($E_{c.m.}$ = 1863 Mev).

[b] There is an additional spread of about ±3 Mev due to the finite momentum spread of the beam of ±21 Mev/c.

weighted by the inverse of this difference, the weights running from about 1.2 to 1.8. Furthermore, the EXAMIN program computed the c.m. kinetic energy and its error for each event, as well as the c.m. angle at which the Λ was emitted. The nominal beam momentum was used to determine the velocity of the center of mass in each case. The resultant kinetic-energy spectrum is shown in Fig. 3. A small number of events in the low-energy region was subtracted to allow for the small contamination of pion-produced associated productions. The size of this correction was obtained by using the number of observed double-V associated productions that satisfied the beam conditions.

We discuss next the procedure for obtaining an estimate of cross sections and angular distributions for $\Sigma^0\pi^0$, $\Lambda\pi^0$, and three-and four-body reactions. One must point out that χ^2 for the $K^- + p \rightarrow \Lambda + \pi^0$ hypothesis is not a very satisfactory criterion in separating $\Lambda\pi^0$ from $\Sigma^0\pi^0$ events. Using it as a criterion for deciding the probability that a given event is a $\Lambda\pi^0$ results in a bias towards a forward-peaked $\Lambda\pi^0$ angular distribution. Similarly, if we use for our sample of $\Sigma^0\pi^0$ events only those in the appropriate energy range which give a bad χ^2 for the $\Lambda\pi^0$ interpretation, a $\Sigma^0\pi^0$ angular distribution results that is biased towards the backward direction. This is because forward-produced Σ^0 hyperons decay into Λ hyperons that are very energetic in the laboratory, and thus the measurements are relatively poor and the resulting errors quite large. In other words a considerable number of forward-produced Σ hyperons give a quite good χ^2 for the $\Lambda\pi^0$ interpretation. On the other hand, backward-produced Σ^0 hyperons tend to give Λ hyperons that are slow in the laboratory, and the resulting fit is very precise (especially if the proton stops; this happens quite often for this configuration). Therefore only a very small fraction of backward-produced Σ^0 hyperons gives a good fit to the $\Lambda\pi^0$ interpretation.

To avoid this difficulty, we determine the total cross section and the angular distribution for $\Sigma^0\pi^0$ events by limiting ourselves to the events with kinetic energy T_Λ lying between 78.2 and 122.7 Mev, i.e. only the lower two-thirds of the $\Sigma^0\pi^0$ spectrum. This means that we are limiting ourselves to those events where the $\Sigma^0 \rightarrow \Lambda$ decay angle in the Σ^0 rest frame satisfies $-1.0 \leqslant \cos\theta_{\Sigma^0\Lambda} \leqslant 0.33$. This in no way

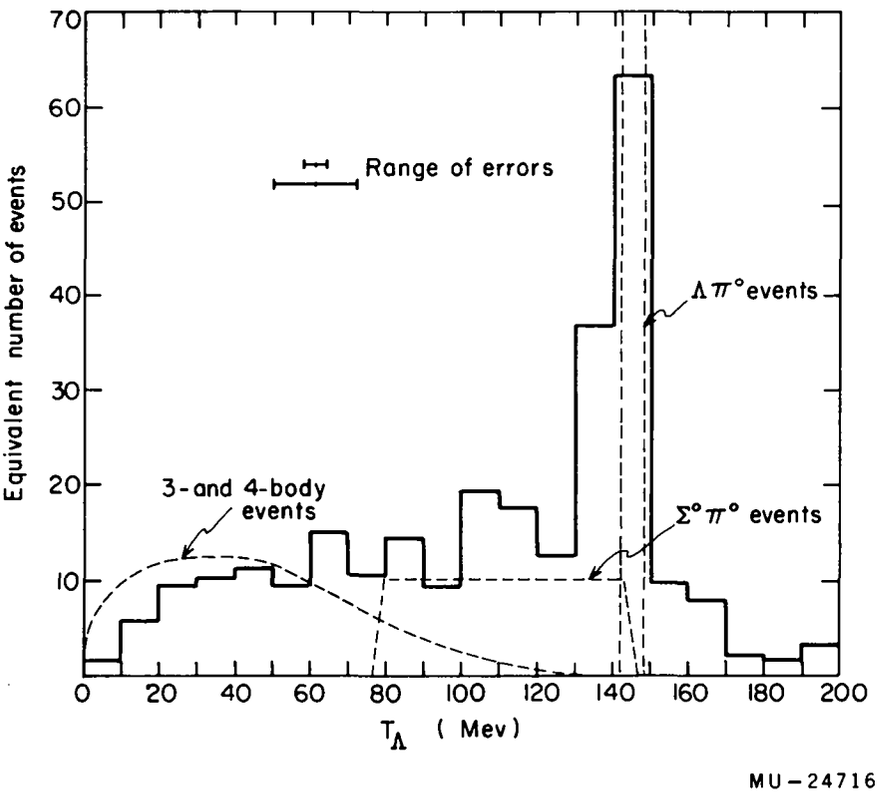

Fig. 3. Kinetic energy spectrum of Λ's in the K^-p_0 c.m. system. The dashed curves are the spectra of $\Lambda\pi^0$, $\Sigma^0\pi^0$, and many-body reactions normalized to the observed cross sections. The $\Lambda\pi^0$ peak should be about three times as high as indicated. Only the spread due to the finite beam width of ±20 Mev/c is folded in. The curve for many-body events was drawn to reproduce the Λ spectrum of V^0 two-prong events. The errors indicated are median values for the better measured and worse measured half of the events.

biases our sample, as the decay is completely isotropic and uncorrelated with the production process. Furthermore the chances that a $\Lambda\pi^0$ event would be so mismeasured as to give T_Λ in this interval are very small. The extent of this $\Lambda\pi^0$ contamination can be estimated by looking at the number of events sufficiently far away on the other side of the line spectrum at 145.3 Mev, i.e. with $T_\Lambda > 168$ Mev. It seems that it is reasonably safe to assume that no more than one $\Lambda\pi^0$ event is included in our sample.

We assume therefore that the sample selected contains only $\Sigma^0\pi^0$ and three- and four-body events. However, it should be emphasized that this many-body contamination cannot give us a bias as can the $\Lambda^0\pi^0$ events, because now we have two canceling effects. Because of measurements errors, it is equally probable that events with $T_\Lambda < 78.2$ Mev lie above 78.2 Mev as it is that events with $T_\Lambda > 78.2$ Mev fall below that value. Since the density of events on both sides of the cutoff is roughly the same, the two effects will compensate each other. This is not true if we work close to the $\Lambda\pi^0$ spectrum, since there we have a line spectrum neighboring on the band spectrum, and accordingly density of events changes suddenly.

We obtain an estimate of the three- and four-body events in this region by looking at the shape of spectrum from the V^0 two-prong events and assuming that the T_Λ spectrum from three- and four-body single-V events is the same. Then by counting the number of V events with $T_\Lambda < 78.2$ Mev, we can calculate the number of many-body events in the band selected. Subtracting this number, and correcting for neutral decays of the Λ, as well as for the fact that we are not looking at the whole $\Sigma^0\pi^0$ spectrum, we finally get the total number of Σ^0 hyperons produced. The number of $\Lambda\pi^0$ events is obtained by subtracting the $\Sigma^0\pi^0$ and three- and four-body events from all single-V events observed. The actual calculations are shown in Appendix D.

It is necessary to emphasize the pitfalls associated with this procedure. First, the hyperon-energy spectra of individual three- and four-body reactions need not be the same when the associated pions are charged as when they are neutral because different combinations of isotopic spins are involved. Secondly, for the same reason the relative

total cross sections need not be the same for the neutral pion reactions as for the charged pion reactions. On the other hand, it must be stated hat since there seems to be no evidence for any sizable π-π interaction in the V^0 two-prong data--which would be the effect that would most violently change the hyperon energy spectrum--we may hope that regardless of details, the over-all spectra are reasonably similar. We feel, however, that the statistical errors on total cross sections and angular distributions should probably be increased by at least 50% to account for these uncertainties.

The angular distribution of the secondary Λ hyperons for the events in the 78.2-Mev $< T_\Lambda <$ 122.7-Mev energy band is shown in Fig. 4. These are believed to be mainly secondary Λ hyperons from the reaction $K^- + p \rightarrow \Sigma^0 + \pi^0$. At this energy the angular distribution of the Σ^0 is reproduced almost completely in the secondary Λ angular distribution; certainly the difference is much smaller than the statistical uncertainties. We must remember that roughly about one-third of these events are really three- and four-body events. The angular distribution of events with $T_\Lambda <$ 78.2 Mev is shown in Fig. 5. It seems reasonable to assume that this distribution for the three- and four-body reactions does not change drastically with the increasing energy of the hyperon, and thus the histogram in Fig. 5 might be a reasonably good estimate of the many-body contamination in Fig. 4. No subtraction was attempted because of the many uncertainties involved, but one might conclude that the angular distribution is somewhat sharper at the two ends than Fig. 4 indicates. Figure 6 shows the angular distribution of all events with $\chi^2 < 2.0$ for $\Lambda\pi^0$ interpretation. As mentioned previously, the actual $\Lambda\pi^0$ distribution will be more depopulated in the forward direction.

3. Polarization of Charged Σ and Single V Events.

We discuss next the study of polarizations of charged Σ hyperons and of Λ hyperons from the single-V events. In general the decay distribution of a spin-1/2 particle in its own rest frame is given by

$$I(\theta) = \frac{1 + \alpha P \cos\theta}{2} ,$$

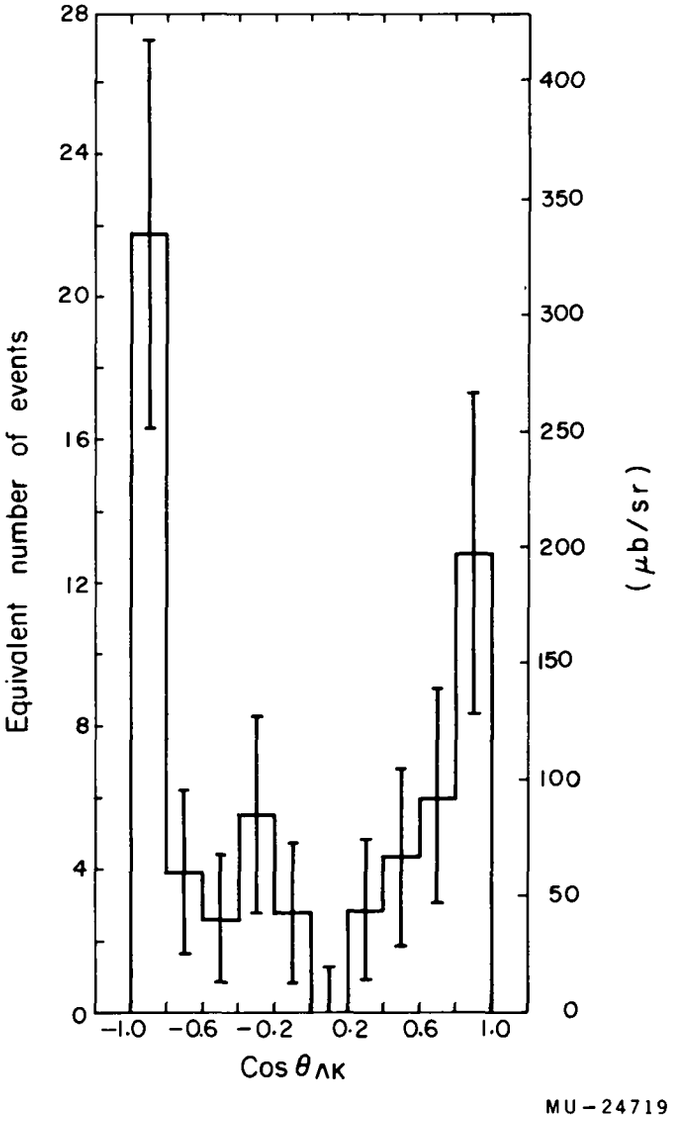

Fig. 4. Angular distribution of Λ's in the K^-p c.m. system. The events included are those with 78.2 Mev < T_Λ < 122.7 Mev., i.e. most likely $\Sigma^0\pi^0$ events. The right-hand scale is based on the total $\Sigma^0\pi^0$ cross section of 1.2 mb.

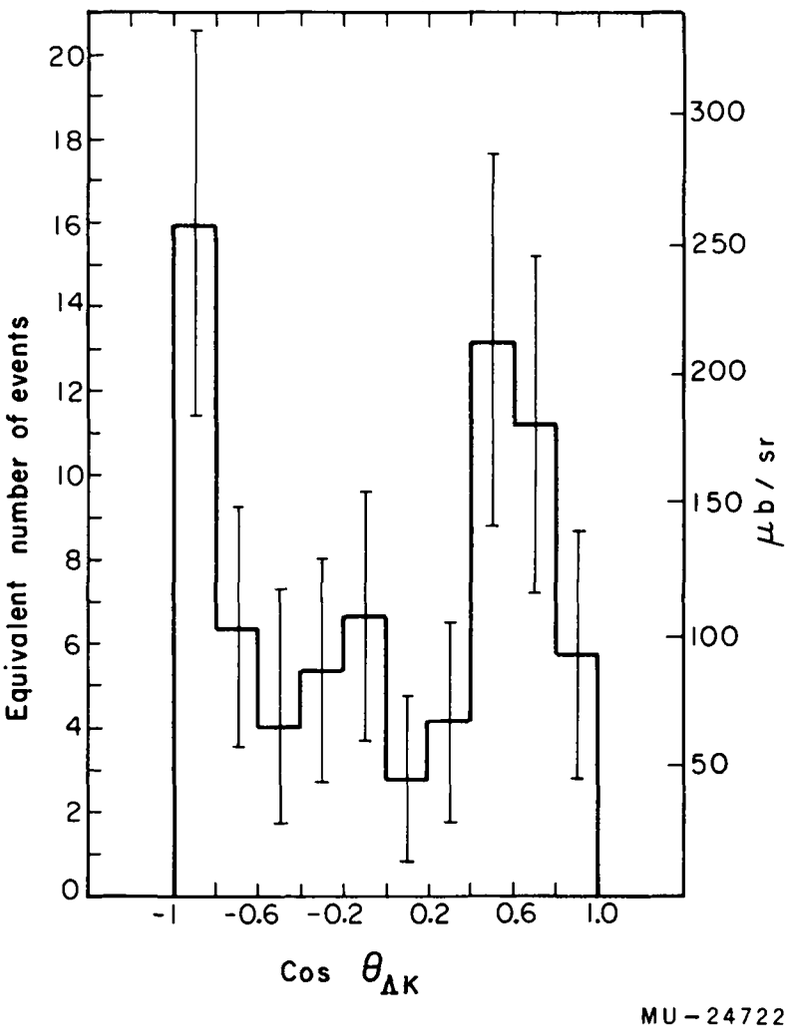

Fig. 5. Angular distribution of Λ's in the K^-p c.m. system. The events included are those with $T_\Lambda < 78.2$ Mev, i.e. most likely three- and four-body events. The right-hand scale is based on the total three- and four-body cross section of 1.5 mb.

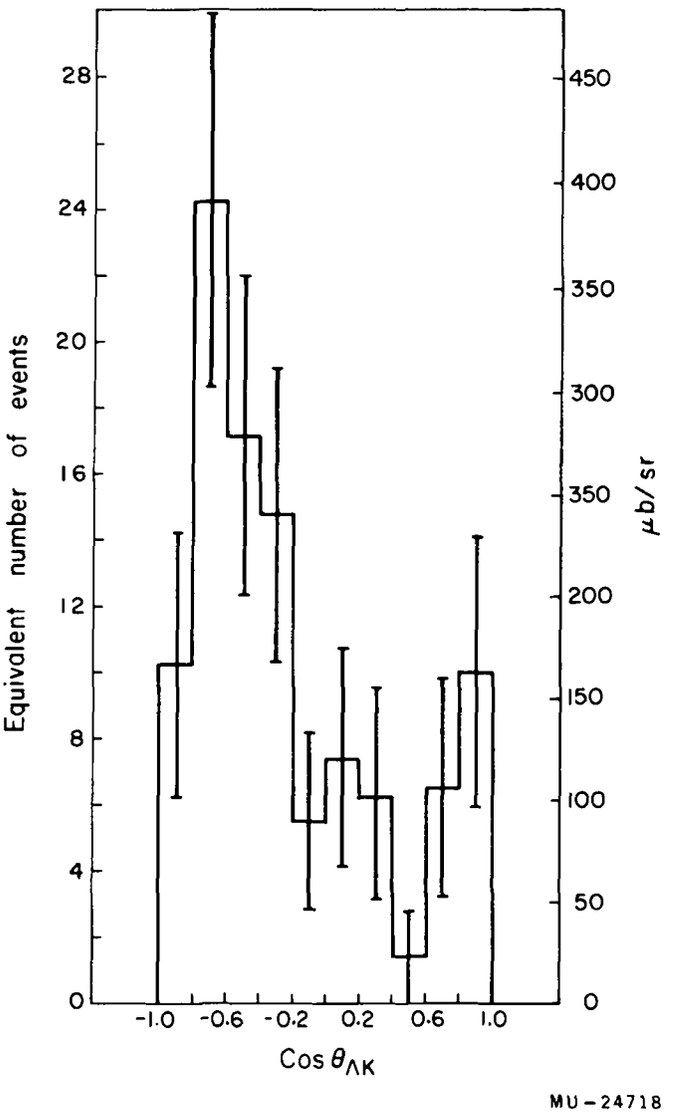

Fig. 6. Angular distribution of Λ's in the K^-p c.m. system. The events included are those giving $\chi^2 < 2.0$ to the $K^- + p \rightarrow \Lambda + \pi^0$ hypothesis. The right-hand scale is based on the total $\Lambda\pi^0$ cross section. The number of forward-produced Λ's is probably overestimated (see text for the discussion of this point).

where α is the decay-asymmetry parameter, $|\alpha| \leq 1$, P is the polarization of the hyperon, depending on the production angle and also obeying $|P| \leq 1$, and $\cos\theta$ is the angle made by the decay product with the direction of polarization. More specifically, since the polarization must be along a direction normal to the production plane, we define

$$\cos\theta = \frac{\vec{P}_N \cdot (\vec{P}_K \times \vec{P}_Y)}{|\vec{P}_K \times \vec{P}_Y| p_N},$$

where $\vec{P}_K$, $\vec{P}_Y$, and $\vec{P}_N$ are momenta of the incident K^-, the visible hyperon, and the decay nucleon, respectively, either in the laboratory or K^-p c.m. system; p_N is the magnitude of the momentum of the nucleon in the hyperon rest frame.

For the processes

$$\left.\begin{aligned} K^- + p &\rightarrow \Sigma^0 + \pi^0 \\ &\rightarrow \Lambda + n\pi^0 \\ &\rightarrow \Sigma^0 + n\pi^0 \end{aligned}\right\} \; n \geq 2,$$

the maximum polarization may exist along directions other than normal to the plane defined by $\vec{P}_K$ and $\vec{P}_\Lambda$. However, as the other particles are invisible, we are restricted of necessity to this plane.

The values of $\alpha\bar{P}$ for all reactions in question are listed in Table IV. $\alpha\bar{P}$ is defined by the expression

$$\alpha\bar{P} = \frac{3}{N} \sum_i \cos\theta_i \pm \sqrt{\frac{3-(\alpha\bar{P})^2}{N}} \; .$$

The expression for the uncertainty in $\alpha\bar{P}$ is precise only if the polarization remains the same for all production angles. We know that this is not true, because the polarization must vanish as $\sin\theta$ for forward and backward production directions. However its behavior off the beam axis will be very sensitive to the partial waves that participate in the production process and so cannot be predicted exactly. As the data are

Table IV. Observed values of $\alpha\bar{P}$

Production Channel	Hyperon decay mode	$\alpha\bar{P}$
$K^- + p \rightarrow \Sigma^+ + \pi^-$	$\Sigma^+ \rightarrow \pi^+ + n$	-0.15 ± 0.27
$\rightarrow \Sigma^+ + \pi^-$	$\Sigma^+ \rightarrow p + \pi^0$	-1.02 ± 0.23
$\rightarrow \Sigma^- + \pi^+$	$\Sigma^- \rightarrow \pi^- + n$	0.20 ± 0.20
$\rightarrow \Lambda + \pi^0$	$\Lambda \rightarrow p + \pi^-$	0.09 ± 0.20
$\rightarrow \Sigma^0 + \pi^0$, $\Sigma^0 \rightarrow \Lambda + \gamma$	$\Lambda \rightarrow p + \pi^-$	0.25 ± 0.26
$\rightarrow \Lambda + a\pi^0$	$\Lambda \rightarrow p + \pi^-$	0.12 ± 0.26
$\rightarrow \Sigma^0 + a\pi^0$, $\Sigma^0 \rightarrow \Lambda + \gamma$ $\Big\}$ $a \geq 2$		

clearly insufficient for a partial wave analysis and since presence of D or F waves would not be surprising, no angle cutoff was imposed and all events were used in determining $\alpha\bar{P}$.

The results on the pionic decay modes of the Σ hyperons are consistent with the observed fact that α vanishes for these modes.[12] On the other hand, the protonic mode of Σ^+ for which α is approximately one exhibits a very large polarization. This distribution of $\cos\theta$ for the $K^- + p \rightarrow \Sigma^+ + \pi^-$, $\Sigma^+ \rightarrow p + \pi^0$ events is shown in Fig. 7. No statistically significant polarization is observed in the single V reactions.

With the limited number of events we have here, no detailed analysis is possible as to the extent to which scanning biases could affect these results. We feel, however, that no bias would seriously discriminate in favor of "up" vs "down" events or vice versa, and thus no serious systematic errors are present.

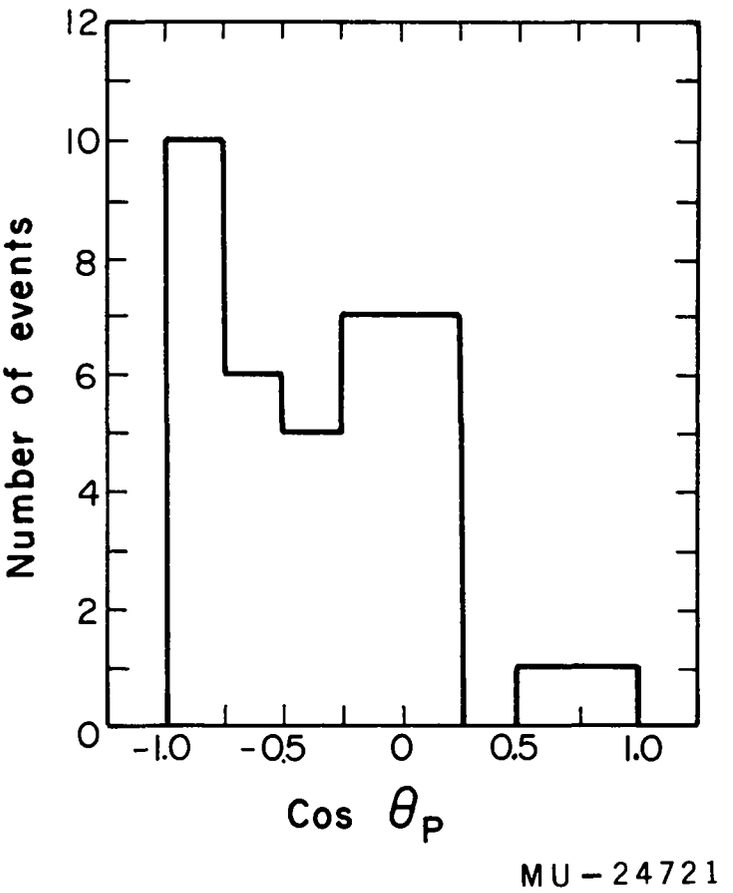

Fig. 7. Decay angular distribution of 37 Σ^+ from the reactions $K^- + p \rightarrow \Sigma^+ + \pi^-$, $\Sigma^+ \rightarrow p + \pi^0$.

B. The $\Sigma 2\pi$ Reactions

The final states to consider here are $\Sigma^+\pi^-\pi^0$, $\Sigma^-\pi^+\pi^0$, $\Sigma^0\pi^+\pi^-$, and $\Sigma^0\pi^0\pi^0$. The last reaction is completely indistinguishable from $\Lambda\pi^0\pi^0$ and the best we can do is to give an upper limit for the sum of these two processes. Therefore, we shall limit our discussion to the first three states. The main experimental difficulty in studying these reactions is the problem of resolving ambiguities: between the reactions in question and $\Sigma^\pm\pi^\mp\pi^0\pi^0$ for the charged hyperons, and between $\Sigma^0\pi^+\pi^-$ and $\Lambda\pi^+\pi^-$ for the Σ^0. The problem is much less severe in the former case; accordingly we shall treat it first.

1. $\Sigma^+\pi^-\pi^0$ and $\Sigma^-\pi^+\pi^0$ Final States

The main difficulty stems from the fact that one of the outgoing particles (π^0) is invisible and the Σ momentum is ordinarily known so poorly (even after it is determined by using the Σ decay) that the $\Sigma^\pm\pi^\mp\pi^0$ hypothesis is very weakly constrained. This will result in many $\Sigma^\pm\pi^\mp\pi^0\pi^0$ events giving a satisfactory χ^2 to the single π^0 interpretation. The $2\pi^0$ hypothesis has too many quantities missing to obtain a kinematical fit, so one is not able to compare χ^2 distributions for the two interpretations. In other words, if we accept as $\Sigma 2\pi$ events all those reactions giving a sufficiently low χ^2, we are faced with the probability of including in our sample a reasonable large number of $\Sigma 3\pi$ events.

It is necessary therefore to correct the total number of $\Sigma 2\pi$ events for this $\Sigma 3\pi$ contamination. Furthermore, the misidentified $\Sigma 3\pi$ events will bias the energy and invariant mass distribution because in general they will tend to cluster in a specific region of the spectra. Accordingly we have used the $\Sigma^\pm\pi^\mp\pi^+\pi^-$ events to determine which events should be removed from our $\Sigma^\pm\pi^\mp\pi^0$ distributions as being more likely $\Sigma^\pm\pi^\mp\pi^0\pi^0$ events. This study is described in detail in Appendix E. In the following section, all the discussed distributions of $\Sigma^\pm\pi^\mp\pi^0$ events have been corrected already for this contamination.

The question of experimental detection biases discussed above for $\Sigma\pi$ events is not so serious here, because there is now much less direct correlation between c.m. quantities, e.g. Q value of a given two-particle system, and the laboratory configuration with which the biases

are intimately connected. Accordingly, the figures below include all the events found, without any corrections. For the total cross-section determination, however, we have again applied the weighting procedure described previously.

2. The $\Sigma^0\pi^+\pi^-$ Final State

We discuss next the difficulties associated with the study of $\Sigma^0\pi^+\pi^-$ events. Topologically, these are a two-prong associated with a Λ. The fit proceeds by first treating Λ decay and then using the new Λ quantities as input for the production vertex, where a simultaneous fit is made to the Σ^0 production and a subsequent Σ^0 decay. The difficulty lies in the fact that at this energy the kinematics of $\Sigma^0\pi^+\pi^-$ are very much similar to those of $\Lambda\pi^+\pi^-$; more specifically, a $\Lambda\pi^+\pi^-$ reaction will very frequently give a reasonably low χ^2 for the $\Sigma^0\pi^+\pi^-$ interpretation, since the difference between the two is only a γ-ray of energy around 100 Mev. The pions being quite relativistic, the extra 100 Mev of momentum and energy can be quite easily absorbed by a small fractional change in the momenta of the pions. On the other hand, we would expect the opposite not to be true: it is not very easy for a real $\Sigma^0\pi^+\pi^-$ event to simulate a $\Lambda\pi^+\pi^-$ reaction. The reason is that if the γ does not lie along a direction of either one of two pions, real drastic changes in momenta and angles of all particles are necessary to arrive at final quantities satisfying the constraining equations of conservation of energy and momentum. A slightly more general way of saying this would be that the $\Lambda\pi^+\pi^-$ reaction being much more constrained (four-constraint fit since no particles are missing) is much harder to fit accidentally than a $\Sigma^0\pi^+\pi^-$ reaction (two-constraint, two-vertex fit, since we see neither the Σ^0 nor the γ-ray).

The detailed reasoning behind the arrived estimate of the actual number of $\Sigma^0\pi^+\pi^-$ events is given in Appendix E. It will suffice here to merely quote our conclusion, namely that roughly 1/3 of all $\Sigma^0\pi^+\pi^-$ events will give also a satisfactory fit to $\Lambda\pi^+\pi^-$ interpretation.

3. Representation of the Data

The energy distribution of the outgoing particles for three-body final states is best represented in terms of Dalitz plots.[13] If the correlation with the beam direction is of no interest, then all the other physical parameters of the reaction in the c.m. system are determined if we specify energies of two particles. The data can thus be conveniently exhibitied in two dimensions, each event represented by a point whose x and y coordinates are the kinetic energies of two final-state particles. Furthermore, for each total c.m. energy, a kinematic boundary exists within which all the events must lie. This representation of the data is known as a Dalitz plot, since it was first used by Dalitz to study energy distribution of pions in τ decay. It has the property that if the matrix element for the reaction is constant (i.e., population of final states is determined solely by phase space), then the region inside the kinematical limit is uniformly populated.[14]

The Dalitz plots for the three reactions discussed above are shown in Figs. 8, 9, and 10. Only unambiguous $\Sigma^0\pi^+\pi^-$ events have been plotted, and the events believed to be examples of $\Sigma^{\pm}\pi^{\mp}\pi^0\pi^0$ have been removed from the $\Sigma^{\pm}\pi^{\mp}\pi^0$ plots.

C. The $\Sigma 3\pi$ Events

The six possible charge states here are $\Sigma^{\pm}\pi^{\mp}\pi^+\pi^-$, $\Sigma^{\pm}\pi^{\mp}\pi^0\pi^0$, $\Sigma^0\pi^0\pi^+\pi^-$, and $\Sigma^0\pi^0\pi^0\pi^0$. Of these, only the first two are sufficiently overconstrained to permit a complete analysis. The next three reactions, in so far as they can be separated from the similar topological configurations can yield us some information, even though the complete reconstruction of the event is impossible. The last one is completely hopeless, being lost among other indistinguishable single V events, and as such will not be discussed any further.

The results of the study of these reactions lend themselves much better to presentation in the following section; accordingly, here we only comment briefly regarding the handling of these data.

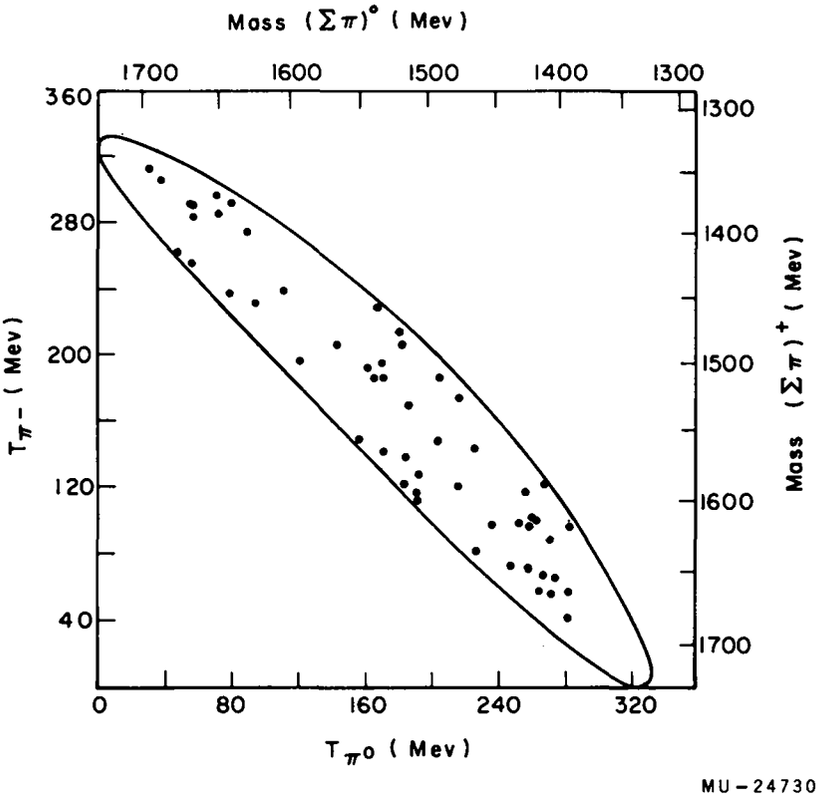

Fig. 8. Dalitz plot for the reaction $K^- + p \rightarrow \Sigma^+ + \pi^- + \pi^0$. The mass of the $(\Sigma-\pi)$ system is calculated on the basis of a nominal beam momentum of 1.15-Bev/c.

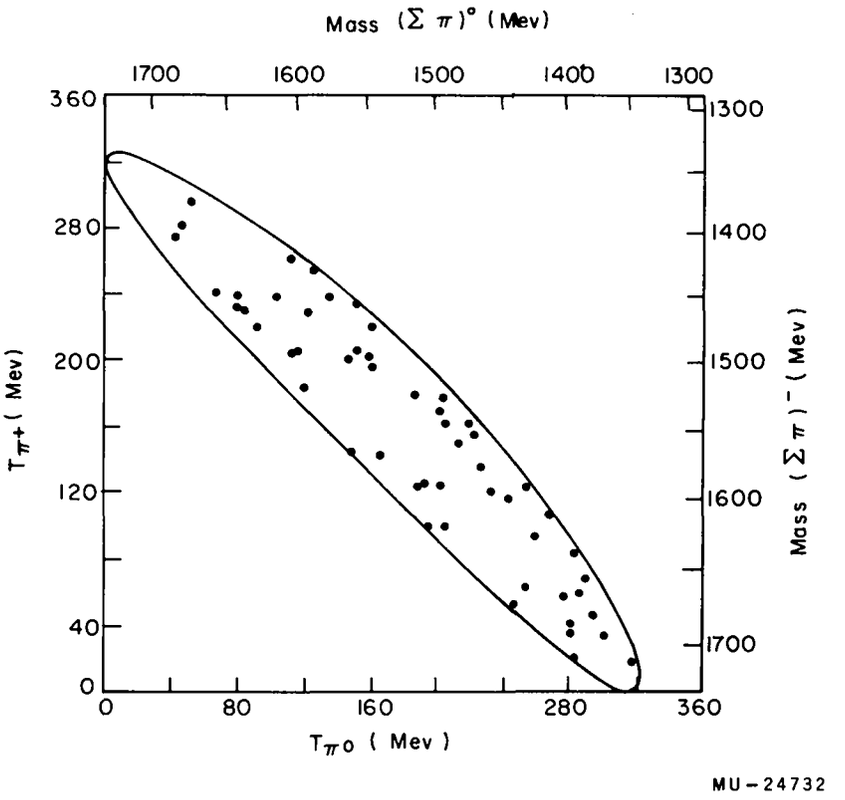

Fig. 9. Dalitz plot for the reaction $K^- + p \rightarrow \Sigma^- + \pi^+ + \pi^0$. The mass of the $(\Sigma-\pi)$ system is calculated on the basis of a nominal beam momentum of 1.150B ev/c.

1. The $\Sigma^{\pm}\pi^{\mp}\pi^{+}\pi^{-}$ Reactions

We start with these reactions since they are readily distinguishable and quite easy to analyze because no particles are missing. A typical example of a $\Sigma^{+}\pi^{-}\pi^{+}\pi^{-}$ event is shown in Fig. 11. The only ambiguity present here is the decay mode of Σ^{+}, which is either readily resolvable or else irrelevent to the main vertex fit. The only other interpretation for these topological configurations is the same reaction with an extra π^{0}, which however does not seem to be the case for any of these events. For the purpose of the distributions presented in Section VC, all the events found were used, because the question of experimental scanning biases is of relatively minor importance here for the same reason as for the three-body events. However, the total cross sections were again obtained by the method of weighting each event by the reciprocal of their detection efficiency to take account of any possible scanning biases.

2. The $\Sigma^{\pm}\pi^{\mp}\pi^{0}\pi^{0}$ Reactions

The difficulty associated with separating out these two reactions has been discussed above. We would emphasize here that only a small fraction of the events believed to be examples of $\Sigma^{\pm}\pi^{\mp}\pi^{0}\pi^{0}$ can be assigned with certainty to this interpretation. These are the events that do not fit $\Sigma^{\pm}\pi^{\mp}\pi^{0}$ hypothesis. The rest of them are more likely four-body processes rather than three-body because of arguments given in Appendix E. This conclusion, however, can only be made on statistical basis, and possible large $\Sigma^{\pm}\pi^{\mp}\pi^{0}$ contamination in this group cannot be excluded.

3. The $\Sigma^{0}\pi^{+}\pi^{-}\pi^{0}$ Reaction

For the $\Sigma^{0}\pi^{0}\pi^{+}\pi^{-}$ reaction, the situation is equally difficult. Topologically these are V^{0} two-prong events and as such can have many other interpretations, even after the V has been identified as a Λ. More specifically, the possible interpretations are

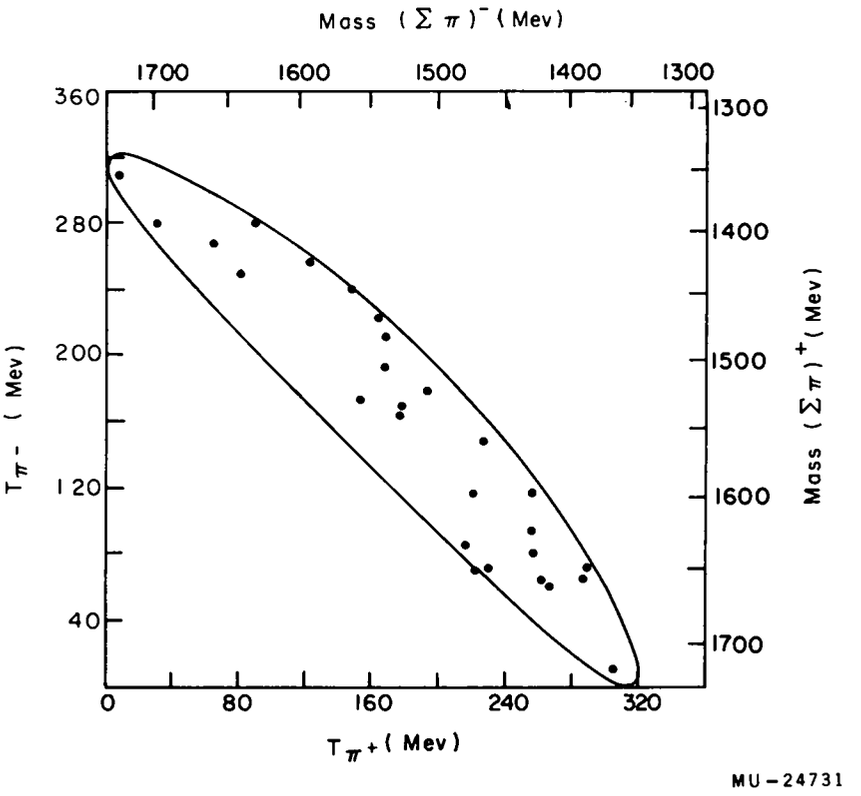

Fig. 10. Dalitz plot for the reaction $K^- + p \rightarrow \Sigma^0 + \pi^+ + \pi^-$. The mass of the $(\Sigma\text{-}\pi)$ system is calculated on the basis of a nominal beam momentum of 1.15-Bev/c.

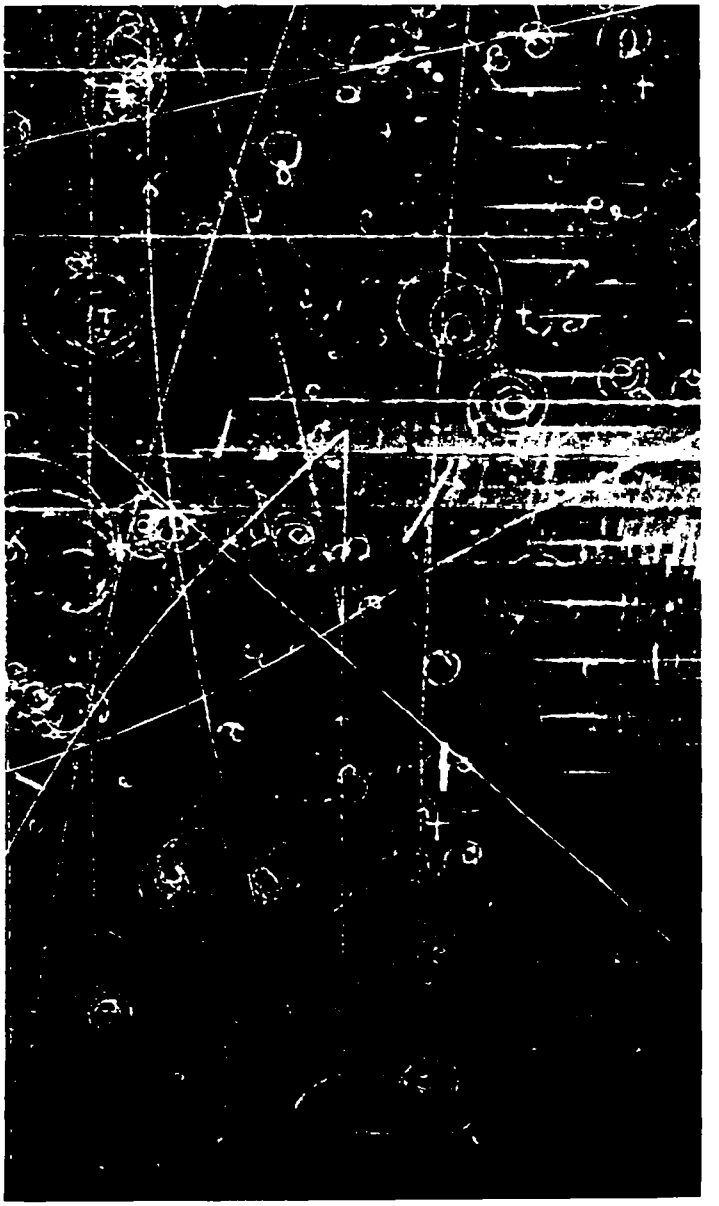

ZN-2937

Fig. 11. Typical example of the reaction $K^- + p \rightarrow \Sigma^+ + \pi^- + \pi^- + \pi^+$ followed by the decay $\Sigma^+ \rightarrow \pi^+ + n$.

$$
\begin{aligned}
K^- + p &\rightarrow \Lambda + \pi^+ + \pi^- \\
&\rightarrow \Sigma^0 + \pi^+ + \pi^- \\
&\rightarrow \Lambda + \pi^+ + \pi^- + \pi^0 \\
&\rightarrow \Sigma^0 + \pi^+ + \pi^- + \pi^0 \\
&\rightarrow \Lambda + \pi^+ + \pi^- + \pi^0 + \pi^0 \\
&\rightarrow \Sigma^0 + \pi^+ + \pi^- + \pi^0 + \pi^0,
\end{aligned}
$$

Furthermore, since the $\Sigma^0\pi^0\pi^+\pi^-$ interpretation is not overconstrained, no kinematical fit to it is possible.

However, the events that have very high a priori probability of being examples of this reaction can be separated out. First we eliminate all the events that give a sufficiently low χ^2 to the first two hypotheses because these are highly overconstrained and their kinematics are quite distinct from those of the $\Sigma^0\pi^0\pi^+\pi^-$ events. We are left then with 39 events that must be examples of the last four reactions. Only one case of $\Lambda\pi^+\pi^-\pi^+\pi^-$ and no cases of $\Sigma^\pm\pi^\mp\pi^+\pi^-\pi^0$ were found, so it seems safe to assume that the last two reactions would be quite rare. The $\Lambda\pi^+\pi^-\pi^0$ hypothesis is sufficiently constrained so that a kinematical fit is possible; however, a satisfactory χ^2 for this interpretation does not exclude the possibility that the event is an example of $\Sigma^0\pi^0\pi^+\pi^-$, since the kinematics of these two reactions are very similar. One would expect, however, that the $\Sigma 3\pi$ events would tend to give generally a higher χ^2 for the $\Lambda 3\pi$ interpretation than the genuine $\Lambda 3\pi$ events. Second, using the measured quantities of the two pions and the Λ data obtained from fitting its decay, we can calculate the missing mass of the reaction. This quantity should be always 135 Mev for $\Lambda 3\pi$ reactions, and greater than 135 Mev for $\Sigma 3\pi$ reactions. Thus, by imposing some sort of cutoff on these two variables, we would expect to obtain a group of events containing a high percentage of examples of $\Sigma^0\pi^0\pi^+\pi^-$ reaction.

V. DISCUSSION OF RESULTS

In this section we discuss our results in light of other strange-particle phenomena and the existing theories. We deal first with the reactions $K^- + p \rightarrow \Sigma + \pi$ and their possible connection with the recently observed T=0 resonance in the $\bar{K}N$ system. Next we discuss the relationship of the data to the recently discovered T=1 resonance in the Λ-π system and the evidence provided by the data for the existence of a T=0 resonance in the Σ-π system. Finally we say a few words about the influence that other Σ-π resonances might have on the interpretation of the data.

A. Discussion of the Reactions $K^- + p \rightarrow \Sigma + \pi$

We would like to point out first the evidence that exists for the predominance of production from the T=0 state. The three cross sections are equal within statistical errors (Table I), although the figure for the $\Sigma^0\pi^0$ reaction is not too well determined because of the previously discussed experimental difficulties. An even stronger evidence is afforded by the angular distributions of the three reactions. The distributions for the two charged Σ hyperons (Fig. 2) are strikingly similar; although not known as precisely, the neutral-hyperon distribution (Fig. 4) is the same within experimental uncertainties. Furthermore, if one looks at the structure inside the backward peak, one sees that in all three reactions it shows sharp peaking towards $\cos\theta_{K\Sigma} = -1$.

We must mention here that this is all circumstantial evidence. Because of large errors in the $\Sigma^0\pi^0$ cross section, a T=1 amplitude equal to about 80% of the T=0 amplitude cannot be excluded. This would require orthogonality of the two I-spin amplitudes to give equal cross sections for $\Sigma^+\pi^-$ and $\Sigma^-\pi^+$ reactions. Furthermore, (although here experimental uncertainties do not allow one to make too strong a statement), the similarity of charged and neutral Σ angular distribution would have to be a coincidence. Thus, even though it cannot be proven,

it seems likely that the $\Sigma\pi$ production at this energy is dominated by the T=0 amplitude.

We can interpret the data as still being dominated strongly by the T=0 resonance discovered recently by Cook et al.[15] in the 1-Bev/c region in the K^-p interaction.[16] It is surprising, though, that the T=1 $\Sigma\pi$ production is so strongly suppressed at this energy, especially since the $\Lambda\pi^0$ cross section seems not too small, i.e. ~ 2mb (Table I). If this T=0 resonance manifests itself so strongly in the Σ-π reactions, one might hope to obtain its spin by looking at the angular distributions involved. Our data clearly show odd powers of $\cos\theta$, characteristic of two or more partial-wave interference effects. This is not surprising since even if the resonant amplitude dominates completely right at the resonance, we would expect other partial waves to be relatively more important at this energy.

It is interesting to speculate along with Kerth and Pais[17] upon the existence of global-symmetry resonances in the pion-hyperon systems that are analogous of the pion-nucleon resonances at similar energies (the latter might also not be proper resonances[16]). More specifically, the question is posed whether the Cook et al. resonance is related to the third pion-nucleon resonance. If so, one might hope to find similarities between the pion-hyperon angular distributions and the pion-nucleon angular distributions at the resonant energies. Resolution of this problem obviously needs a detailed investigation of the angular distribution behavior at several energies in the resonance region. We merely would like to point out that our data seems to require higher powers than $\cos^2\theta$, and thus predominance of $J > 3/2$ seems not unreasonable.

Another interesting fact is the existence of complete polarization at this energy. The value of $\alpha_{\bar{p}}$ of -1.02 ± 0.23 (Table IV) for the protonic decay mode of Σ^+ was obtained by imposing no cutoff on the production angle. The polarization thus must persist up to very small production angles. As the polarization is an interference phenomenon between two partial waves, we see that several partial waves

contribute strongly to the production process, a fact indicated also by the angular distribution, as we remarked above. Furthermore, if many different partial waves interfere, we would expect on the basis of purely statistical arguments that the different interference terms would come in with different signs, and the over-all effect would vanish. Large polarization indicates this predominance of two (or at least only a few) partial waves.

If the three reactions indeed proceed mainly through the T=0 channel, then the Σ^0 and Σ^- hyperons should also be 100% polarized. Unfortunately, it is impossible to check Σ^- polarization, since α_{Σ^-} vanishes. However, Σ^0 polarization can be studied by looking at up-down asymmetry of the Λ resulting from Σ^0 decay. The sign of this asymmetry would then yield the relative sign of α_Λ vs α_{Σ^+}.

Unfortunately, in addition to the impossibility of isolating the pure sample of $\Sigma^0\pi^0$ events, two other difficulties exist. Firstly, the chain of decays $\Sigma^0 \to \Lambda + \gamma$, $\Lambda \to p + \pi^-$ washes out the polarization by a factor of three (in addition to changing the sign of polarization).[18] Secondly, we do not know precisely the Σ^0 production plane. This plane, however, will be approximated quite closely at our energy by the $K^-\Lambda$ plane because of the relatively small Q value of Σ^0 decay compared to Σ^0 momentum. From Table IV we see that the value of $\alpha\bar{p}$ of the $\Sigma^0\pi^0$ events selected by methods outlined in Section IVA,2 is 0.25 ± 0.26.

We feel that no conclusions can be drawn from this result either about the existence of Σ^0 polarization or relative $\alpha_\Lambda - \alpha_{\Sigma^+}$ sign. Even if we assume 100% Σ^0 polarization, no conclusive answer as to the sign of $\alpha_\Lambda - \alpha_{\Sigma^+}$ can be given, because our sample of $\Sigma^0\pi^0$ events contains roughly 30% many-body events. Even if these were unpolarized, they would reduce the polarization of the whole sample to about 0.25. A small polarization of the opposite sign in many-body events, which is not excluded by the data (Table IV), would lower the value considerably and make the experimental result consistent with both $\alpha_\Lambda/\alpha_{\Sigma^+}$ greater than or less than zero. A much more precise experiment is needed to resolve this question.

B. T=1 Resonance (Y_1^*)

The problem of correct interpretation of the $\Lambda\pi$ resonance is still unresolved. As yet there is no conclusive data to distinguish between the two explanations put forth, i.e. the global-symmetry interpretation[19] and the $\bar{K}N$ bound-state model.[20] We would like next to give a short background on these two ideas.

1. Global Symmetry Description of Y_1^*

The basis of global symmetry is equality of all pion-baryon couplings, an equality that is only broken by the weaker K couplings. Accordingly, as an analogue of the 3/3 resonance in the pion-nucleon system one expects the existence of a T=1 resonance in the pion-hyperon system. One can provide a simple argument for the mass and width of this resonance.[17] One considers the observed isotopic spin T as composed of two spins, I and K, in the manner $\vec{T}=\vec{I}+\vec{K}$, where I is the fundamental spin that specifies the state completely in the global-symmetry approximation (i.e., if there were no K couplings) and K is the isotopic spin due to the K couplings that break this symmetry. Λ and the three charge states of the Σ in this approximation are composed of components of the two doublets Y and Z, which are split by K coupling. Table V shows the I and K spin assignments of the strongly interacting particles.

We write a general phenomenological mass formula for nucleons and Σ and Λ hyperons:

$$M = m(K^2) + \Delta\, \vec{I}\cdot\vec{K},$$

where $m(K^2)$ is the general hyperon or nucleon mass depending only the K spin and Δ is the Σ-Λ mass difference. Then by analogy we can write the mass for the resonant states:

$$M = m(K^2) + \Delta\, \vec{I}\cdot\vec{K} + \mu + Q,$$

where μ is the pion mass and Q the resonant energy of the pion-nucleon system. For T=1, I=3/2, and K=1/2 we get about 1380 Mev for the mass of the resonance.

Table V. Assignments of K and I spin for elementary particles in the doubletapproximation

Particle	Global-symmetry description	Conventional description	T	T_z	I	I_z	K	K_z
	π^+	π^+		1		1		0
π	π^0	π^0	1	0	1	0	0	0
	π^-	π^-		-1		-1		0
	K^+	K^+		1/2		0		1/2
K			1/2		0		1/2	
	K^0	K^0		-1/2		0		-1/2
	p	p		1/2		1/2		0
N			1/2		1/2		0	
	n			-1/2		-1/2		0
	Y^+	Σ^+	1	1		1/2		1/2
Y					1/2		1/2	
	Y^0	$(\Sigma^0-\Lambda)/\sqrt{2}$	1, 0	0, 0		-1/2		1/2
	Z^0	$(\Sigma^0+\Lambda)/\sqrt{2}$	1, 0	0, 0		1/2		-1/2
Z					1/2		1/2	
	Z^-	Σ^-	1	-1		-1/2		-1/2
	Ξ^0	Ξ^0		1/2		1/2		0
Ξ			1/2		1/2		0	
	Ξ^-	Ξ^-		-1/2		-1/2		0

The width can be obtained from the corresponding width for the pion-nucleon system by scaling it down by the kinematical factor (due to different momenta involved in the two cases) and the isotopic-spin weight factor. The former is the product of available phase space times the centrifugal barrier-penetration factor. Since Y_1^* resonance in this interpretation must have spin $3/2$ and even Y_1^*-Λ parity (i.e., p-wave resonance) in analogy with pion-nucleon $3/3$ resonance, the kinematic factor is just $(P_\Lambda/P_N)^3$. As shown below, the $\Lambda\pi$ system has an isotopic-spin weight of $2/3$, and the contribution of the $\Sigma\pi$ decay to the width is negligible. Accordingly the isotopic-spin weight factor is $\sim 2/3$. The estimated width thus turns out to be 23 Mev.

The resonance must also be able to decay into the $\Sigma\pi$ system in the $T=1$ state. To obtain the relative rates, we write down the resonant state as a linear superposition of the $\Lambda\pi$ and $\Sigma\pi$ systems in the "real world":

$$Y_1^* = A \mid \Lambda\pi \rangle + B \mid \Sigma\pi \rangle$$

and of the $Y\pi$ and $Z\pi$ systems in the doublet approximation of the "global-symmetry world":

$$Y_1^* = C \mid Y\pi \rangle + D \mid Z\pi \rangle .$$

Considering now specifically Y_1^{*+} and imposing the restrictions of charge independence (i.e., in the first case we form the $T=1$ state, and in the second an $I=3/2$ state), we get

$$A(\Lambda\pi^+) + \frac{B}{\sqrt{2}}(\Sigma^+\pi^0 - \Sigma^0\pi^+) = C(\sqrt{1/3}Y^0\pi^+ + \sqrt{2/3}Y^+\pi^0) + D(Z^0\pi^+).$$

Substituting for Y and Z

$$Y^+ = \Sigma^+,$$

$$Y^0 = \frac{\Sigma^0 - \Lambda}{2},$$

and

$$Z^0 = \frac{\Sigma^0 + \Lambda}{2},$$

we obtain the result $A = -\sqrt{2}B$. The relative rates for the three states are then:

$$\Lambda\pi^+ : \Sigma^+\pi^0 : \Sigma^0\pi^+ = 4:1:1.$$

To obtain the observed decay rates from this isotopic-spin weight ratio, we must again compensate for the different momenta involved. Phase space gives us a factor of P_Σ/P_Λ, and the p-wave contributes $(P_\Sigma/P_\Lambda)^2$, giving us an over-all $(P_\Sigma/P_\Lambda)^3$ of 0.225. Thus the observed branching ratio R for a given charge state of the $\Sigma\pi$ system will be about 5%. The same argument can be reproduced fully for the other three charge states of the Y_1^*, with the same results. Furthermore, by charge independence, the rates for different charge states of the $\Sigma\pi$ system will be the same, i.e.:

$$\frac{Y^{*+} \to \Sigma^+ + \pi^0}{Y^{*+} \to \Sigma^0 + \pi^+} = \frac{Y^{*-} \to \Sigma^- + \pi^0}{Y^{+-} \to \Sigma^0 + \pi^-} = \frac{Y^{*0} \to \Sigma^+ + \pi^-}{Y^{*0} \to \Sigma^- + \pi^+} = 1.$$

2. The $\bar{K}N$ Bound-State Model Description of Y_1^*

We turn next to the ideas embodied in the "bound-state resonance" model. As a very thorough discussion of this subject has been given recently by Dalitz,[21] we limit ourselves to a brief summary of the main conclusions of his paper. Treating the $\bar{K}$-N and hyperon-pion interactions by means of the zero-range approximation, we find

that if the imaginary part of the scattering length, b, is small and the real part, a, large and negative, hen the $\bar{K}$-N wave function can be approximated by a bound state. If one neglects the pion-hyperon interaction, then the mass of this state M^* is given by

$$M^* = M_N + M_K - 1/(2\mu_K a^2),$$

where a is the real part of the scattering length and μ_K is the reduced mass of the $\bar{K}$-nucleon system. Furthermore the half width $\Gamma/2$ is given by $\Gamma/2 = b/\mu_K a^3$. Dalitz uses the data presented by Alvarez at Kiev[22] for a⁻ solution (which alone out of the four possible scattering-length solutions of Dalitz and Tuan[20] satisfies the above-mentioned conditions for the bound state in the T=1 channel) and obtains $M^* = 1382 \pm 20$ Mev and $\Gamma/2 \approx 18$ Mev.

Recently, a much more precise analysis of the old low-energy K^-p data has been performed by Humphrey and Ross.[23] They find that only two scattering-length solutions satisfy the data, and neither meets the above requirements for a pion-hyperon resonance in the T=1 channel below the K^-p threshold, i.e. large negative real part and small imaginary part of the T=1 scattering length (or at least the approximations made in deducing the existence of resonance are no longer valid with these solutions). We must point out here, however, that the Dalitz-Tuan theoretical arguments as well as the Humphrey-Ross analysis are based on zero-effective-range theory. The effects of nonzero effective ranges are being investigated by Ross and Shaw.[24] These could not only affect the fitted solutions, but also, as Ross and Shaw point out, even if the inclusion of nonzero effective ranges has little effect on data in physical regions, it could seriously affect the behavior of the pion-hyperon cross section below the K^-p threshold. Without a further theoretical treatment, we do not feel justified therefore in saying that the experimental data rules as a bound-state-model resonance.

The bound-state model being the S 1/2 state, the Y_1^* resonance must have spin one-half, and the Y_1^*-Λ relative parity is odd or

even depending on whether K-Λ parity is odd or even, respectively. The Σ-to-Λ-decay branching ratio of Y_1^* depends strongly on the experimental value of the Σ/Λ ratio in the I=1 channel at the K-N threshold R_t, on the relative Σ-Λ parities, and on the assumptions that one makes about the behavior of amplitudes for Σ and Λ production below threshold. Assuming that the centrifugal barrier-penetration factor dominates this behavior and calling the relative orbital momenta in the Σ and Λ channels ℓ_Σ and ℓ_Λ, we obtain for the Σ/Λ ratio (we include here both charges of the Σ) at the resonance R_r

$$R_r = R_t(q_{\Sigma r}/q_{\Sigma t})^{2\ell_\Sigma+1}/(q_{\Lambda r}/q_{\Lambda t})^{2\ell_\Lambda+1}$$

where $q_{\Sigma r}$ is the Σ momentum at resonance and $q_{\Sigma t}$ at the $\bar{K}N$ threshold. Using the recent value of 0.40 ± 0.03, for R_t,[23] we can obtain a value as low as 16% (i.e. 8% for each charge) by taking $\ell_\Sigma = 1$ and $\ell_\Lambda = 0$, i.e., opposite Σ-Λ parity. It should be pointed out that inclusion of effective ranges can significantly alter this branching ratio.

The present experimental values for Y_1^* mass and width are 1385 and 20 to 30 Mev, respectively.[25] The latter is uncertain because of Bose-statistics effects[26] in the $\Lambda\pi^+\pi^-$ events at low energy, as well as the conflicting results from the study of the $\theta_2 p$ interaction.[27] The spin and parity of Y_1^* are still unknown; it is clear thus that the existing data agree with global-symmetry prediction, and because of previously mentioned difficulties we cannot exclude the bound-state model. We may hope that analysis of $\Sigma 2\pi$ data will elucidate the proper interpretation of Y_1^*.

3 The $\Sigma 2\pi$ Experimental Results

Since we know the production rate of Y_1^{*+} and Y_1^{*-} from the study of the $\Lambda\pi^+\pi^-$ reaction,[5] we can obtain the decay branching ratio R of the resonance by looking at the mass distribution of the positively and negatively charged (Σ-π) systems in our $\Sigma 2\pi$ reactions. On the three Dalitz plots (Figs. 8, 9, and 10), a large Σ-Λ branching ratio

would exhibit itself as a bunching of events along $T_{\pi}+$ and $T_{\pi}-$ lines of about 280 Mev. We see that there is no evidence of any enhancement in this region, and so the branching ratio must be quite low.

To obtain a quantitative lower limit on this ratio, we combine the events in such a way as to be able to plot composite spectra of the $(\Sigma-\pi)$ systems in all three charge states (Figs. 12 and 13a). Now the Y_1^{*+} and Y_1^{*-} events would show up as events in the $(\Sigma\pi)^+$ and $(\Sigma\pi)^-$ plots (Fig. 12) around a mass value of 1385 Mev. For definiteness we take all the events with the mass in the 60-Mev band centered at 1385 Mev, assume that they are all Y_1^*, and compare them with the number of $\Lambda\pi^+\pi^-$ events with the $(\Lambda\pi^+)$ or $(\Lambda\pi^-)$ mass in the same band. This gives us an upper limit of 8% on the value R. This limit appears to be rather unrealistic, since there seems to be no peaking above the phase-space curve (see however Sec. VD, 2 for a further discussion of this point). The value R=0 certainly cannot be excluded by the data.

We should point out here that the difficulty (discussed in Appendix E and Sec. IVB, 1) associated with distinguishing the $\Sigma^{\pm}\pi^{\pm}\pi^0$ events from the $\Sigma^{\pm}\pi^{\pm}\pi^0\pi^0$ events does not affect this result because the mass of the $(\Sigma^{\pm}\pi^0)$ system is determined once one knows the c.m. momentum of the charged pion, which is ordinarily measured accurately enough so that the fit will not change the value significantly. For a $(\Sigma\pi)$ mass low enough to be included in this calculation, the energy of the pion must be quite high, well above the kinematical limit allowed by the four-body reaction. In other words the events that are hard to identify will fall in the region of high $T_{\pi}0$ and therefore necessarily low $T_{\pi}\pm$. As such, it does not make much difference whether they are classified as three- or four-body events for the purpose of the above calculation.

It must be admitted that the events of interest in this calculation are those most likely to give spurious fits to the $\Sigma^{\pm}\pi^{\mp}$ reactions, because these will have relatively high charged-pion energies (and therefore low neutral-pion energies). However, the 19 events that are ambiguous (see Table II) have a perfectly normal χ^2 distribution for the two-body hypotheses and poor χ^2 distribution for the three-body hypotheses. This

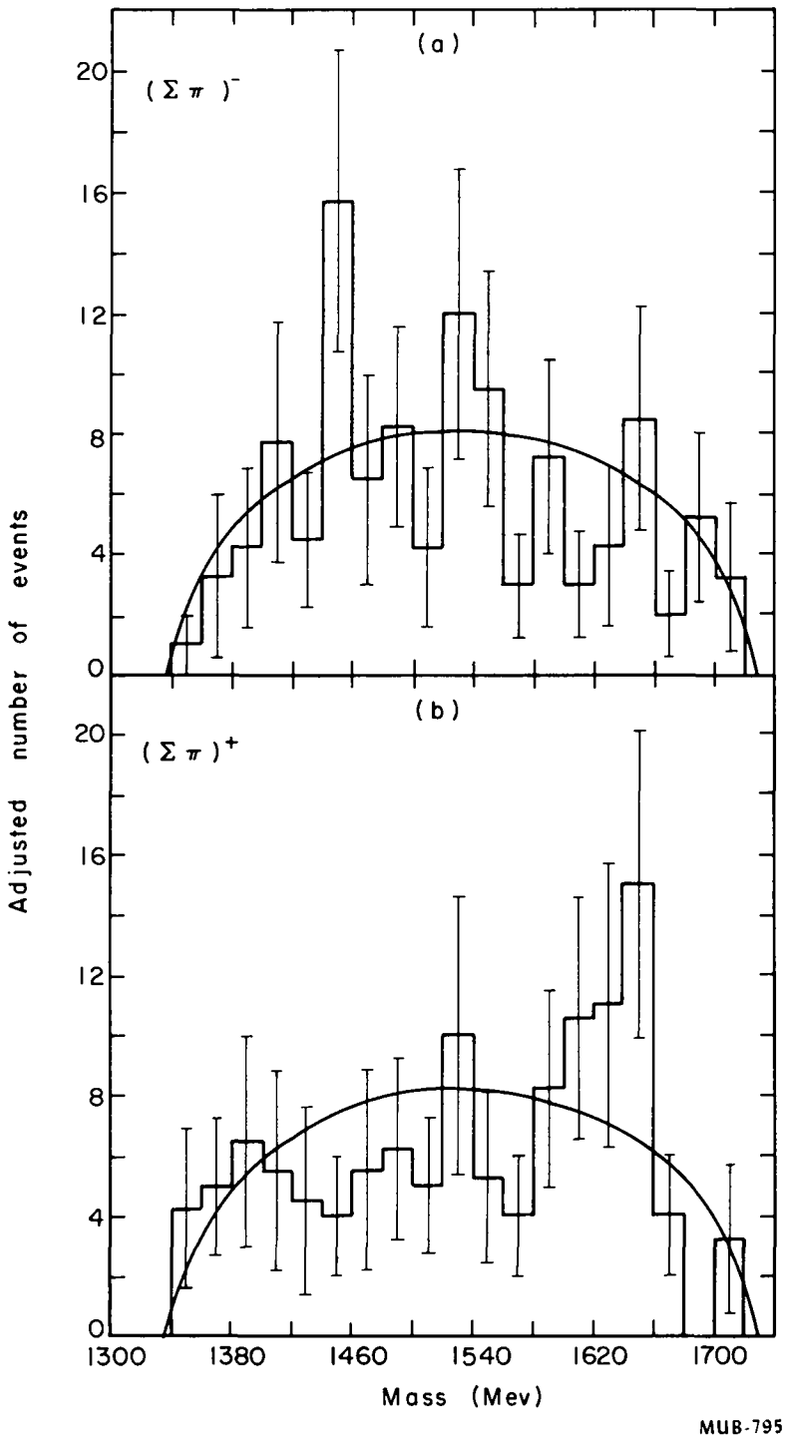

Fig. 12. Mass spectra of (a) $(\Sigma\pi)^-$ and (b) $(\Sigma\pi)^+$ systems from the reactions $K^- + p \rightarrow \Sigma^+\pi^-\pi^0$, and $\Sigma^0\pi^+\pi^-$. Each observed $\Sigma^0\pi^+\pi^-$ event has been given a weight of 2.25 to allow for the difficulties discussed in the text as well as the neutral decay mode of the Λ.

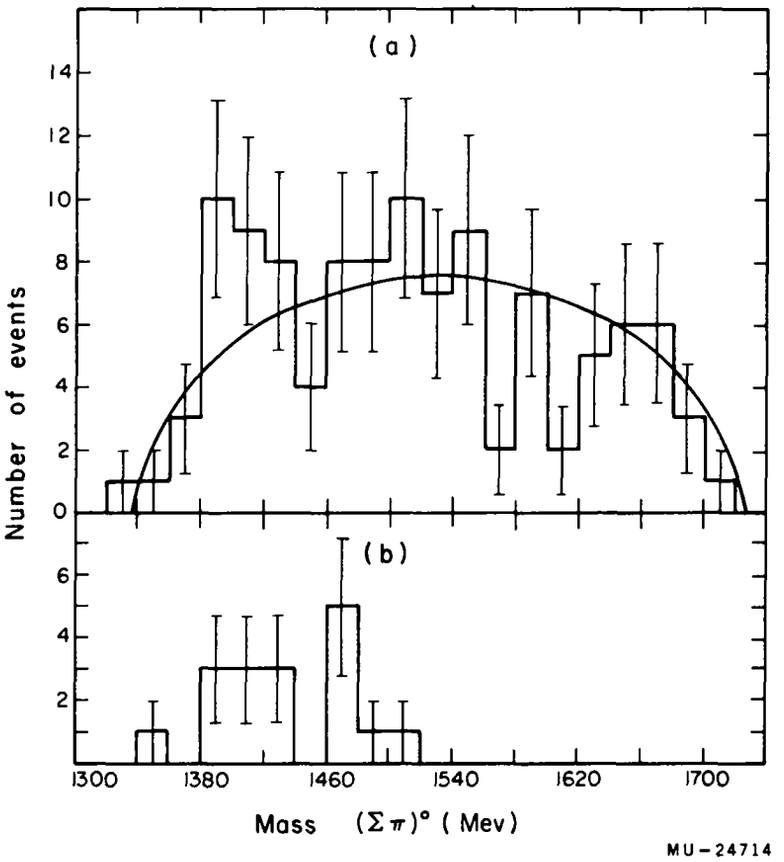

Fig. 13. (a) Mass spectra of the $(\Sigma\pi)^0$ system from the reactions $K^- + p \rightarrow \Sigma^+\pi^-\pi^0$, and $\Sigma^-\pi^+\pi^0$. Only events that are believed to be examples of the three-body final state are included.

(b) Mass spectra of the $(\Sigma^{\pm}\pi^{\mp})$ system from the events that are believed to be examples of $K^- + p \rightarrow \Sigma^{\pm} + \pi^{\mp} + \pi^0 + \pi^0$ but yet give a satisfactory fit to the $\Sigma^{\pm}\pi^{\mp}\pi^0$ hypothesis (see Appendix E for selection criterion). The mass values in the figure were obtained by using quantities resulting from the fit to the $\Sigma^{\pm}\pi^{\mp}\pi^0$ hypothesis.

coupled with the fact that a four-constraint fit is much more difficult to fit spuriously than a one-constraint fit leads us to conclude that probably no more than one or two of these events are indeed examples of the three-body reaction--certainly not enough to affect our conclusion.

It should be mentioned here that the observed average mass of the Y_1^* as observed through the Σ-π decay mode will not necessarily be identical to that obtained by looking at the Λ-π mode. This is due to the difference in the two decay momenta; in other words a Y_1^* with a low mass will probably not decay into a $\Sigma\pi$ system because of the smaller phase space and (or) centrifugal-barrier penetration factor. Thus we would expect to observe that the mass of Y_1^* as observed through the $\Sigma\pi$ decay mode would be displaced to higher energies. However, as this is a strong function of the shape of the resonance curve and the spin of the excited state (neither one of which is known) and is not a very large effect, for simplicity we have taken 1385 Mev as the central value for both decay modes.

The low Σ/Λ branching ratio of Y_1^* unfortunately does not allow us to distinguish between the two theoretical interpretations of the resonance. The limit is still above the prediction of global symmetry, and by taking effective ranges into account in the $\bar{K}N$ bound-state model, we can reduce R to below the observed value. Bastien et al.[28] have recently obtained a result also consistent with R=0 by studying $\Sigma 2\pi$ production by 760-and 850-Mev/c K^- mesons.

C. The T=0 Resonance (Y_0^*)

We discuss next the evidence presented by the data regarding the existence of a T=0 resonance in the (Σ-π) system. At the beginning, we must sound a word of caution. The conclusions below are drawn on the basis of some 40 events, and as such a statistical fluctuation cannot be excluded. Accordingly, we admit that the data is not conclusive in establishing the existence of a T=0 resonance. We present it to show that the data can be explained reasonably well in the framework of this resonance, and at the same time to outline the method of analysis to be

followed when more events are available. We must also mention that Bastien et al. have recently reported some evidence supporting the T=0 resonance hypothesis.[28] Recently Shult and Capps have invoked a T=0 resonance to explain the observed branching ratios for K^- interactions in deuterium.[29]

1. The $\Sigma^{\pm}\pi^{\mp}\pi^{+}\pi^{-}$ Events

We start with the discussion of the $\Sigma^{\pm}\pi^{\mp}\pi^{+}\pi^{-}$ events in so far as these are the highest quality data from the experimental point of view. To investigate the possibility of strong final-state interactions, we plot the mass spectra of all possible $(\Sigma\text{-}\pi)$ systems in these reactions. Thus for each event we obtain three mass values--two for the neutral and one for the doubly charged $(\Sigma\text{-}\pi)$ system. These two spectra are displayed in Fig. 14. It seems quite clear that the two histograms are significantly different. Furthermore, the doubly charged system shows no statistically significant departure from phase-space predictions, and the neutral system exhibits a bunching of events around 1405 Mev.

It is attractive to interpret the data in terms of a resonance in the $(\Sigma\text{-}\pi)$ system. To explore this possibility in more detail, one wishes to present the data in a form analogous to that used for study of the Y_1^* resonance in the $K^- + p \rightarrow \Lambda + \pi^+\pi^-$ reaction, i.e. Dalitz plots. To do this, we isolate the system consisting of the Σ hyperon and the two pions of unlike charge (that is, of charge different from that of the Σ) and treat them as a three-body final state. In essence this amounts to the statement that the third pion is relatively "inert" and does not affect the strong final-state interaction between the Σ hyperon and the other two pions, an assumption that seems to be justified at least to a certain extent by the phase-space-like distribution of the $(\Sigma\text{-}\pi)^{\pm\pm}$ system.

We can transform now the $(\Sigma 2\pi)$ system under consideration into its own rest frame and obtain the energy available in that frame. Furthermore, we can obtain the boundaries of the Dalitz plot corresponding to this particular energy. Insofar the energy distribution of these particles is governed by the statistical considerations, there is

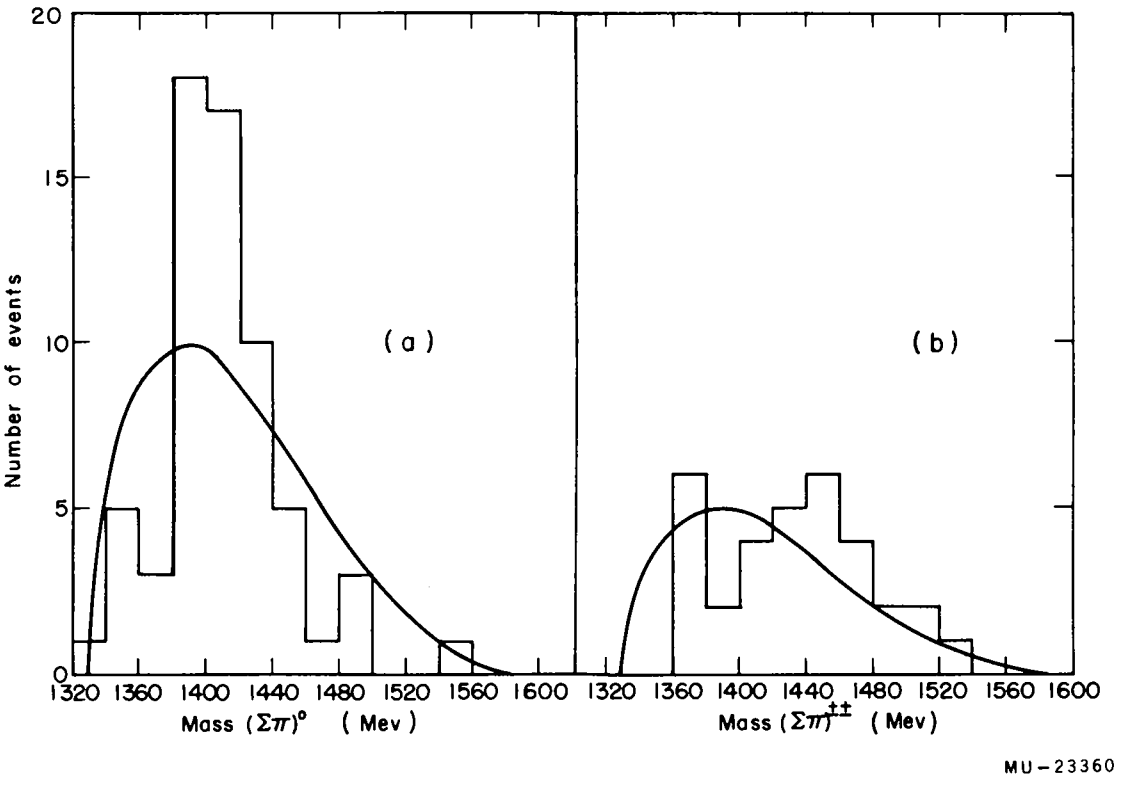

Fig. 14. Invariant mass spectra of the (a) neutral and (b) doubly-charged (Σ-π) systems from the reactions $K^- + p \rightarrow \Sigma^{\pm} + \pi^+ + \pi^+ + \pi^-$.

an equal a priori probability that the point representing a given event will fall within any given element of area in the Dalitz plot. The conventional Dalitz plots, however, are not completely suitable for our representation since, because of various c.m. energies for each event, there is no constant relation between the kinetic energy of one pion and the mass of the system consisting of the Σ and the other pion. For this purpose it turns out to be more suitable to label the axes in terms of the mass squared of the $(\Sigma-\pi)$ system. This still preserves the property that every element of area has equal a priori probability of being populated, and at the same time permits all the events with the same mass of the $(\Sigma-\pi)$ system to fall on the same line.

All the Dalitz-plot envelopes will now be tangent to one of two sets of orthogonal axes, one set corresponding to the mass of the $(\Sigma^+-\pi^-)$ system squared, the other to that of the $(\Sigma^-\pi^+)$ system squared. The minimum-energy envelope (corresponding to an event in which all three particles move with the same velocity) becomes just a point at the intersection of the two axes. As the three-body c.m. energy increases, the ellipse gets larger and moves away from the interaction point.

The final plot will consist of superposition of all envelopes, each one corresponding to one event. It will now be a three dimensional figure, and the points with equal a priori density of events will have the same height. This is achieved by remembering that each ellipse, corresponding to one observed event, must have the same volume. Its height is therefore given by the inverse of its area. In this way, the experimentally observed energy distribution of the third pion is taken into account. To illustrate graphically this process of superposition of envelopes corresponding to different events, we show in Fig. 15 the addition of envelopes for three different events in three dimensions and the resulting contour map.

The contour map for the actual 32 events together with the experimental points is shown in Fig. 16. Only half of the plot is shown because of its symmetry around the 45 deg line (i.e. because the two pions are identical). The events can be seen to fall into two bands, each

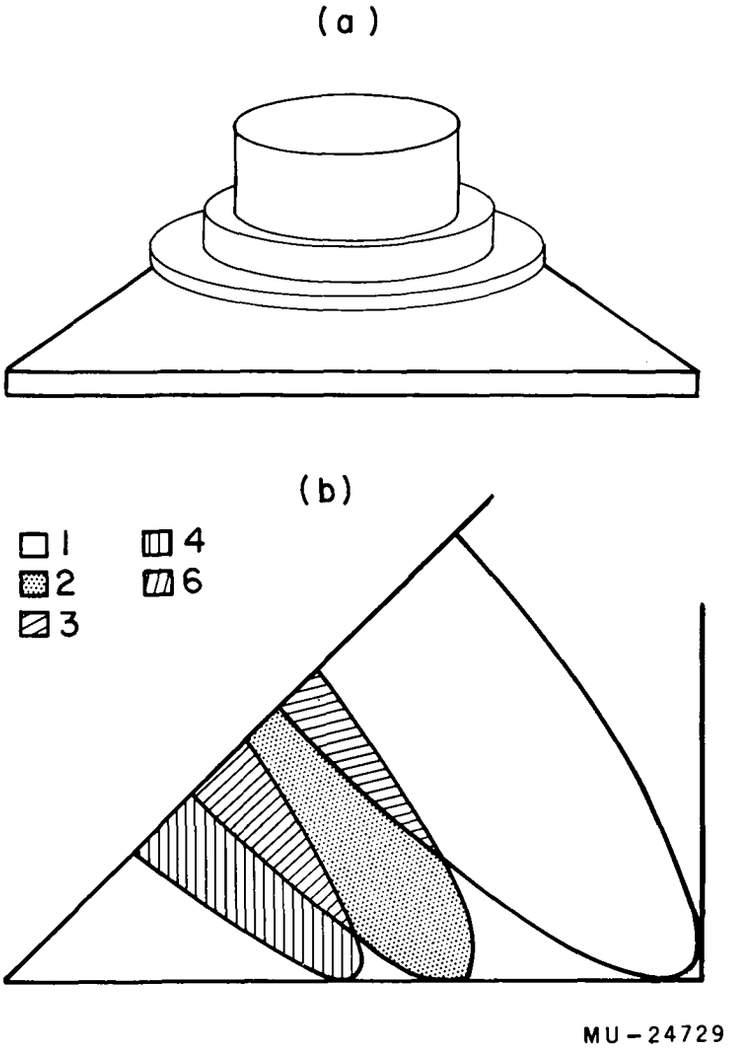

Fig. 15. (a) Three-dimensional view of superposition of three Dalitz envelopes of different c.m. energy to give a composite figure representing phase space for these three events.

(b) Contour map resulting from these three events. Relative densities are shown for an assumed 4:2:1 ratio of areas of the three ellipses.

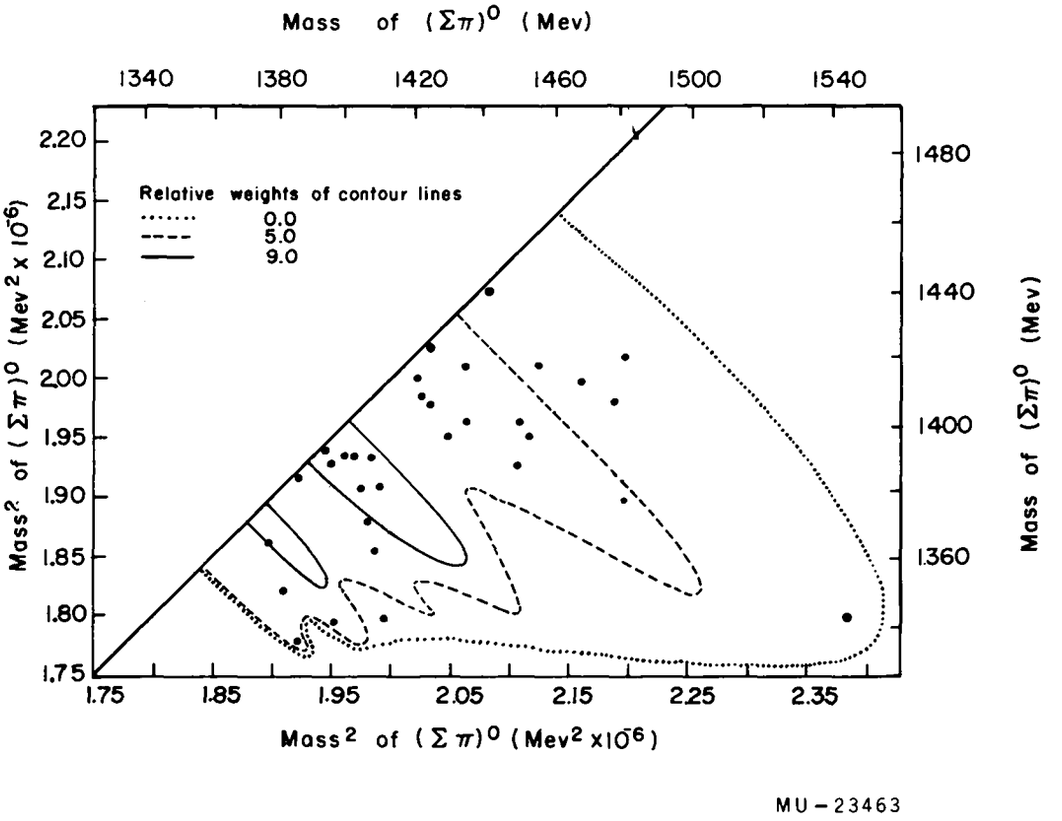

Fig. 16. Contour map resulting from the superposition of Dalitz envelopes representing the 32 examples of the reactions $K^- + p \rightarrow \Sigma^{\pm} + \pi^+ + \pi^{\mp} + \pi^-$. The solid circles represent the experimental points.

one centered about 1405 Mev (1.97×10^6 Mev^2), accentuating our belief that the phenomenon observed is due to a resonance in the (Σ-π) system. Indeed, one can ask what is the probability that 26 events out of 32 fall in one of the bands with full width of 40 Mev and centered at 1405 Mev, if phase space is the sole factor governing the reaction. The answer is that the odds against this are greater than 10^3 : 1. This exaggerates the point because of arbitrary selection of the band position, but the odds are nevertheless impressive.

We should like to dwell here for a moment on the advantage of this representation over the simple mass-spectrum histograms. Aside from the fact that this representation allows one to view each event individually and observe the two-band structure, one also has the possibility of being able to study the interference effects between the two amplitudes, which might enable one to deduce properties like spin and parity of the resonance. It should be emphasized, however, that these considerations are based on an assumption that needs a deeper theoretical justification than the crude arguments given above.

We would like to emphasize that if we see here a real effect (as opposed to a statistical fluctuation) then it must be due to a strong interaction in the Σ-π system and not in the π-π system. This is because we are dealing with a four-body system, and therefore a given mass of a dipion system does not determine uniquely the mass of the other two particles. Furthermore, experimentally the invariant dipion mass spectra do not show any significant departure from phase space.

2. The $\Sigma^0\pi^0\pi^+\pi^-$ Events: Determination of the Isotopic Spin of the Resonance

The data so far presented are still insufficient to determine the isotopic spin of the resonance. The assignment of T=0 or T=1 seems most logical in view of the absence of the 1405-Mev peak in the doubly charged system. However the T=2 assignment cannot be excluded because of the many amplitudes that can be involved in this reaction. As an example, if the reaction proceeds dominantly through the over-all T=1 channel with the two nonresonating pions also in T=1, then a T=2 resonance could not exhibit itself in the spectrum of the

doubly charged (Σ-π) system. The only unambiguous determination of the I spin can be obtained through the study of the $K^- + p \rightarrow \Sigma^0 + \pi^0 + \pi^+ + \pi^-$ reaction. More specifically, the decay branching ratio ρ of the resonance, defined by

$$\rho = \frac{(\Sigma\pi)^0 \rightarrow \Sigma^0 + \pi^0}{(\Sigma\pi)^0 \rightarrow \Sigma^+ + \pi^- + (\Sigma\pi)^0 \rightarrow \Sigma^- + \pi^+} ,$$

is 2, 0, or 1/2 depending on whether the I spin state is 2, 1, or 0, respectively.

In other words, if we assume that all 32 examples of $\Sigma^{\pm}\pi^{\mp}\pi^+\pi^-$ reactions proceed by the resonant mode, then we would expect 64 (for T=2), 0 (for T=1), or 16 (for T=0) examples of the $\Sigma^0\pi^0\pi^+\pi^-$ reaction, with a $\Sigma^0\pi^0$ mass around 1405 Mev. If we allow for the neutral decay mode and the typical escape correction of the Λ, the numbers are reduced to 33, 0, and 8 events.

The experimental difficulties associated with the study of this reaction have been discussed in the previous section (Sec. IVC, 3). However, to obtain some idea of the effect of the postulated resonance on this reaction, we divide our V^0 two-prong events that do not fit $\Lambda\pi^+\pi^-$ or $\Sigma^0\pi^+\pi^-$ into two groups. The first group includes events for which (a) χ^2 for the $\Lambda\pi^+\pi^-\pi^0$ interpretation is greater than 2.0 and (b) the missing mass carried off by the unseen neutrals is greater than 135 Mev. The second group includes the rest of the events. Thus the latter group is expected to contain mainly $\Lambda\pi^+\pi^-\pi^0$, while the former probably contains mainly examples of $\Sigma^0\pi^0\pi^+\pi^-$, $\Lambda 4\pi$, and $\Sigma^0 4\pi$. For each event, we calculate the invariant mass of the emitted neutral particles by using only the PANG data for the two charged pions and the beam momentum (Thus this system includes the Λ particle in addition to the unseen neutrals). Thus we need not hypothesize on the identity of a given event to obtain this quantity. Since the errors will vary quite a bit from event to event because no kinematical fit is involved (from 15 to 40 Mev), we present the data in both histogram and ideogram form (Figs. 17 and 18).

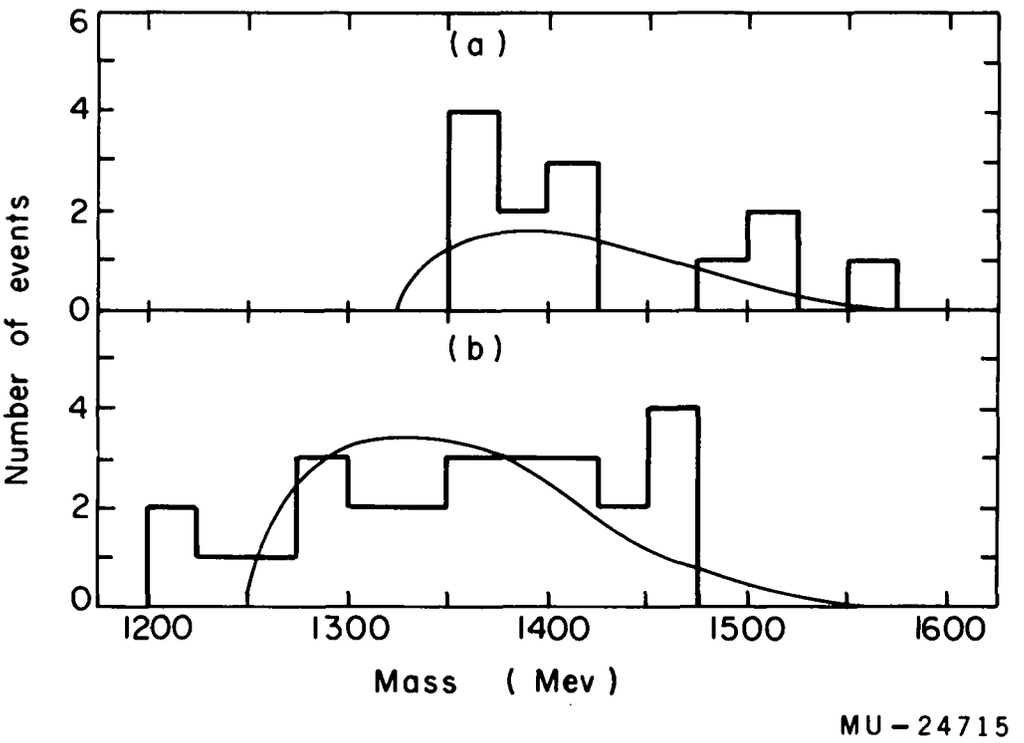

Fig. 17. Histograms of missing mass for 39 V^0 two-prong events which do not fit $\Lambda\pi^+\pi^-$ or $\Sigma^0\pi^+\pi^-$ hypotheses. (a) Thirteen events that give $\chi^2>2.0$ for $\Lambda\pi^+\pi^-\pi^0$ interpretation and a missing mass for the unseen neutrals > 135 Mev. The solid curve is the phase-space curve for the $\Sigma^0\pi^+\pi^-\pi^0$ reaction normalized to nine events (the other four are probably examples of $\Lambda 4\pi$ events). (b) The other 26 events. The solid curve is the phase-space curve for the $\Lambda\pi^0\pi^+\pi^-$ reaction normalized to 26 events.

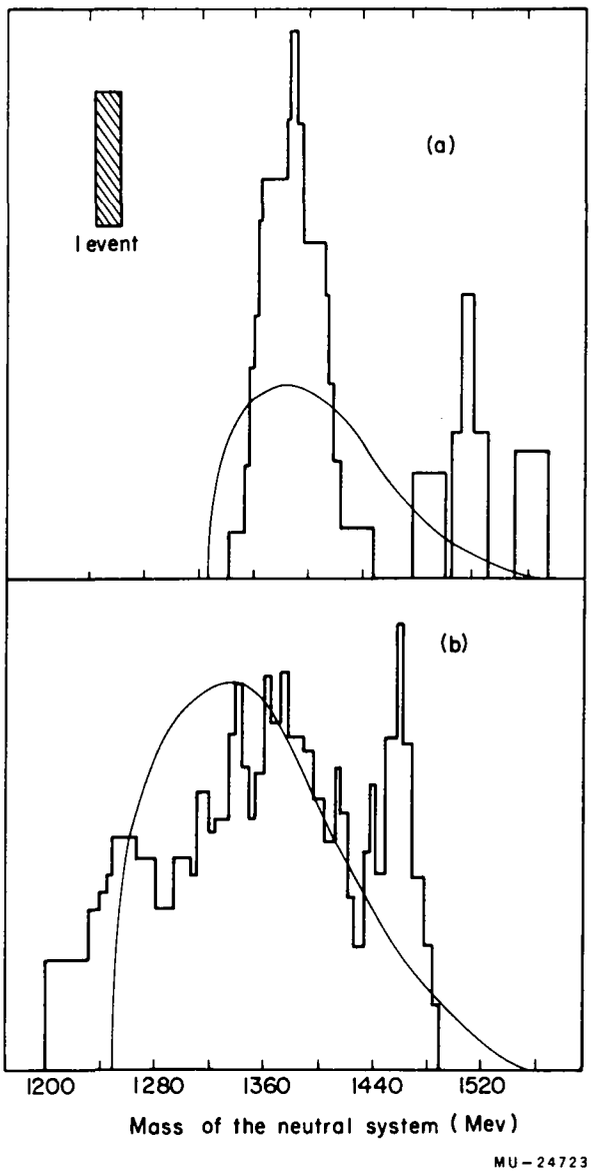

Fig. 18. Ideogram of missing mass for the 39 V^0 two-prong events that do not fit $\Lambda\pi^+\pi^-$ or $\Sigma^0\pi^+\pi^-$. The division of the events is the same as Fig. 17.

The only safe conclusion that can be drawn from the data is that the T=2 assignment is excluded. There does seem to be a clustering of nine events in Figs. 17a and 18a around 1390 Mev, and clustering that is absent in Figs. 17b and 18b. In view of this (we ignore for a moment the discrepancy between 1390 and 1405 Mev), we feel that the data seem to favor the T=0 isotopic spin assignment. However, because of scarcity of data, we cannot exclude the possibility that this clustering of events is due to a statistical fluctuation. Our belief that the isotopic spin of the resonating system is zero as opposed to one is accentuated by the fact that a T=1 resonance could decay into a Λ-π system. Thus we would see an excess of events in the $(\Lambda\pi)^{\pm}_{0}$ mass spectrum from the $\Lambda\pi^{+}\pi^{-}\pi^{0}$ reaction around 1405 Mev, a fact not substantiated by the data (Fig. 19). Accordingly, in the following discussion we assume that the isotopic spin of the resonance is zero.

We must mention one possible objection. If we accept the statement that the bunching of events in Figs. 17a and 18a is a significant phenomenon (as opposed to a statistical fluctuation), then two different explanations suggest themselves. The first one is the hypothesis postulated above, i.e. that the events in Figs. 17a and 18a are mainly $\Sigma^{0}\pi^{0}\pi^{+}\pi^{-}$ events and we see the effect of a resonance in the $\Sigma^{0}\pi^{0}$ system. The second one is that these are really poorly measured $\Lambda\pi^{0}\pi^{+}\pi^{-}$ events, and we observe the resonance in the $\Lambda\pi^{0}$ system (i.e. the previously discussed Y_{1}^{*}).

We feel that the latter is rather unlikely for the following three reasons: (a) If we assume that the bunching in Figs. 17a and 18a is real (and not a statistical accident), then nine out of 13 events in that group are dominated by the resonance. This would mean that at least a comparable fraction, i.e. 18 out of 26 events in Figs. 17b and 18b (since these then would be presumably better measured $\Lambda\pi^{0}\pi^{+}\pi^{-}$ events) should fall around 1390 Mev--a significant departure from phase-space prediction. This requirement is not satisfied by the data (Figs. 17b and 18b). (b) The events around 1390 Mev in Figs. 17a and 18a move away from this value when one uses the fitted (to the $\Lambda\pi^{0}\pi^{+}\pi^{-}$ interpretation) values of the Λ and π^{0} variables to calculate the mass of the neutral system.

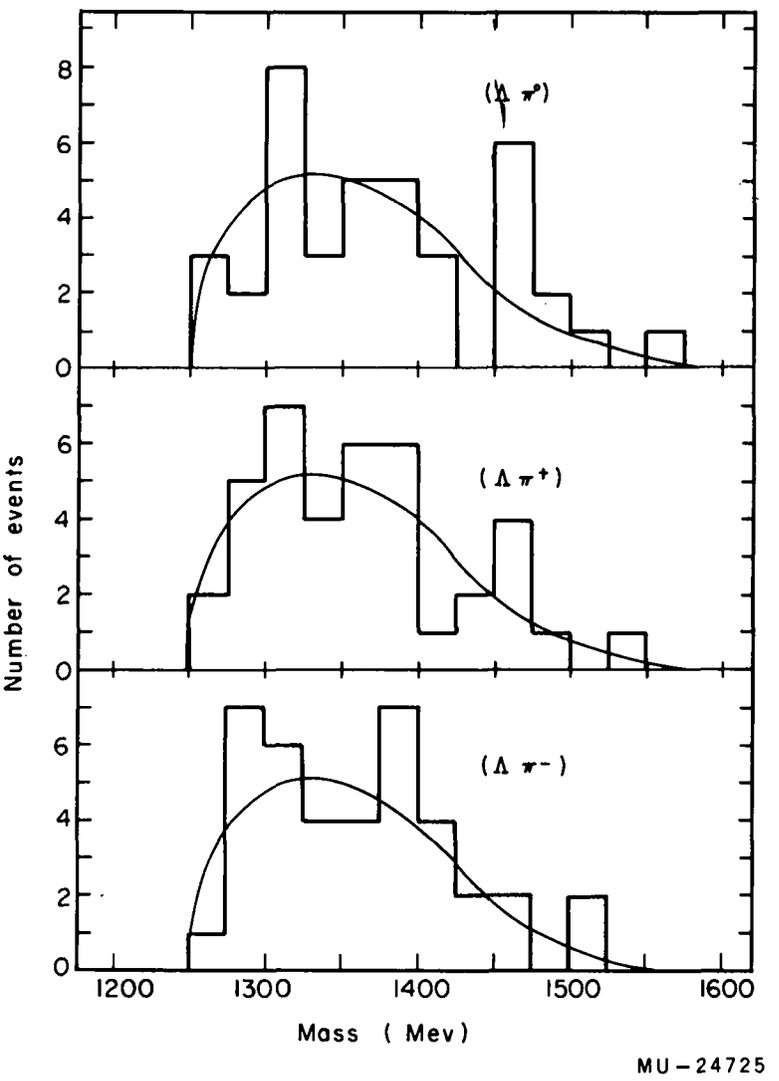

Fig. 19. Mass spectra of $\Lambda\pi^+$, $\Lambda\pi^+$, and $\Lambda\pi^0$ systems for the 39 events that do not fit $\Lambda\pi^+\pi^-$ or $\Sigma^0\pi^+\pi^-$ hypotheses. Values used were those obtained from the fit to the $\Lambda\pi^+\pi^-\pi^0$ hypothesis.

(c) If we assume that all 39 events are examples of the $\Lambda\pi^+\pi^-\pi^0$ reaction and calculate the invariant masses of the $(\Lambda\pi^+)$, $(\Lambda\pi^-)$ and $(\Lambda\pi^0)$ systems from the fitted values, there seems little evidence for presence of Y_1^* in any of these spectra (Fig. 19). In other words, either Y_1^* for some reason plays no dominant role in the $K^-+p\rightarrow\Lambda+\pi^++\pi^-+\pi^0$ process, or its effect is now very obscured because of the interference phenomena. It appears, therefore, that the observed phenomenon (if it is not a statistical accident) is due to the $K^-+p\rightarrow\Sigma^0+\pi^0+\pi^++\pi^-$ reaction.

3. The $\Sigma^\pm\pi^\mp\ \pi^0\pi^0$ Reactions

The T=0 resonance should exhibit itself also in the mass spectrum of the $(\Sigma^\pm\pi^\mp)$ system from the $\Sigma^\pm\pi^\mp\ \pi^0\ \pi^0$ reactions. As there were 32 $\Sigma^\pm\pi^\mp\ \pi^+\ \pi^-$ events, the number of $\Sigma^\pm\pi^\mp\ \pi^-\pi^0$ reactions should be somewhere between zero and 16, depending on the relative importance of the T=0 and T=1 channels in the production process. The mass spectrum for the 22 events of this kind is shown in Fig. 20. Unfortunately, the large errors on some of these events (since here again no production fit is made) as well as the possibility of $\Sigma 2\pi$ contamination does not allow us to draw any supporting conclusions either in favor or against the resonance hypothesis in the $(\Sigma\text{-}\pi)$ system.

4. Discussion of $\Sigma^\pm\pi^\mp\pi^0$ Events in Light of the T=0 Resonance

We must now turn to the two problems that face our interpretation of the data. These are the relative absence of the resonance effect in the $\Sigma^\pm\pi^\mp\pi^0$, and the discrepancy in the mass of the resonance as obtained from its charged and from its neutral decay modes. We discuss first $\Sigma^\pm\pi^+\pi^0$ events.

The T=0 resonance should exhibit itself as the enhancement of the 1400-Mev region in the $(\Sigma^\pm\pi^\mp)$ mass spectrum. This is true to a certain extent (Fig. 13a), but the effect is hardly statistically significant and not as strong as might be expected from the influence that the resonance has on the $\Sigma^\pm\pi^\mp\pi^+\pi^-$ events (Fig. 14). In answer to this objection, we must first point out that this region of low $(\Sigma^\pm\pi^\mp)$ mass has a large experimental uncertainty because of possible contamination of the

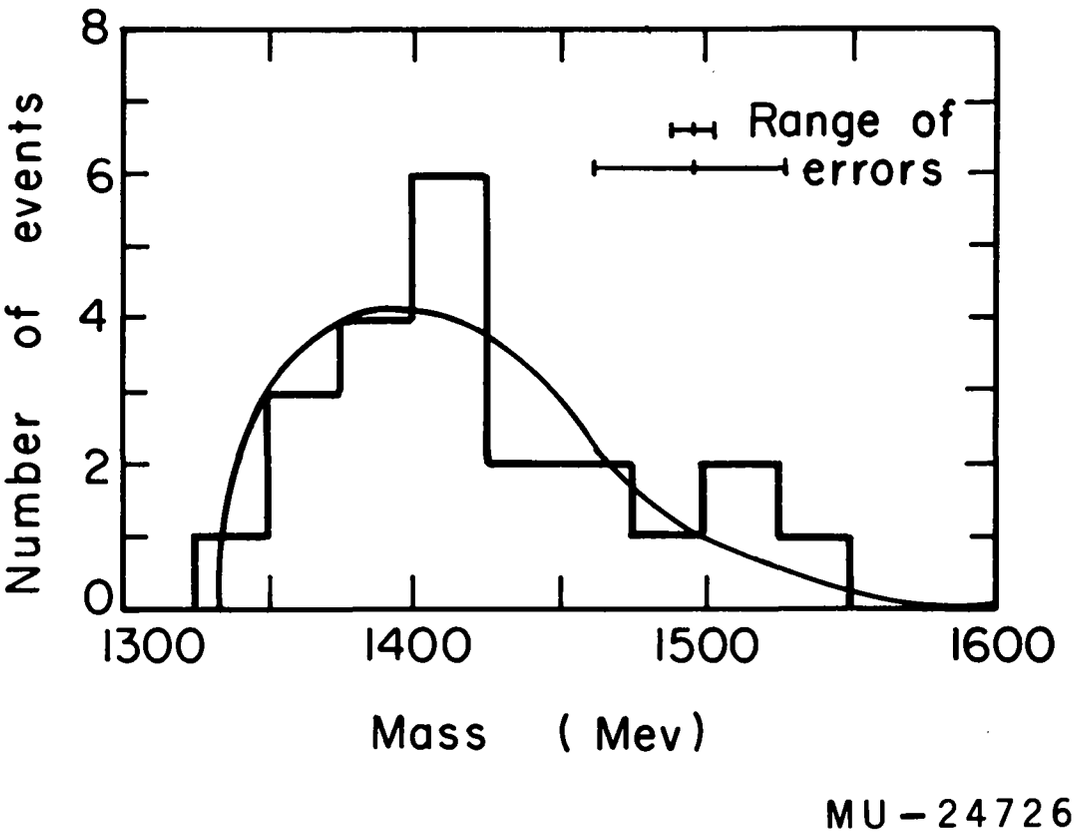

Fig. 20. Mass spectrum of ($\Sigma^{\pm}\pi^{\mp}$) system from the events believed to be examples of $K^- + p \rightarrow \Sigma^{\pm} + \pi^{\mp} + \pi^0 + \pi^0$ reactions. The solid curve is the phase-space curve for the $\Sigma 3\pi$ reaction normalized to 22 events.

$\Sigma^{\pm}\pi^{\mp}\pi^0\pi^0$ events discussed in Section IVC, 3. In other words, due to the difficulty of correcting for this effect, the number of events in this part of the spectrum is rather uncertain. Thus the excess of events in this region could be easily more pronounced if too many events were subtracted out (see Fig. 13b for the spectrum of subtracted events). However, even after allowance for this effect we must still admit that the T=0 resonance plays a relatively minor role in the $\Sigma^{\pm}\pi^{\mp}\pi^0$ events.

The second point we would like to make is that a mechanism does exist which forbids the resonance in the $\Sigma^{\pm}\pi^{\mp}\pi^0$ events, namely production through a pure T=0 channel. For the production from the T=0 channel, the two pions must always be in a T=1 state, and thus certain stringent restrictions must be met. The wave function can be written as

$$\psi_0 = \sqrt{\frac{1}{6}}\,\Sigma^+(\pi^-\pi^0 - \pi^0\pi^-) - \sqrt{\frac{1}{6}}\,\Sigma^0(\pi^+\pi^- - \pi^-\pi^+) + \sqrt{\frac{1}{6}}\,\Sigma^-(\pi^0\pi^+ - \pi^+\pi^0).$$

Thus the three charge states are all characterized by the same production amplitudes. This requires not only that the cross sections for these three charge states be equal, but also that all the other distributions be the same. Furthermore, the $\Sigma^0\pi^0\pi^0$ reaction should be totally absent, because two neutral pions cannot be in a T=1 state.

It should be pointed out that this argument of identity of the three charge states holds only for the T=0 production. For a T=1 channel, the two pions can be in T=0, 1, or 2. Thus we deal now with three different amplitudes, which would make it quite unlikely that these would produce the same cross sections and same distributions for all three charge states.

To test this hypothesis, we note first that the cross sections for $\Sigma^{\pm}\pi^{\mp}\pi^0$, $\Sigma^{\mp}\pi^{\pm}\pi^0$, and $\Sigma^0\pi^+\pi^-$ are roughly equal (Table I) although the last one is rather uncertain due to ambiguity with $\Lambda\pi^+\pi^-$ as outlined previously (Sec. IVB, 2). It is impossible to obtain any estimate of the number of $\Sigma^0\pi^0\pi^0$ events except for an upper limit of ~1.5 mb (Table 1). However, many other processes are included in this group, so the limit is probably unrealistic. Thus the total-cross-section data does not exclude a hypothesis of production from T=0 only.

The Dalitz plots for the three reactions (Figs. 8, 9, and 10) are not too different and are reasonably symmetric, so no evidence against production from the T=0 hypothesis can be drawn from these. We look next at the angular distributions for the three reactions. The angular distribution of the three Σ hyperons must be the same, and the angular distributions of the two pions in each reaction must be identical to each other as well as to the pion distributions in the other two reactions. The nine angular distributions are shown in Fig. 21. No effort was made to assure that these should not have any experimental biases inherent in them, because the number of events is too small for any careful analysis. It is felt that no strong biases exist that would significantly affect the data, at least for the two charged Σ states. Slightly more caution is necessary when looking at the $\Sigma^0\pi^+\pi^-$ reaction because a significant number of these events are missing from the spectrum presented in Fig. 21. We feel, however, that there is relatively little correlation between a configuration of the $\Sigma^0\pi^+\pi^-$ system in the K^-p c.m. frame and the probability that this event will fit a $\Lambda\pi^+\pi^-$ hypothesis. Therefore the $\Sigma^0\pi^+\pi^-$ angular distribution should also be reliable. The distributions appear different, but it would be dangerous to conclude that this is statistically significant, especially since some small experimental biases could be present that would affect different reactions in a different way. Furthermore, it must be remembered that, by proper choice of phases, even a small T=1 contribution can significantly affect the distributions observed.

To conclude the discussion regarding the possibility of production from a pure T=0 channel, we state that no strong evidence exists against this hypothesis, but at the same time there is no strong evidence for it.

One more point should be made before leaving the $\Sigma^\pm\pi^\mp\pi^0$ reactions. We know that the $\Lambda\pi^+\pi^-$ reaction seems to be governed almost entirely by the Y_1^* resonant amplitude, the phase-space factor being completely irrelevant. It is tempting therefore to ask to what extent is the phase-space factor relevant in the $\Sigma^\pm\pi^\mp\pi^0$ reactions, and to what extent is it meaningful therefore to speak about departures from

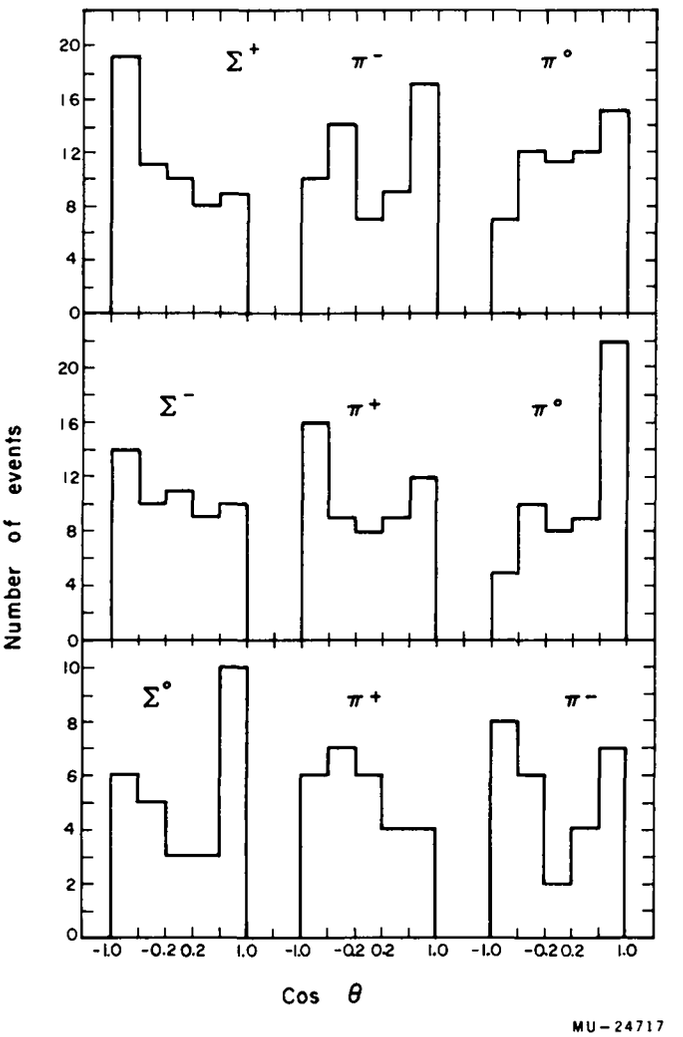

Fig. 21. Angular distribution of the three final-state particles for the reactions $K^- + p \rightarrow \Sigma^{\pm} + \pi^{\mp} + \pi^0$, $\Sigma^0 + \pi^+ + \pi^-$.

phase-space predictions. More specifically we ask whether a more correct view would be to think in terms of several resonant amplitudes dominating the reaction, which when superimposed might resemble a phase-space curve. This is a point obviously quite important when talking about the extent to which the T=0 resonance is seen in the $\Sigma^{\pm}\pi^{\mp}\pi^{0}$ reactions, and we shall return to it later (Sec. VD).

5. Mass Discrepancy

We turn now to the problem of mass discrepancy. As observed through the charged-Σ decay mode, the central value for the mass of the T=0 resonance is 1405 ± 2.5 Mev, and the half-width after unfolding of experimental errors is ± 10 Mev. From the V^{0} two-prong events (Figs. 17a and 18a), if we assume that all nine events around 1390 Mev are examples of $\Sigma^{0}\pi^{0}\pi^{+}\pi^{-}$ proceeding through the resonant channel, we obtain for the central value 1387 ± 5 Mev and a width consistent with ±10 Mev. Even though on the first glance this might appear as a statistically significant mass discrepancy, we feel that it would be dangerous to draw such a strong conclusion from only nine events. Since the identification of $\Sigma^{0}\pi^{0}\pi^{+}\pi^{-}$ events is so difficult, it is not inconceivable that a few examples of $\Lambda\pi^{0}\pi^{+}\pi^{-}$ have been included in Figs. 17a and 18a and that they tend to bring down the central value.

Determination of whether there is a real mass difference will have to await further data. We merely mention here some of the phenomena that could give a mass shift: electromagnetic mass differences between the $\Sigma^{-}\pi^{+}$, $\Sigma^{+}\pi^{-}$, and $\Sigma^{0}\pi^{0}$ systems, interference between the two resonating amplitudes in the case of $\Sigma^{\pm}\pi^{\mp}\pi^{+}\pi^{-}$ reactions, and interference with the nonresonant amplitude. However, a quantitative discussion of these points is probably premature at this stage.

D. Influence of Other Possible Σ-π Resonances

In this section we would like to discuss briefly the effect of other resonances on our data and to what extent the data support or deny the production of these resonances by 1.15-Bev/c K^{-} mesons. We turn our attention first to the T=2 global-symmetry analogue of the 3/2, 3/2 pion-nucleon resonance in the pion-hyperon system.

1. The T=2 Global Symmetry Resonance

In connection with the still unresolved status of the Y_1^* resonance interpretation, a considerable amount of speculation has been centered around the question of the T=2 resonance. The existence of a j= 3/2, T=2 resonance in the Σ-π system would greatly strengthen our belief in the validity of global symmetry and would provide an indirect support for the global symmetry interpretation of Y_1^*. If we use arguments outlined in Section VB1, the position and width of this resonance are 1530 Mev and 70 Mev, respectively.[17]

Accordingly, we consider to what extent our data can provide evidence for or against the existence of T=2 resonance. The most obvious place to look for it would be in the spectrum of the doubly charged $\Sigma\pi$ system in the $\Sigma^{\pm}\pi^+\pi^+\pi^-$ reactions (Fig. 14). Unfortunately, the 1530-Mev region is at the tail end of the available spectrum, and so it would be very surprising if this resonance could indeed dominate the reaction. Therefore, the absence of any clustering of events in this region hardly can be construed as anything except a purely kinematical effect. In the $\Sigma 2\pi$ reactions, however, there is ample phase space in this part of the spectrum, and so one would expect that the investigation of those reactions might tend to be more fruitful.

Even though no obvious excess of events in this region is present, this per se does not constitute any conclusive argument against the presence of the T=2 resonance. The width of this resonance is such that the resonant events would be hard to separate out from background, but in addition the interference effects could be expected to affect the spectrum considerably, because the two resonant bands would intersect inside each Dalitz ellipse. Because in this system the resonance would have to be produced from a T=1 state we can write the wave function for the final-state consisting of Y_2^* (resonating Σ-π in a T=2 state) and the other π:

$$\psi_1 = \sqrt{\frac{3}{10}}\ Y_2^{*+}\pi^- - \sqrt{\frac{4}{10}}\ Y_2^{*0}\pi^0 + \sqrt{\frac{3}{10}}\ Y_2^{*-}\pi^+ .$$

Next we substitute the decay wave function for each charge state of Y_2^* to obtain

$$\psi_1 = \sqrt{\frac{3}{20}}\left[(\Sigma^+\pi^0)\pi^- - (\Sigma^0\pi^+)\pi^-\right] - \sqrt{\frac{1}{15}}\left[(\Sigma^+\pi^-)\pi^0 + 2(\Sigma^0\pi^0)\pi^0 + (\Sigma^-\pi^+)\pi^0\right] + \sqrt{\frac{3}{20}}\left[(\Sigma^-\pi^0)\pi^+ - (\Sigma^0\pi^-)\pi^+\right],$$

where the system in parentheses is the resonating system. Finally, we collect the terms for each one of the three charge states under consideration:

$$\Sigma^+\pi^-\pi^0 \rightarrow \sqrt{\frac{3}{20}}(\Sigma^+\pi^0)\pi^- - \sqrt{\frac{1}{15}}(\Sigma^+\pi^-)\pi^0$$

$$\Sigma^-\pi^+\pi^0 \rightarrow \sqrt{\frac{3}{20}}(\Sigma^-\pi^0)\pi^+ - \sqrt{\frac{1}{15}}(\Sigma^-\pi^+)\pi^0$$

$$\Sigma^0\pi^+\pi^- \rightarrow \sqrt{\frac{3}{20}}(\Sigma^0\pi^+)\pi^- + \sqrt{\frac{3}{20}}(\Sigma^0\pi^-)\pi^+.$$

Thus the two resonant amplitudes contributing to each reaction have a definite phase relation with respect to each other and accordingly will interfere with each other. Specifically, the interference effects between the two contributing coherent amplitudes change sign as we go from the neutral Σ case to the charged Σ reactions, though in the latter case the interference is not complete.

We have investigated to what extend the experimental mass distributions and Dalitz plots are consistent with this resonance. We have used the treatment introduced by Dalitz and Miller[26] to study the lower energy energy $\Lambda\pi^+\pi^-$ reaction by writing a phenomenological matrix element of the form used by these authors that would be dominated by the resonant amplitude and also satisfy the symmetry properties of the wave function. The Breit-Wigner, one-level formula was used as appropriate for a resonance which is an analogue of the 3/2, 3/2 pion-nucleon resonance. Even though our statistics are quite limited, we find it hard to reproduce the distribution of the center parts of the three Dalitz plots simultaneously by means of only s-and p-wave

production. It seems that if a $T = 2$ resonance exists, it does not play any significant role in the Σ production at this energy, or else higher partial waves dominate.

2. The 1520-Mev $T = 0$ Resonance

Recently evidence has been reported for the existence of a $T = 0$ resonance in the $\Sigma\pi$ system with the mass of 1520 Mev.[30] We again ask whether any effect of this resonance is seen in any of our reactions. Again because of the limited amount of phase space in that region for the $\Sigma^{\pm}\pi^{\mp}\pi^{+}\pi^{-}$ events, lack of any effect in those reactions is not surprising (Fig. 14). The resonance, however, should also appear in the $\Sigma^{\pm}\pi^{\mp}\pi^{0}$ events as a bump in the mass spectrum of $(\Sigma^{\pm}\pi^{\mp})$ (Fig. 13a). At first glance, no obvious excess of events above the phase space is noticeable, but we would like to explore this possibility a little further.

As we mentioned before, the $\Lambda\pi^{+}\pi^{-}$ reaction is dominated exclusively by the Y_1^* resonance; the three-body phase space is rather irrelevant here. Therefore, we do not feel that it is necessarily correct to compare the $\Sigma 2\pi$ spectra with the phase-space predictions. We can present an alternative hypothesis, which--at least with our limited statistics--cannot be easily disproved, a hypothesis that here also the reactions are dominated entirely by strong final-state interactions. More specifically we can say that these reactions proceed almost exclusively through the $T = 0$ resonances at 1405 and 1520 Mev and the $T = 1$ Y_1^* at 1385 Mev. If we look at the mass spectrum of $(\Sigma^{\pm}\text{-}\pi^{\mp})$ in these terms, we can think of the low-mass events as due to the 1405-Mev resonance, the center of the spectrum as due to the 1520-Mev, $T = 0$ resonance, and the high-mass events as due to projection onto the $(\Sigma^{\pm}\pi^{\mp})$ axis of events with $(\Sigma^{\pm}\pi^{0})$ mass around 1385 Mev, namely Y_1^* events. This hypothesis would require relative depopulation of the center of the $\Sigma^{0}\pi^{+}\pi^{-}$ Dalitz plot. Some events are found here, indicating that some "background" must be present, but because of experimental difficulties associated with this reaction (which were mentioned before) and the limited statistics, we cannot exclude the possibility that the same region in the charged Σ events is considerably

more populated.

We would like to emphasize the spirit in which we make these comments. Rather than attempting to prove any hypothesis, a task we are unable to do with this small amount of data, our primary purpose is merely to sound a word of caution. For, if indeed the hypothesis of production mainly through resonant channels is true, then the statement that the 1405-Mev $T = 0$ resonance is absent in the $\Sigma 2\pi$ reactions loses most of its validity. Furthermore, the Y_1^* branching ratio R, for which we obtained an upper limit of 8% may actually be quite close to this number, even though at first glance the limit seems unrealistically high. We want merely to emphasize that the most elementary treatment of looking at departures from phase space may not be the correct one.

ACKNOWLEDGMENTS

This work has been part of an experiment conducted jointly with Profs. Luis W. Alvarez, Myron L. Good, and Harold K. Ticho, Drs. Margaret H. Alston and Philippe Eberhard, and Mr. William Graziano.

The author would like to express his deep appreciation to Prof. Luis W. Alvarez for his continual interest, advice, and encouragement. Sincere thanks are due Profs. Myron L. Good and Harold K. Ticho for their help, guidance, and suggestions at all stages of this work. The advice of and discussions with Dr. Margaret Alston have been invaluable in the data-analysis part of the experiment. The author has profited greatly from discussions with Dr. Philippe Eberhard during the early stages of experiment. The continuing help, suggestions, and cooperation of Mr. William Graziano are acknowledged with deep gratitude.

The author would like to express his thanks to Profs. Donald H. Miller and Arthur H. Rosenfeld for many enlightening discussions. Dr. Frank Solmitz has always given freely of his time, and his advice during the early stages of the experiment has been invaluable. The author has profited considerably from the series of lectures given by Profs. Richard H. Dalitz and Abraham Pais during their stay in Berkeley, as well as several informal discussions.

This experiment would have been impossible without the highly developed digital-computer data-analysis system. Drs. Frank Solmitz, William Humphrey, and Ronald Ross have been responsible mainly for the PANG program, and Profs. Arthur H. Rosenfeld, James Snyder, and Horace Taft, Dr. Frank Solmitz, and Mr. Jon Peter Berge for the KICK system. Mr. William Graziano is responsible for the EXAMIN program used in this experiment.

The cooperation of the Bevatron crew under the direction of Dr. Edward Lofgren, and of the bubble-chamber crew under the direction of Messrs. Donald Gow, Robert Watt, and Glenn Eckman is acknowledged with many thanks.

Finally, special thanks are due to the scanners who participated in this experiment, especially Messrs. Joseph Waldman and Jon Folkman.

This work was done under the auspices of the U. S. Atomic Energy Commission.

APPENDICES

A. Path Length Determination

The amount of K^- path length in the experiment was determined by counting K decays, because at the energy used here the K mesons are minimum-ionizing and thus indistinguishable from the lighter particles. The maximum decay angle possible for a 1-Bev pion (which was the average momentum of the pion contamination) is 3 deg, and thus a wide-angle decay is a unique signature of a K meson.

Before converting the number of K decays to a total path length, we must apply the following several corrections.

a. Small angle decays. Only decays with opening angles larger than 4 deg were included, because below that limit, the scanning efficiency becomes very poor, and one begins to see pion decays. Even this limit is probably too small. The ability to detect K mesons dipping directly downward at 4 deg becomes marginal, and in the future, a slightly larger cutoff should be imposed. This 4-deg limit corresponds to a certain forward cone in the K-meson rest frame and a smaller backward cone (since all visible decay products except electrons must go forward in the laboratory at this energy). To calculate the size of this cone, we start with the two simultaneous transcendental equations:

$$P \cos\Theta = \gamma p \cos\theta + \eta\epsilon$$
$$P \sin\Theta = p \sin\theta,$$

where capitals refer to laboratory quantities and small letters to K-meson rest-frame quantities. Using the small-angle approximation for $\cos\theta$ and $\sin\theta$, we get for the two predominant decay modes:

$$K_{\mu 2} \rightarrow \cos\theta = 0.941$$
$$K_{\pi 2} \rightarrow \cos\theta = 0.928$$

in the forward cone. The backward cone gives a completely negligible contribution.

We make the approximation that the less frequent decay modes have, on the average, the same cutoff as the average of these two modes (except for τ decays for which the detection efficiency is 100%). Averaging the cutoffs of all decay modes according to their decay rate, we get $\cos\theta = 0.940$. Since the K meson is spinless, it must decay isotropically in its rest frame, and so the final correction here is 3.0%.

b. Scanning efficiency. Because all the film was scanned twice, one can use the first scan to calculate the efficiency of the second scan. This procedure assumes that every K decay is equally easy to find, i.e., that there are no intrinsically "well-hidden" decays. This is obviously not completely true, but in view of the 4-deg small-angle limit and the choice of the fiducial volume at a reasonable distance from the actual walls of the chamber, it may be hoped that the procedure does not depart very much from reality. Besides, the scanning-efficiency correction turns out to be small enough that this is not too important. The relevant numbers are:

Total number of K decays	3023
Number missed on first scan	533
Number missed on second scan	117.

To obtain the actual number of K decays, we must calculate the scanning efficiency for these events. The scanning efficiency S of the second scan is given by the fraction of the decays found on the first scan which were also found during the second scan:

$$S = \frac{3023 - 533 - 117}{3023 - 533} = \frac{2373}{2490} = 95.3\%.$$

The actual number of K decays is given by

$$\frac{3023 - 117}{0.953} = \frac{2906}{0.953} = 3049.$$

The over-all scanning efficiency for K decays is thus $3023/3049 = 99.1\%$. In the first scan, the scanning efficiency for K decays was much lower than in the subsequent scan because the emphasis in the former was

mainly on double V's.

In addition we must apply the following three corrections, which would have been applied automatically had all K decays been measured and fitted.

c. Nonbeam decay correction. During the sketching operation, all interactions or decays produced by tracks within 5 deg to the beam direction were recorded. In the final analysis, a more stringent criterion was applied for all accepted interactions by means of EXAMIN program. Since not all K decays were measured, we used our τ decays to determine what fraction of K decays would fail to meet the new criterion. It was found that 16 out of 174 events would not meet this new beam definition.

d. Low-energy correction. In addition, a certain number of tracks may meet the beam criterion on direction and yet be below the nominal beam momentum. Again we use the highly overconstrained τ decays to determine this number. The correction turns out to be four out of 158 decays.

This assumes that all categories of events are equally strongly constrained as τ decays. In other words we assume that all interactions produced by low-momentum K^- mesons are just as unlikely to give satisfactory fits when beam-averaged as τ decays. This is obviously not true when we deal with incoming K^- mesons with momenta only slightly below the beam momentum (e.g. ~50 Mev/c). However, the main fraction of below-beam-energy K^- mesons had momentum sufficiently low that when they were beam-averaged a satisfactory fit could not be obtained, even for a one-constraint hypothesis.

e. Fiducial-volume correction. During scanning and sketching, the fiducial volume was defined by means of a projected plane in one view. For the final analysis, the accepted region was defined in terms of an actual volume which was contained entirely in the previous definition. We must therefore correct for the decays satisfying the original fiducial volume but not the final one. Again using τ decays, we find this correction to be three out of 154 events. The over-all correction for these three factors is then 23 out of 174 events, i.e. 13%.

Combining all these corrections, we get for the actual number N of K decays satisfying all beam criteria

$$N = \frac{0.87 \times 3023}{0.970 \times 0.991} = 2736.$$

To determine the path length, we multiply the number of decays by the decay length of a 1.150-Bev/c K meson. Thus the total path length, L, in the experiment is given by

$$L = \eta \tau \, cN = \frac{1150}{494} \times 3 \times 10^{10} \times 1.224 \times 10^{8} \times 2736 = 2.34 \times 10^{6} \text{ cm}.$$

Finally we calculate the cross section corresponding to the observation of one interaction. The relationship between the cross section, σ, path length, L, and number of events observed, n, is given by

$$n = N_0 \, \rho \, \sigma \, L/A,$$

where ρ is the density of hydrogen at bubble-chamber operating conditions (0.0586 gm/cm^3),[31] N_0 is the Avogadro's number (6.025×10^{23}), and A is the atomic weight of the material used (1.008 for hydrogen). Thus the cross section corresponding to one event is given by

$$\sigma = A/N_0 \, \rho \, L = \frac{1.008}{(6.025 \times 10^{23})(0.0586)(2.34 \times 10^{6})}$$

$$= 1.22 \times 10^{-29} \text{ cm}^2 = 12.2 \ \mu\text{b}.$$

The statistical uncertainties associated with this calculation of path length are insignificant, since in each case under consideration the main uncertainty comes from the statistical error on the number of interactions observed.

B. Study of Measurement Errors

This experiment is the first one in which the PANG and KICK programs were used to study high-energy events. In the preceding low-energy experiment where the momentum, P, was typically ~200 Mev/c, the uncertainties in the angle and momentum measurements were dominated in most cases by the multiple Coulomb scattering (the rms. projected angle due to multiple Coulomb scattering is proportional to $\sqrt{L}/P\beta$, where L is the measured length of the track and β is its velocity in units of c). The Coulomb contribution to angle errors at that energy would be typically of the order of 1 deg. Furthermore, the typical curvatures, K, observed at low momenta in the 15-in. chamber (~ 12 kgauss H field) were such that typical value of the sagitta, S (given by $S = KL^2/8$) would be in the vicinity of 1 cm. Accordingly, at low energy the precise knowledge of measurement errors (which are typically ~ 0.2 deg with the existing measuring equipment and the precise fit performed by PANG) is not very important; in addition, the effects of systematic curvature shifts due to turbulence are insignificant, as these amount to spurious sagittas of the order of a small fraction of a millimeter.

In the 1-Bev region, the Coulomb contribution to the angle errors is of the order of few minutes of arc. Accordingly, the measurement errors, which previously were obscured by much larger Coulomb scattering begin to dominate. Furthermore, the typical sagittae are now 1 to 2 mm, and thus small systematic spurious curvature due to turbulence can affect significantly the measured momenta.

A considerable amount of time was spent therefore in the early stages of analysis studying the measurement errors and the "turbulence" in the chamber. We discuss first the latter point. An ideal but experimentally difficult way to study "turbulence" would be to pass high-energy tracks through the chamber at different heights and going in different directions. In addition the magnetic field should be turned off. Unfortunately, this was impossible because of lack of time during the exposure, and so a different technique had to be used. In essence,

it consisted of studying the mean momentum and the momentum spread of the K^- beam as obtained from curvature measurements. Tracks that showed wide-angle decays were selected because this characteristic identified them surely as K mesons. Furthermore, the momentum as well as the spread of the K^- particles could be independently obtained to a high accuracy by studying $K\mu_2$ decays (Appendix C). Specifically, K mesons that travelled about three-fourths of the length of the chamber before decaying were chosen so as to minimize measuring errors and enable one to study the "turbulence" effects in various parts of the chamber.

It should be pointed out here that we use the word "turbulence" rather loosely. Without a more detailed study, we can not distinguish between actual turbulence and effects like optical distortion and systematic optical-system imperfections. As a matter of fact, some evidence exists that not all the effects described below are due to turbulence. We shall continue, however, to use the word turbulence as a general term for all of these effects.

Three separate sets of optical correction constants have been calculated in PANG for the film used in this experiment, the three sets of rolls being 557 to 598, 600 to 696, and 702 to 786. We will discuss the turbulence effects for each of these three sets. Some modifications were introduced in the operation of the chamber between the second and third sets, and so the "true turbulence" might easily be different in the last set of rolls. However, only changes in the optics were made between the first and second sets, and so the extent to which the measurements discussed below differ for these two sets is a rough measure of the size of the contribution of optical effects to these errors.

Table VI presents the data on the momentum measurements of the whole track, from its entrance to the chamber to the point of decay, as well as the data on the two halves of the track treated as two separate tracks. From the data, one can draw two conclusions: (a) there is a systematic spurious curvature which can be thought of as long-wavelength turbulence tending to lower the momentum of the negative tracks moving along the direction of the beam, and (b) the basic intrinsic measurement uncertainty of each point must be higher than

Table VI. Results of "turbulence" study on K decays.

Film interval	Part of track	Mean observed momentum (Mev)	Observed σ (Mev)	Expected σ (Mev)
	whole	1136	48	35
557-598	first half	1170	215	120
	second half	1079	150	85
	whole	1088	70	34
600-696	first half	1110	205	120
	second half	1032	145	80
	whole	1032	56	32
702-780	first half	1007	215	115
	second half	1000	150	75

the assigned value (possibly due to short-wavelength turbulence), as exhibited by the above expected momentum spread of the short tracks. This latter effect would not show up too strongly in the data on whole tracks, since there the Coulomb-error contribution becomes significant (the typical Coulomb-to-measurement error ratio for a track going through the chamber is ~ 1.5).

Unfortunately, it is not practical to remove the systematic shift in the curvature, because no information is available on the turbulence effects at other depths than at the beam level or along other directions. One can, however, increase the errors appropriately. This was done in two ways. Firstly, the basic measurement uncertainty was increased from 5 to 7 microns to compensate for short-wavelength turbulence, and secondly, a given spurious curvature corresponding to the observed systematic shift was folded in with the other measurement errors. We can look at the second point in the following way. For a track of a given length, a spurious curvature K, (momentum $P = 1/K\cos\theta$) corresponds to a spurious sagitta δS proportional to K. Thus the actual measured sagitta S_m is shifted by δS, and we treat this by assigning to S_m an additional error δS to be folded in with the other errors. But S_m is proportional to the actual curvature K_m (momentum $P_m = 1/K_m \cos\theta$) and so the fractional error to be added to S_m is just $\delta S/S_m$ or P_m/P. Thus we fold into the quoted error, dp/p, an additional contribution equal to P_m/P, where P_m is the measured momentum, and P the momentum equivalent to the spurious curvature. The actual values of P are listed in Table VII.

Finally we discuss the analysis of the angle errors. The PANG optical parameters (which correct for the nonlinear effects in the optics) represent essentially a best set of corrections to optical imperfections, but are averaged over a group of rolls over which conditions may fluctuate to a certain extent. Therefore it seems logical to expect that there is a certain intrinsic limit on how accurately on the average can an angle be measured. A lower limit therefore should be set on the errors. Furthermore, the azimuth measurements will be affected by the systematic turbulence shift.

Table VII. Final-error floors.

Film interval	$\Delta\lambda_{min}$ (deg)	$\Delta\phi_{min}$ (deg)	Momentum due to spurious curvature (Bev)	Measuring uncertainty
557-598	0.20	0.15	30	7μ
600-696	0.20	0.15	15	7μ
702-780	0.20	0.20	10	7μ

To get a rough idea of lower limit on angle errors, we measured tracks using all possible view combinations and compared the differences between various measurements with the quoted measurement errors. The quoted errors were seen to be on the average too small, as the difference between different values almost always exceeded the quoted errors, sometimes by a factor of three or four. Thus an estimate was obtained of how large an error must be added to the quoted one to obtain reasonable values. In addition, the size of the systematic momentum shifts due to turbulence was used to obtain the size of the contribution to azimuth errors from this source.

However both this study as well as the investigation of turbulence could only indicate the rough size and kind of corrections that were necessary because the data are so limited. For this reason, the final values of all parameters were established by looking at distributions of χ^2 and "pull" quantities for decays. The "pull" quantities are parameters calculated in the KICK program, which give a measure of how far a given measured quantity had to be pulled to give a satisfactory fit. They take into account both the size of the error and the sensitivity of kinematics to that quantity. Their average value should be zero, and they should be Gaussian distributed with a half-width of one. Quantitatively a pull quantity in a variable x is defined as[10]

$$x_{pull} = \frac{x^{meas.} - x^{fitted}}{(x^{meas.} - x^{fitted})_{rms}} .$$

The error floors and turbulence corrections were varied until χ^2 and pull quantities had proper distributions. The advantages of using τ decays for error-floor study are their unambiguous interpretation and absence of any high-energy tracks (except incident K which is beam-averaged) that would be greatly affected by the systematic turbulence shift. All the distributions therefore may be expected to show proper behavior if the errors are adjusted correctly. The χ^2 distributions and the distributions of the nine pull quantities are shown in Figs. 22 through 25.

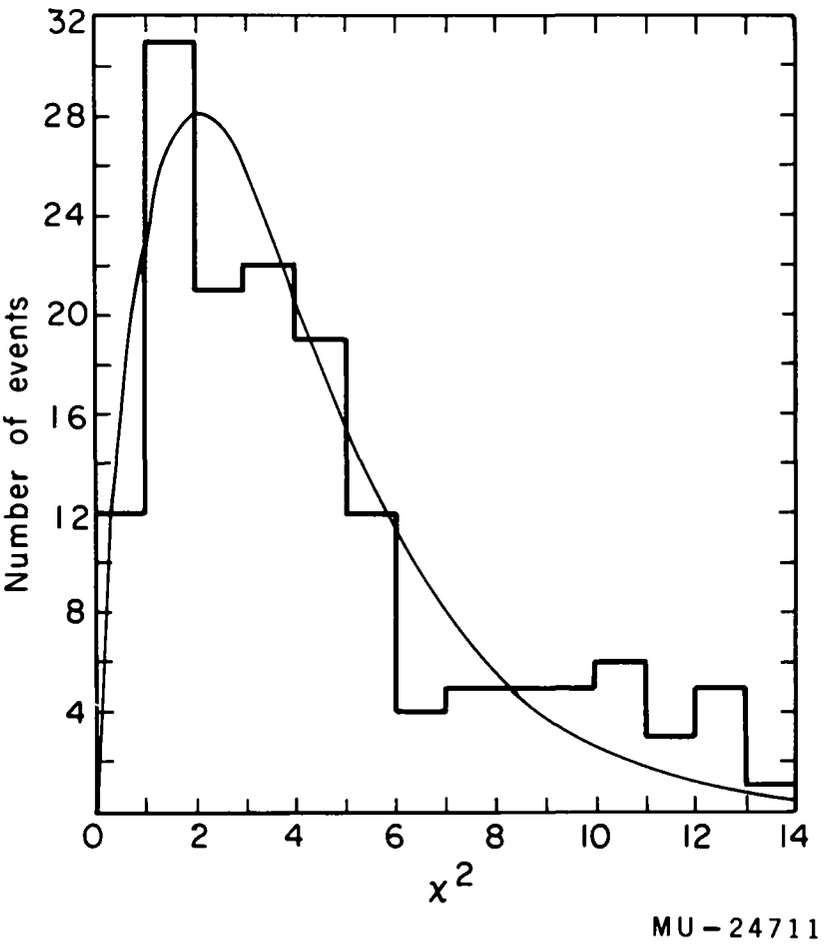

Fig. 22. The χ^2 distribution for the τ decays. The solid curve is the expected χ^2 distribution. The median is 3.48; the expected median, 3.4. The average is 4.34; the expected average, 4.0.

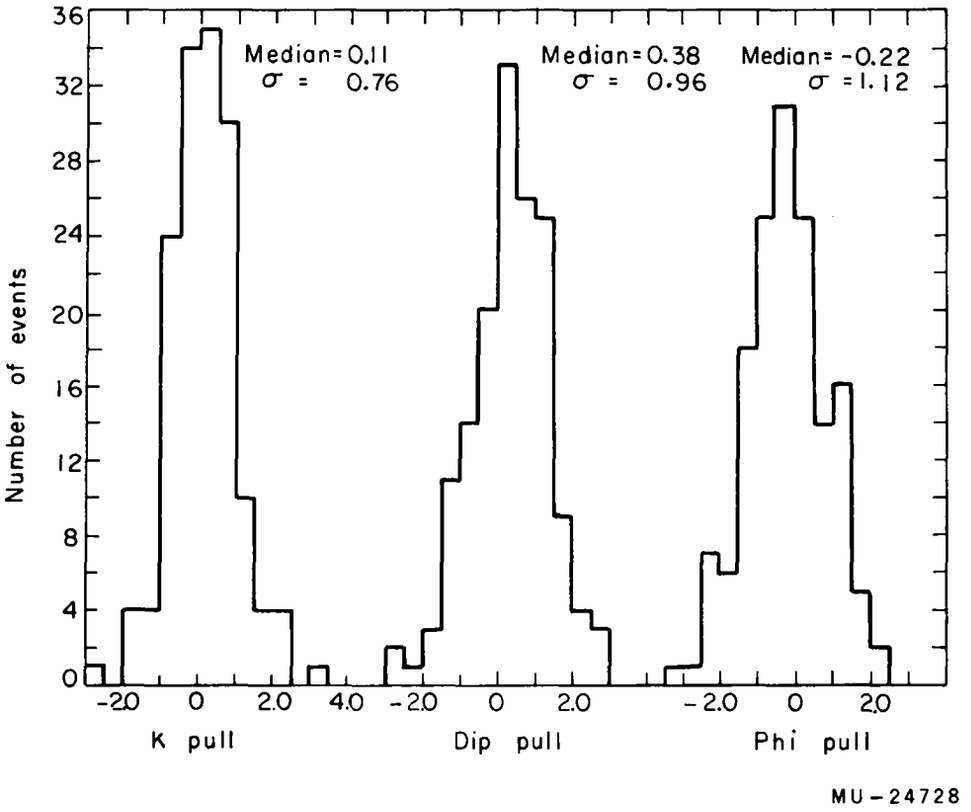

Fig. 23. Distribution of the three pull quantities for the incoming K^- in τ decays.

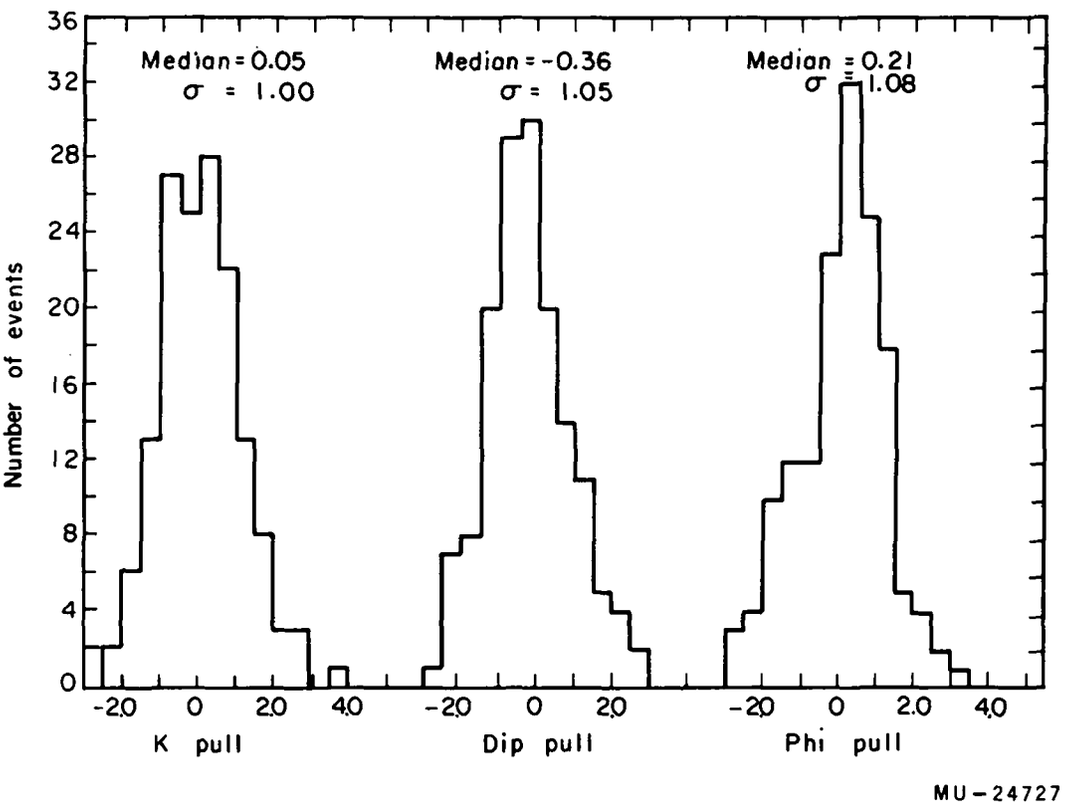

Fig. 24. Distribution of the three pull quantities for the outgoing π^+ from τ decays.

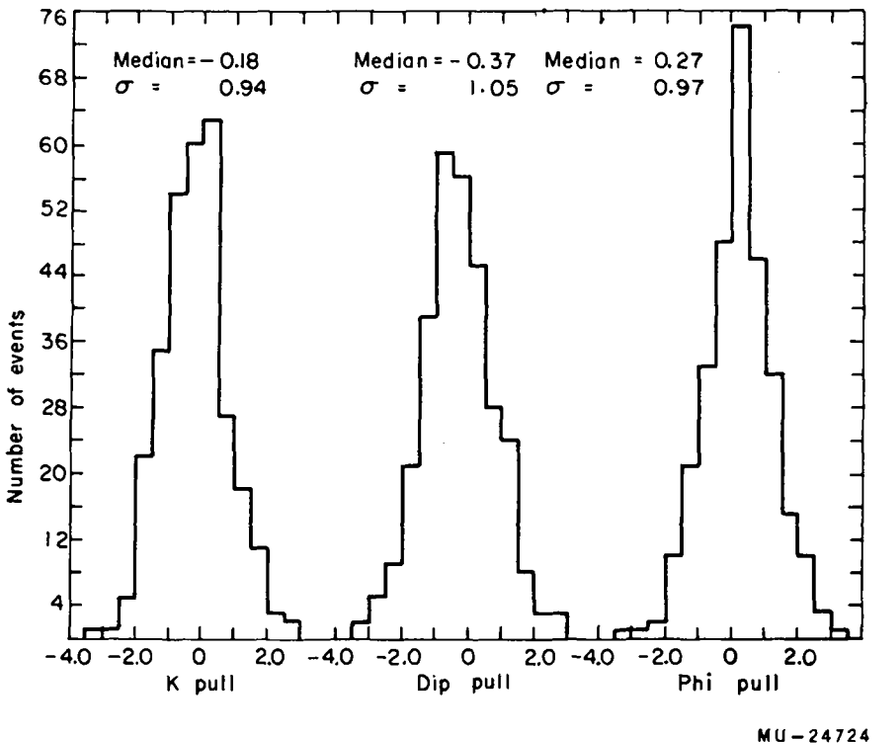

Fig. 25. Distribution of the three pull quantities for the two outgoing π^- mesons from the τ decays.

It can be seen that, if not absolutely correct, the errors represent a very good approximation. The worst systematic shifts seem to be in dip angles. However, the actual shift of the mean of about 1/3 corresponds to a systematic error of less than 1/10 deg, and as such does not represent a serious problem. The final values for the error floors are listed in Table VII.

C. Determination of the Beam Momentum

The beam was designed for the nominal momentum of 1.173 Bev/c at the target inside the Bevatron. The collimator in the second quadrupole was set to accept a band with a full width of 2.5%. For analysis it is important to determine the exact value of beam momentum in the bubble chamber as well as its spread, since the curvature measurement is not only relatively inaccurate at high energy but also is subject to systematic errors due to turbulence and optical imperfections (Appendix B).

For these reasons it is desirable to use a class of interactions or decays of beam particles to determine their momentum by applying the constraints of energy and momentum. Thus the measurement of the momentum and angle of emission of the muon in $K \rightarrow \mu + \nu$ decay determines uniquely the momentum of the K mesons. The difficulties with this method are the large measurement uncertainty of the μ momentum, as well as the impossibility of identifying the K decay as proceeding by this mode. Both of these are overcome if the muon stops in the chamber, since its range then determines the momentum very accurately, and the characteristic subsequent μ-e decay identifies the secondary as a sure μ.

Fortunately the beam momentum in this experiment is in the energy range where a reasonably large fraction of $K\mu_2$ decays will give a stopping muon. A muon from a $K\mu_2$ decay mode of a K meson of momentum 1101 Mev/c, which goes directly backward in the K^- rest frame will come out at rest in the laboratory system. At our energy, roughly 1.5% of all K decays will give a sufficiently slow muon that will come to rest in the chamber.

The advantages of this method for determination of the beam momentum are its great accuracy, complete lack of significant biases, and negligible contamination. If we consider first the accuracy of the method, the K momentum, P_K, depends solely on the momentum of the muon, P_μ, and its angle of emission, $\theta_{K\mu}$. These two quantities can be determined to a fraction of an Mev/c and a fraction of a degree respectively. The sensitivity of P_K to these two quantities over the range of kinematics under consideration is as follows:

$$\frac{dP_K}{dP_\mu} = 0 \text{ to } 25$$

$$\frac{dP_K}{d\theta_{K\mu}} = 5 \text{ to } 15 \text{ Mev/c deg.}$$

The exact variation of P_K with muon range and $\theta_{K\mu}$ is illustrated in Fig. 26. Thus for each individual decay, the momentum can be determined to a few Mev/c.

As for biases, the method is obviously completely independent of scanning efficiency or of any scanning biases. There are two small systematic errors that, however, turn out to be insignificant. First, the probability of decay goes as $1/P_K$, and thus the lower-momentum beam tracks will tend to decay more often, and the mean value will be shifted downward. Secondly the probability that a beam track will give a stopping muon also has a weak dependence on P_K, in the direction that a higher-momentum track is less likely to produce a stopping muon secondary, resulting again in a lower observed mean value. For small momentum spread, like in our case, these two effects are rather insignificant (they shift the observed mean downward by less than 1 Mev/c). No correction was therefore made for these two effects.

The only possible source of contamination are $K\mu_3$ decays, but these are expected to be few and also easily identifiable, since they would presumably give anomalously large P_K. Most of the $K\mu_3$ muon spectrum can not produce a muon so slow in the lab that it could stop in

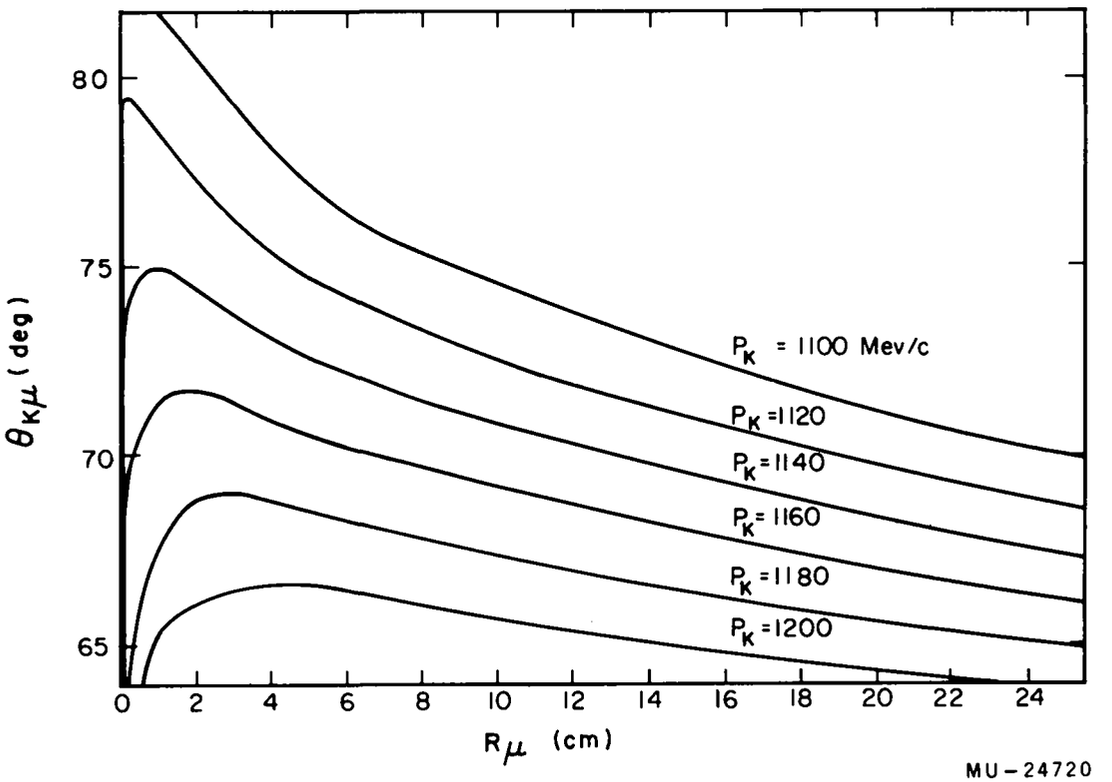

Fig. 26. Curves of constant P_K as a function of range and angle of the muon from K_{μ_2} decay.

the chamber. However, even if the muon spectrum was a delta function at the most favorable momentum, we would still expect only two or three $K\mu_3$ decays because of a much rarer decay rate for this mode. Actually one decay out of 47 was observed which could be safely ascribed to $K\mu_3$ mode.

Altogether 46 $K\mu_2$ decays were found with a stopping muon, three of which were distinctly below the nominal beam momentum (i.e. the K^- meson probably scattered before entering the chamber). The mean value of the beam momentum based on these 43 events is 1150 ± 3 Mev/c, (i.e. standard error on the mean value of $\pm 0.3\%$) with the width after unfolding of experimental uncertainties of ± 21 Mev/c. It should be pointed out that the mean value agrees very well with the beam design value, as the expected energy loss due to ionization in the walls of the chamber is about 20 Mev/c.

D. Estimate of Rates for Different Reactions in Single-V Events

We assume:

(a) The hyperon spectra from the single-V reactions are identical to their V^0 two-prong counterparts, e.g. the energy spectra of the Λ from the $\Lambda\pi^0\pi^0$ and $\Lambda\pi^+\pi^-$ reactions are the same.

(b) The relative rates for single V reactions are the same as their V^0 two-prong counterparts, e.g. $\sigma(\Lambda\pi^0\pi^0)/\sigma(\Lambda\pi^+\pi^-) = \sigma(\Sigma^0\pi^0\pi^0)/\sigma(\Sigma^0\pi^+\pi^-)$.

(c) By taking a sample of events with 78.2 Mev $< T_\Lambda <$ 122.7 Mev we are sufficiently far away from the $\Lambda\pi^0$ peak so that no $\Lambda\pi^0$ events are included in the selected sample.

We work with the equivalent number of events, i.e. each event has been multiplied by the inverse of its probability of detection.

We have 62.4 ± 9.5 events in the selected T_Λ interval, i.e. 78.2 Mev $\leqslant T_\Lambda \leqslant$ 122.7 Mev. We want to estimate next what fraction of these are three-and four-body events. Accordingly, we treat first all V^0 two prong events as if they were single V's; that is we just use the decay fit of the Λ to obtain its c.m. energy and its probability of detection. From the resulting energy spectrum of the Λ's we see that 23.1% of all

V^0 two-prong events with $T_\Lambda < 122.7$ Mev lie in the selected energy interval. Furthermore, we have 70.1 single V^0 events with $T_\Lambda < 78.2$ Mev. Some of these, however, are $\Sigma^0\pi^0$ events which fall under 78.2 Mev because of measurement errors. On the basis of an average error or 8.0 Mev, we estimate that 2.8 events below 78.2 Mev are $\Sigma^0\pi^0$ events.

There are $(70.1-2.8)/(1-0.231) = 87.5$ many-body events with $T_\Lambda < 122.7$ Mev. This yields $87.5 - (70.1 - 2.8) = 20.2$ many-body events in the selected energy interval. Therefore there are $62.4 - 20.2 + 2.8 = 45.0$ $\Sigma^0\pi^0$ events in the sample selected. Correcting for the fact that we look at only 2/3 of the $\Sigma^0\pi^0$ spectrum, we obtain $45.0 \times 3/2 = 67.5$ $\Sigma^0\pi^0$ events.

To obtain the total number of many-body events, we correct for the few V^0 two-prong events that lie above 122.7 Mev. This yields $1.02 \times 87.5 = 89.2$ many-body events. The number of $\Lambda\pi^0$ events is then obtained by subtracting these two from the total number of single V's observed. This yields $271.7 - 67.5 - 89.2 = 115.0$ $\Lambda\pi^0$ events.

Finally we must correct for the fact that even though some of these events satisfy the beam criteria as far as their direction is concerned, they are below the nominal beam momentum. Because these events are not fitted at the production vertex, we have to make this correction on statistical bases. From Appendix A, the fraction of low-energy events is four out of 158, and thus we multiply our results by 96.5%.

To correct for the neutral decay of the Λ, we divide the numbers by 0.64 ± 0.03.[32] Finally, to obtain the total cross sections, we use the conversion factor of 12.2 μb for each equivalent event observed. The computed cross sections in millibarns with their statistical errors are accordingly:

$$\Lambda\pi^0 \rightarrow 2.1 \pm 0.2$$
$$\Sigma^0\pi^0 \rightarrow 1.2 \pm 0.3$$
$$\left.\begin{matrix}\Lambda a\pi^0 \\ \Sigma^0 a\pi^0\end{matrix}\right\} \rightarrow 1.5 \pm 0.2 \quad \text{for } a \geq 2$$

To allow for the uncertainties inherent in this separation, we feel that the errors should be increased by about 50%.

E. Study of Ambiguities in the $\Sigma 2\pi$ Reactions

1. The $\Sigma^+\pi^-\pi^0$ and $\Sigma^-\pi^+\pi^0$ Reactions

We are interested in estimating the fraction of $\Sigma^{\pm}\pi^{\mp}\pi^0\pi^0$ events that will give a satisfactory fit to the $\Sigma^{\pm}\pi^{\mp}\pi^0$ hypothesis. In addition we want to know whether these events can be separated out on statistical grounds from the genuine examples of $\Sigma^{\pm}\pi^{\mp}\pi^0$ events. We can obtain some information on these points by fitting the $\Sigma^{\pm}\pi^{\mp}\pi^+\pi^-$ events to the $\Sigma 2\pi$ hypothesis. This is done by taking the Σ track and each one of the three pions in turn and trying to fit it as a $\Sigma 2\pi$. We can also calculate the missing mass for each pair of tracks. The results on a sample of $\Sigma 3\pi$ events are given in Table VIII and Figs. 27 and 28. We can draw two conclusions: (a) the probability that a $\Sigma 3\pi$ event will fit $\Sigma 2\pi$ is quite high ($\sim 65\%$) and (b) most of the $\Sigma 3\pi$ events will give a reasonably high missing mass. Specifically, 80% of the fitting events will give a missing mass greater than 270 Mev. Except for smearing due to measurement errors, this quantity should be always greater than 270 Mev.

To purify our sample of $\Sigma 2\pi$ events, we reject all the events with a missing mass greater than 270 Mev as those most likely be $\Sigma 3\pi$ events. This results in the removal of 17 out of 128 events. To these 17, we must add the five events that did not fit the $\Sigma^{\pm}\pi^{\mp}\pi^0$ hypothesis. We call all of these 22 events examples of $\Sigma^{\pm}\pi^{\mp}\pi^0\pi^0$. Thus 77% (17 out of 22) of these $\Sigma^{\pm}\pi^{\mp}\pi^0\pi^0$ events gave a satisfactory χ^2 to $\Sigma^{\pm}\pi^{\mp}\pi^0$, as opposed to 65% for the $\Sigma^{\pm}\pi^{\mp}\pi^+\pi^-$ events. This leads us to believe that the size of the correction is reasonable--if anything, slightly too large--and the remaining group of $\Sigma^{\pm}\pi^{\mp}\pi^0$ is relatively free from contamination. We have tacitly assumed here that all the internal distributions are the same for the $\Sigma^{\pm}\pi^{\mp}\pi^+\pi^-$ as for the $\Sigma^{\pm}\pi^{\mp}\pi^0\pi^0$ processes. However, very drastic and unrealistic differences would be required to significantly alter this result, so the assumption seems justified.

2. The $\Sigma^0\pi^+\pi^-$ Reactions

We discuss in the next few paragraphs the arguments used to estimate the total number of $\Sigma^0\pi^+\pi^-$ events. First, those $\Sigma^0\pi^+\pi^-$

Table VIII. Results of fitting $\Sigma 3\pi$ events to the $\Sigma 2\pi$ hypothesis

Serial number	Σ charge	χ^2 for $\Sigma 2\pi$ hypothesis[a]	Missing mass (Mev)	Error in missing mass (Mev)
		0.34	305	224
563 239	+	0.16	imaginary[b]	
		0.01	imaginary[b]	
		0.56	293	86
570 068	+	0.23	303	203
		0.23	307	208
		reject[c]		
594 023	+	reject[c]		
		28.5	378	21
		3.30	396	75
684 330	+	0.68	302	128
		18.3	395	28
		3.66[d]	419	100
739 066	+	0.74	329	160
		26.5	343	13
745 155	+	11.9	319	27
		23.8	326	13
		7.97	479	51
755 231	+	4.98	451	67
		0.53	323	169
		1.32	325	77
645 155	-	15.6	405	41
		7.00	390	16
		26.1[d]	386	22
677 111	-	14.9	365	23
		1.85	350	43
682 076	-	3.10	383	37
		3.85	372	12
		0.89	308	146
723 046	-	0.05	209	281
		0.17	imaginary[b]	
		5.44	422	39
742 017	-	8.14	445	29
		0.31	281	174
		reject[c]		
751 269	-	0.21	267	182
		1.11	347	81

a. The $\langle \chi^2 \rangle$ for a genuine $\Sigma 2\pi$ event is 1.0. The 1% χ^2 cutoff is 6.6.

b. Missing mass is imaginary when the magnitude of the missing momentum exceeds the missing energy.

c. Reject in the χ^2 column refers either to a case in which constraints cannot be satisfied by KICK method or, after the first iteration, χ^2 is greater than 500.

d. Sometimes only two χ^2 values are given for an event. This corresponds to a condition in which one pion momentum is measured so poorly that its value is rejected, and the $\Sigma 2\pi$ hypothesis is no longer overconstrained.

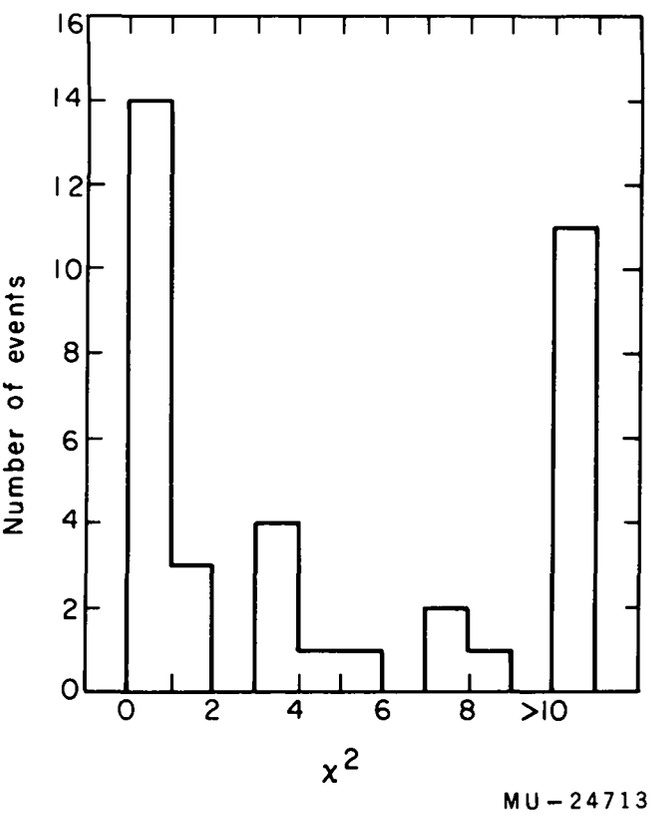

Fig. 27. The χ^2 distribution for the $\Sigma^{\pm}\pi^{\mp}\pi^{+}\pi^{-}$ events when they are fitted to the $\Sigma 2\pi$ hypothesis.

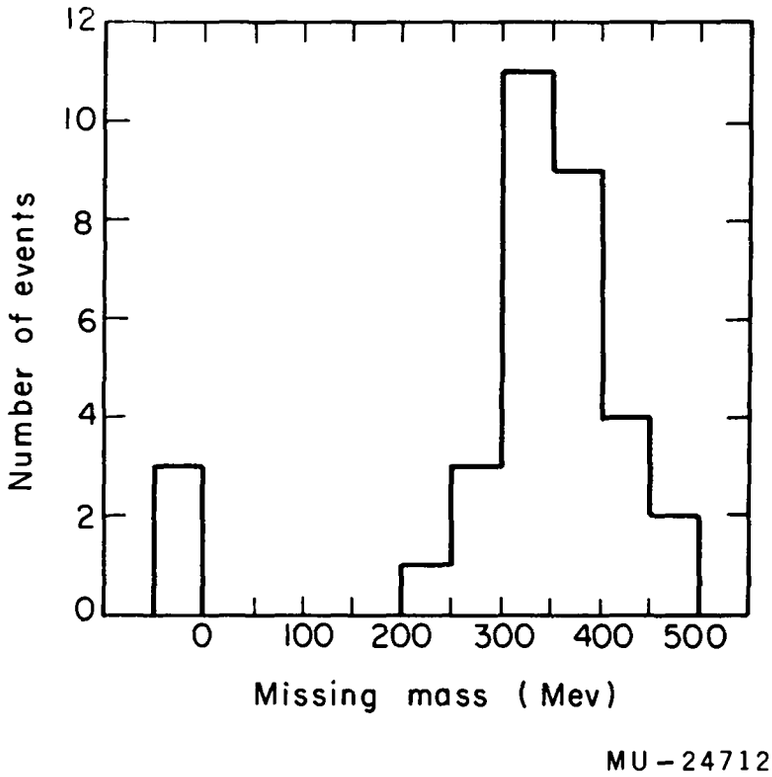

Fig. 28. Missing-mass distribution for the $\Sigma^{\pm}\pi^{\mp}\pi^{+}\pi^{-}$ events obtained from the measured quantities of the Σ track and one of the three pions. The events with MM < 0 represent the cases when missing momentum is greater than the missing energy.

events misidentified as $\Lambda\pi^+\pi^-$ should give a worse χ^2 distribution for the $\Lambda\pi^+\pi^-$ interpretation than the genuine $\Lambda\pi^+\pi^-$. A similar statement can be made for the $\Lambda\pi^+\pi^-$ events misidentified as $\Sigma^0\pi^+\pi^-$. Some of the parameters that give a measure of how good are the fits to different hypotheses are listed in Table IX. We conclude that as far as the χ^2 distribution is concerned, the assumption that majority of ambiguous events are $\Lambda\pi^+\pi^-$ seems to be pretty good. As a matter of fact, the unambiguous $\Lambda\pi^+\pi^-$ events seem to give on the average a higher χ^2 than the ambiguous events. This is probably because the errors on long, well-measurable tracks are probably underestimated, since it is these events that would be least likely to give a good χ^2 to a spurious interpretation.

Another argument can be based on an analysis of V^0 two-prong events without using the data on the V. We calculate χ^2 for the $\Lambda\pi^+\pi^-$ and $\Sigma^0\pi^+\pi^-$ interpretations for all V^0 two-prong events. Now, since both reactions have only one constraint, the probability for a spurious fit is the same in both cases. If we define:

P = probability that a $\Lambda\pi\pi$ event will give a better χ^2 fit to a $\Sigma^0\pi\pi$ interpretation than to a $\Lambda\pi\pi$, or the probability that $\Sigma^0\pi\pi$ event will give a better χ^2 fit to a $\Lambda\pi\pi$ interpretation than to a $\Sigma^0\pi\pi$

N_Σ = actual number of $\Sigma^0\pi\pi$ events

N_Λ = actual number of $\Lambda\pi\pi$ events

M_Σ = number of events with a lower χ^2 value for $\Sigma^0\pi\pi$ interpretation

M_Λ = number of events with a lower χ^2 value for $\Lambda\pi\pi$ interpretation,

we have the two equations

$$M_\Sigma = PN_\Lambda + (1 - P)\, N_\Sigma = 57$$

and

$$M_\Lambda = PN_\Sigma + (1 - P)\, N_\Lambda = 104.$$

The third equation, $N_\Sigma + N_\Lambda = M_\Sigma + M_\Lambda = 161$, is just a linear combination of these two and contributes nothing new.

Table IX. χ^2 Distributions for the ambiguous and unambiguous V^0 2P events.[a]

	$\Sigma^0\pi^+\pi^-$ interpretation (two constraints)					$\Lambda\pi^+\pi^-$ interpretation (four constrants)				
	No. of events	Median	Expected median	Average	Expected average	No. of events	Median	Expected median	Average	Expected average
Unambiguous	27	1.5	1.4	1.8	2.0	47	5.8	3.4	6.2	4.0
Ambiguous	87	3.0	1.4	3.4	2.0	87	4.0	3.4	4.7	4.0

a. Only events that are four-constraint cases for $\Lambda\pi^+\pi^-$ interpretation and two constraints for $\Sigma^0\pi^+\pi^-$ interpretation are included.

We want to estimate the value of parameter P. We know that physically P must range from zero, corresponding to zero measurement errors or completely different kinematics, to 1/2, corresponding to very large errors or identical kinematics. However, a more stringent statement can be made. We can obtain a lower limit for P by looking at our 27 "sure" $\Sigma^0\pi\pi$ events and seeing what fraction of them gives a lower χ^2 value for a $\Lambda\pi\pi$ interpretation than for a $\Sigma\pi\pi$ interpretation in this one-constraint fit. This is a lower limit for P since, if this is a biased sample of $\Sigma^0\pi\pi$ events, it is biased in such a way that these are less likely to give a good fit to $\Lambda\pi\pi$ interpretation than an average $\Sigma^0\pi\pi$ event. This lower limit on P turns out to be 26% and gives us an upper limit on the fraction of $\Sigma^0\pi\pi$ events in the group of ambiguous events. Using this value for P, we get 32 ± 13 for the maximum number of $\Sigma^0\pi\pi$ events in the whole film sample, which means a very small but statistically rather uncertain contamination (i.e. $< 5 \pm 13$ events).

We can obtain some lower limit on the number of $\Sigma^0\pi\pi$ events by looking at the distribution of the γ ray in the Σ^0 rest frame. A forward γ ray will have more energy in the laboratory system, and so it will be more difficult to absorb it by changing the momenta of the two pions. We would expect, therefore, that events with forward γ rays would be very unlikely to fit the $\Lambda\pi\pi$ interpretation. This coupled with the fact that the Σ^0, being a spin-1/2 particle, must decay isotropically allows us to obtain a lower limit on the number of $\Sigma^0\pi\pi$ events. The experimental numbers for the γ-ray distribution for the 27 "sure" $\Sigma^0\pi\pi$ events is 20 forward and seven backward γ rays. If we assume 100% efficiency for distinguishing $\Sigma^0\pi\pi$ events with forward γ rays, this corresponds to a lower limit on the number of $\Sigma^0\pi\pi$'s of 40 ± 9 events (i.e. contamination greater than 13 ± 9 events). Even though these are rough estimates based on very limited statistics, they do indicate that there are 10 to 15 $\Sigma^0\pi\pi$ events in the ambiguous group, since both the

lower and upper limits are roughly the same. For the purposes of future discussion, we assume then that one-third of all $\Sigma^0 \pi\pi$ events will give a satisfactory fit to a $\Lambda\pi\pi$ interpretation.

REFERENCES AND FOOTNOTES

1. P. Eberhard, M. L. Good, and H. K. Ticho, Rev. Sci. Instr. 31, 1054 (1960).
2. M. Gell-Mann, Suppl. Nuovo cimento 4, 848 (1956); K. Nishijima, Progr. Theoret. Phys. (Japan) 13, 285 (1955).
3. L. W. Alvarez, P. Eberhard, M. L. Good, W. Graziano, H. K. Ticho, and S. Wojcicki, Phys. Rev. Letters 2, 215 (1959).
4. B. Cork, G. Lambertson, O. Piccioni, and W. Wenzel, Phys. Rev. 106, 167 (1957).
5. M. Alston, L. W. Alvarez, P. Eberhard, M. L. Good, W. Graziano, H. K. Ticho, and S. Wojcicki, Phys. Rev. Letters 5, 520 (1960).
6. M. Alston, L. W. Alvarez, P. Eberhard, M. L. Good, W. Graziano, H. K. Ticho, and S. Wojcicki, Phys. Rev. Letters 6, 698 (1961).
7. These interactions are currently being studied by Mr. William Graziano of this Laboratory.
8. C. Coombes, B. Cork, W. Galbraith, G. Lambertson, and W. Wenzel, Phys. Rev. 112, 1303 (1958).
9. W. Humphrey, A Description of the PANG program, Alvarez Group Memo 111, September 18, 1959, and Memo 115, October 25, 1959 (unpublished); A. H. Rosenfeld, "Digital-Computer Analysis of Data from Hydrogen Bubble Chambers at Berkeley", in Proceedings of the International Conference on High-Energy Accelerators and Instrumentation, CERN, 1959 (CERN, Geneva, 1959).
10. A. H. Rosenfeld and J. N. Snyder, Digital-Computer Analysis of Data from Bubble Chambers, IV. The Kinematic Analysis of Complete Events, UCRL-9098, February 16, 1960 (to be published in Rev. Sci. Instr.); J. P. Berge, F. T. Solmitz, and H. Taft, Digital Computer Analysis of Data from Bubble Chambers, III. The Kinematical Analysis of Interaction Vertices, UCRL-9097, March 15, 1960 (also Rev. Sci. Instr. 32, 538 (1961).

11. The EXAMIN program used in this experiment has been written mainly by Mr. William Graziano, with some subroutines written by Dr. George Kalbfleisch, Mr. Dave Johnson, and this author. A slightly different form of the EXAMIN system has been described by Mr. Dave Johnson in Alvarez Group Memo 271, March, 1961 (unpublished).
12. R. Cool, B. Cork, J. Cronin, and W. Wenzel, Phys. Rev. 114, 912 (1959); P. Franzini, A. Garfinkel, J. Keren, A. Michelini, R. Plano, A. Prodell, M. Schwartz, J. Steinberger, and S. E. Wolf, Bull. Am. Phys. Soc., Ser. II, 5, 224 (1960).
13. R. H. Dalitz, Phys. Rev. 94, 1046 (1954).
14. For a general proof of this point see M. Gell-Mann and A. H. Rosenfeld, Ann. Revs. of Nuclear Sci. 7, 407 (1957).
15. V. Cook, B. Cork, T. F. Hoang, D. Keefe, L. T. Kerth, W. A. Wenzel, and T. T. Zipf, K^--p and K^--n Cross Sections in the Momentum Range 1 to 4 Bev/c, UCRL-9386, January 4, 1961.
16. At present, it is not clear whether this K-N resonance as well as the higher pion-nucleon resonances are genuine dynamical effects or just kinematical manifestations of other phenomena. The data on π-p angular distributions in the region of these resonances indicates the presence of more than just one partial wave; see C. D. Wood et al., Phys. Rev. Letters 6, 481 (1961).
17. L. T. Kerth and A. Pais, On the Gentle Art of Hunting Bumps, UCRL-9706, May 19, 1961.
18. R. Gatto, Phys. Rev. 109, 610(L)(1958).
19. M. Gell-Mann, Phys. Rev. 106, 1297 (1957); P. Amati, A. Stanghellini, and B. Vitale, Nuovo cimento 13, 1143 (1959) and Phys. Rev. Letters 5, 524 (1960).
20. R. H. Dalitz and S. F. Tuan, Ann. Phys. 10, 307 (1960); R. H. Dalitz and S. F. Tuan, Phys. Rev. Letters 2, 425 (1959).
21. R. H. Dalitz, Phys. Rev. Letters 6, 239 (1961).

22. L. W. Alvarez, in Ninth International Annual Conference on High-Energy Physics, Kiev, 1959 [Academy of Sciences (IUPAP), Moscow, Russia, 1960], 2 vols; The Interactions of Strange Particles, UCRL-9354, August 11, 1960 (unpublished).
23. W. E. Humphrey, Hyperon Production by K^- Mesons Incident on Hydrogen (thesis), UCRL-9752, June 12, 1961 (unpublished); R. Ross, Elastic and Charge-Exchange Scattering of K^- Mesons in Hydrogen (thesis), UCRL-9749, June 21, 1961 (unpublished).
24. M. Ross and G. Shaw, Ann. Phys. 9, 391 (1960), Ann. Phys. 13, 147 (1961), and Phys. Rev. Letters 5, 578 (1960).
25. For a review of data on Y_1^* through December, 1961, see M. H. Alston, and M. Ferro-Luzzi, Revs. Modern Phys. (to be published) and Pion-Hyperon Resonances, UCRL-9587, March 7, 1961.
26. R. H. Dalitz and Donald H. Miller, Phys. Rev. Letters 10, 562 (1961).
27. H. J. Martin, L. B. Leipuner, W. Chinowsky, F. T. Shively, and R. K. Adair, Phys. Rev. Letters 6, 283 (1961).
28. P. Bastien, M. Ferro-Luzzi, and A. H. Rosenfeld, Phys. Rev. Letters 6, 702 (1961).
29. R. L. Schult and R. H. Capps, Phys. Rev. 122, 1659 (1961).
30. R. Tripp, M. Ferro-Luzzi, and M. Watson, Bull. Am. Phys. Soc. Series II, 4, 350 (1961).
31. G. Clark and W. F. Diehl, Range-Energy Relation for Liquid Hydrogen Bubble Chambers, UCRL-3789, May 1957.
32. G. A. Snow and M. M. Shapiro, Revs. Modern Phys. 33, 231 (1961).